VIRGINIA MARCIA CONCATO-LOPES

ATIVIDADE ANTITUMORAL DO 3,3',5,5'-TETRAMETOXIBIFEENIL-4,4'-DIOL E TRILOBOLIDO-6-*O*-ISOBUTIRATO EM MODELO EXPERIMENTAL EM CÉLULAS A549 E NCI-H460:

EXPLORANDO OS EFEITOS METABÓLICOS E OS MECANISMOS DE AÇÃO

Londrina
2023

VIRGINIA MARCIA CONCATO-LOPES

ATIVIDADE ANTITUMORAL DO 3,3',5,5'-TETRAMETOXIBIFEENIL-4,4'-DIOL E TRILOBOLIDO-6-*O*-ISOBUTIRATO EM UM MODELO EXPERIMENTAL *IN VITRO* EM CÉLULAS A549 E NCI-H460:

EXPLORANDO OS EFEITOS METABÓLICOS E OS MECANISMOS DE AÇÃO

Tese apresentada ao Programa de Pós-Graduação em Patologia Experimental da Universidade Estadual de Londrina, como requisito à obtenção do título de Doutora em Patologia Experimental.

Orientador: Prof. Dr. Wander R. Pavanelli.

Londrina
2023

Ficha de identificação da obra elaborada pelo autor, através do Programa de Geração Automática do Sistema de Bibliotecas da UEL

Concato-Lopes, Virginia Márcia Concato-Lopes.
Atividade antitumoral do 3,3\',5,5\'-tetrametoxibifeenil-4,4\'-diol e trilobolido-6-O-isobutirato em um modelo experimental in vitro em células A549 e NCI-H460: : explorando os efeitos metabólicos e os mecanismos de ação. / Virginia Márcia Concato-Lopes Concato-Lopes. - Londrina, 2023.
96 f.

Orientador: Wander Rogério Pavanelli Pavanelli.
Coorientador: Mario Sérgio Mantovani Mantovani .
Tese (Doutorado em Patologia Experimental) - Universidade Estadual de Londrina, Centro de Ciências Biológicas, Programa de Pós-Graduação em Patologia Experimental, 2023.
Inclui bibliografia.

1. Câncer de Pulmão - Tese. 2. Tratamento Alternativo - Tese. 3. Indução de morte celular - Tese. I. Pavanelli, Wander Rogério Pavanelli. II. Mantovani , Mario Sérgio Mantovani . III. Universidade Estadual de Londrina. Centro de Ciências Biológicas. Programa de Pós-Graduação em Patologia Experimental. IV. Título.

CDU 616

VIRGINIA MARCIA CONCATO-LOPES

ATIVIDADE ANTITUMORAL DO 3,3',5,5'-TETRAMETOXIBIFEENIL-4,4'-DIOL E TRILOBOLIDO-6-O-ISOBUTIRATO EM UM MODELO EXPERIMENTAL IN VITRO EM CÉLULAS A549 E NCI-H460:

EXPLORANDO OS EFEITOS METABÓLICOS E OS MECANISMOS DE AÇÃO

Tese apresentada ao Programa de Pós-Graduação em Patologia Experimental da Universidade Estadual de Londrina, como requisito à obtenção do título de Doutora em Patologia Experimental.

BANCA EXAMINADORA

_____

Orientador: Prof. Dr. Wander R. Pavanelli
Universidade Estadual de Londrina – UEL

_____

Prof. Dr. Fabio Henrique Kwasniewski
Universidade Estadual de Londrina - UEL

_____

Prof. Dr. Mário Sérgio Mantovani
Universidade Estadual de Londrina – UEL

_____

Profª. Drª. Danielle Lazarin Bidoia
Universidade Estadual de Londrina – UEL

_____

Profª. Drª. Maiara Voltarelli Providello
Universidade Estadual de Londrina – UEL

Londrina, 20 de outubro de 2023.

Dedico este trabalho à minha mãe, meu esposo, minha filha e minha família, por todo seu amor incondicional e por sempre acreditar em mim, motivos estes que me fazem seguir em frente.

AGRADECIMENTOS

Agradeço primeiramente a Deus, por ter me dado força, calma e coragem para trilhar os caminhos durante o doutorado, à Ele toda honra e toda glória por sempre me guiar e confortar.

À minha Mãe e rainha Nossa Senhora, por sempre interceder por mim.

Ao meu orientador, professor Dr. Wander R. Pavanelli, por ter me aceitado em seu laboratório desde a iniciação científica, pelos conselhos, pelas dicas e por ter confiado a mim este projeto no qual fui muito feliz em desenvolvê-lo. Meus sinceros agradecimentos.

Agradeço à professora Drª Ivete Conchon-Costa que abriu as portas de seu laboratório, por toda atenção e carinho concedido, e por todo o seu ensinamento.

Agradeço imensamente ao Prof. Dr. Mário Sérgio Mantovani, por ter aberto as portas de seu laboratório, por ter se disponibilizado a me ajudar e me ensinar todos os protocolos. Agradeço pelas dicas e conselhos e por contribuir grande e estritamente com o desenvolvimento deste trabalho.

Agradeço a profª. Drª. Aneli M. Barbosa-Dekker, ao Professor Dr. Robert F. H. Dekker e ao Professor Dr. Nilton Arakawa por ceder o composto e seu tempo, que contribuíram muito para a realização do meu trabalho.

Agradeço à profª. Drª. Idessania Nazareth Costa pelos ensinamentos e por toda a sua contribuição na minha formação.

À todos os meus amigos do mundo cientifico, por deixarem meus dias mais felizes, por toda loucura compartilhada e por deixarem mais leve a rotina de trabalho. Em especial, à Mariana Barbosa Detoni, Ellen Mayara Souza Cruz, Ana Carolina Jacob Rodrigues, Amanda Cristina Machado Carloto, Elaine da Silva Siqueira, Manoela Daiele Gonçalves, Taylon Felipe Silva, Bruna Taciane da Silva Bortoleti, Fernanda Tomiotto- Pellissier, Maria Beatriz Madureira, Yasmin Munhoz, Juliana Bitencourt, Rachel Arruda, Angélica Paulina, Natalia Concimo, Fabrício Inoue Seydi, Ricardo de Matos e João Emanoel.

À todos os professores e funcionários do departamento de Ciências patológicas.

Agradeço à CAPES e CNPq pela bolsa concedida e financiamento de meu projeto.

Aos integrantes da banca de qualificação e defesa, Dr. Mário Sérgio Mantovani e Dr. Fabio Henrique Kwasniewski, Professora Drª. Danielle Lazarin Bidoía e Professora Drª. Maiara Voltarelli Providello pelo tempo concedido e dedicação para a correção do meu trabalho.

Gostaria de agradecer à minha mãe Lourdes, minha amiga, e guerreira, pois se não fosse por seu esforço eu não teria chegado onde estou. Agradeço a ti mãe por todo seu esforço ao longo destes anos todos, por cuidar de mim nos momentos difíceis e estressantes e por sempre me apoiar. Muito obrigada mãe!

Agradeço ao meu amor Gustavo, que acompanhou de perto meus passos e essa etapa em minha vida, por sempre me ajudar e por ter muita paciência e sempre me apoiar. Agradeço também pelo nosso presentinho de casamento, minha amada filha, que é a razão da minha vida e alívio dos meus estresses diários, a qual amo infinitamente.

Agradeço ao meu pai, meus irmãos e sobrinhos, por sempre me compreenderem e estar por perto para me ajudar em diversas situações.

À todos os citados e aos possíveis esquecidos, muito obrigada!

“Não vos inquieteis com nada! Em todas as circunstâncias apresentai a Deus as vossas preocupações, mediante a oração, as súplicas e a ação de graças. E a paz de Deus, que excede toda a inteligência, haverá de guardar vossos corações e vossos pensamentos, em Jesus Cristo. ”

Filipenses 4:6,7

“Não importa o quanto a vida possa ser ruim, sempre existe algo que você pode fazer, e triunfar. Enquanto há vida, há esperança. ”

Stephen Hawking

RESUMO

CONCATO-LOPES, Virgínia Márcia. **Atividade antitumoral do 3,3',5,5'-tetrametoxibifeenil-4,4'-diol e trilobolido-6-*O*-isobutirato em um modelo experimental *in vitro* em células A549 e NCI-H460:** explorando os efeitos metabólicos e os mecanismos de ação. 2023. 135 p. Tese (Doutorado em Patologia Experimental) - Universidade Estadual de Londrina, Londrina, 2023.

O câncer de pulmão, uma doença crônica e heterogênea, é a principal causa de morte relacionada ao câncer mundialmente. Apesar da disponibilidade de diversas opções terapêuticas, sua eficácia continua limitada, frequentemente acompanhada de alta toxicidade, efeitos colaterais significativos, além de resistência medicamentosa que as células cancerígenas desenvolvem. O composto fenólico 3,3',5,5'-tetrametoxibifenil-4,4'-diol (TMBP), obtido por meio da biotransformação do 2,6-dimetoxifenol, mediada por lacase fungica, e a lactona sesquiterpênica extraída de *Sphagneticola trilobata*, trilobolide-6-*O*-isobutirato (TBB), demonstraram na literatura efeitos leishmanicida, antitumorais e imunomoduladores. No entanto, seus mecanismos de ação em câncer de pulmão de células não pequenas (CPCNP) não foram investigadas. Neste estudo, avaliamos o efeito antitumoral *in vitro* do TMBP e do TBB nas linhagens A549 e NCI-H460, elucidando os mecanismos indutores de morte celular. O tratamento com TMBP (12,5-200 μM) sobre as células NCI-H460 resultou na redução da proliferação em 24, 48 e 72 h. O IC_{50} (154 μM) foi obtido e utilizado para os demais experimentos. Após 24 h de exposição, o tratamento com IC_{50}, induziu diversas alterações morfológicas e ultraestruturais nas células NCI-H460, reduziu a migração e a marcação de N-caderina e β-catenina por imunofluorescência, aumento de espécies reativas de oxigênio (ERO) e óxido nítrico (ON), juntamente com a diminuição dos radicais ânion superóxido e atividade reduzida da glutationa redutase (GSH). Além disso, o TMBP induziu estresse metabólico, evidenciado pela redução da captação de glicose, da lactato desidrogenase intracelular e dos níveis de lactato. Outros efeitos observados incluíram a despolarização mitocondrial, aumento na formação de gotículas lipídicas e a presença de vacúolos autofágicos. Notavelmente, o TMBP induziu a parada do ciclo celular na fase G2/M e a morte celular semelhante a apoptose, conforme indicado pelo aumento da atividade da caspase-3/7 e pela redução da marcação de STAT-3 por imunofluorescência. O impacto antitumoral do TMBP foi acompanhado por uma redução nos níveis proteicos de PI3K, AKT, ARG-1 e NF-κB, juntamente com um aumento de iNOS. Em relação ao tratamento com TBB, as previsões *in silico* revelaram um potencial promissor de similaridade com medicamentos para o composto, indicando alta biodisponibilidade oral e eficiente absorção intestinal. O tratamento *in vitro*, sob células humanas A549 e NCI-H460 (12-100 μM) reduziu a viabilidade celular, obtendo valores de IC_{50} de 73 e 54 μM para A549 e NCI-H460, respectivamente, os quais foram usados nas experimentações seguintes. Após a exposição ao tratamento com IC_{50} de 73 e 54 μM, as células apresentaram alterações morfológicas e estruturais, capacidade migratória reduzida e aumento do estresse oxidativo, caracterizado pelo aumento nos níveis de ERO, radicais ânion superóxido e ON, juntamente com uma redução nos marcadores antioxidantes chave, como superóxido dismutase e GSH. Encontramos também estresse celular induzido pelo TBB após tratamento, o qual resultou em mudanças notáveis no metabolismo celular, levando ao acúmulo de gotículas lipídicas e vacúolos

autofágicos, bem como o comprometimento da integridade mitocondrial, um aspecto crucial da função celular. Adicionalmente, o TBB desencadeou uma morte celular semelhante a apoptose por meio da ativação das caspases 3/7. Essas descobertas destacam o grande potencial dos compostos TMBP e TBB como candidatos promissores para estudos futuros, consolidando sua posição como componentes adicionais no desenvolvimento de protótipos de novos medicamentos anticâncer.

Palavras-chave: Câncer de Pulmão; Compostos fenólicos; Lactona Sesquiterpênica; PI3K/AKT; Estresse oxidativo.

ABSTRACT

CONCATO-LOPES, Virgínia Márcia. **Antitumor activity of 3,3',5,5'-tetramethoxybiphenyl-4,4'-diol and trilobolido-6-*O*-isobutyrate in an *in vitro* experimental model in A549 and NCI-H460 cells:** exploration of metabolic effects and mechanisms of action. 2023. 135 p. Tese (Doutorado em Patologia Experimental) - Universidade Estadual de Londrina, Londrina, 2023.

Lung cancer, a chronic and heterogeneous disease, is the leading cause of cancer-related deaths worldwide. Despite the availability of several therapeutic options, their efficacy remains limited, often associated with high toxicity, significant side effects, and drug resistance developed by cancer cells. The phenolic compound 3,3',5,5'-tetramethoxybiphenyl-4,4'-diol (TMBP), obtained by the biotransformation of 2,6-dimethoxyphenol mediated by fungal laccase, and the sesquiterpene lactone extracted from *Sphagneticola trilobata*, trilobolide-6-*O*-isobutyrate (TBB), have been reported in the literature to have leishmanicidal, antitumor and immunomodulatory activities. However, their mechanisms of action in non-small cell lung cancer (NSCLC) have not been investigated. In this study, we evaluated the *in vitro* antitumor effects of TMBP and TBB on A549 and NCI-H460 cell lines and elucidated the mechanisms that induce cell death. Treatment of NCI-H460 cells with TMBP (12.5-200 μM) resulted in reduced proliferation at 24-72 h. The IC_{50} (154 μM) was obtained and used for further experiments. After 24 h of exposure, treatment with IC_{50} induced several morphological and ultrastructural changes in NCI-H460 cells, decreased migration and labeling of N-cadherin and β-catenin by immunofluorescence, increased reactive oxygen species (ROS) and nitric oxide (NO) along with decreased superoxide anion radicals and reduced glutathione reductase (GSH) activity. In addition, TMBP induced metabolic stress as evidenced by decreased glucose uptake, intracellular lactate dehydrogenase, and lactate levels. Other effects observed included mitochondrial depolarization, increased lipid droplet formation and the presence of autophagic vacuoles. Notably, TMBP induced cell cycle arrest in the G2/M phase and apoptosis-like cell death as indicated by increased caspase-3/7 activity and decreased immunofluorescence labeling of STAT-3. The antitumor effect of TMBP was accompanied by a decrease in protein levels of PI3K, AKT, ARG-1 and NF-κB and an increase in iNOS. With respect to TBB treatment, *in silico* predictions revealed a promising drug-like potential for the compound, indicating high oral bioavailability and efficient intestinal absorption. In vitro treatment of human A549 and NCI-H460 cells (12-100 μM) reduced cell viability, yielding IC_{50} values of 73 and 54 μM for A549 and NCI-H460, respectively, which were used in the following experiments. After exposure to treatment with IC_{50} of 73 and 54 μM, cells showed morphological and structural changes, reduced migratory capacity, and increased oxidative stress, characterized by an increase in the levels of ROS, superoxide anion radicals and NO, together with a reduction in markers of key antioxidants such as superoxide dismutase and GSH. We also found cellular stress induced by TBB after treatment, which resulted in significant changes in cellular metabolism, leading to the accumulation of lipid droplets and autophagic vacuoles, as well as the impairment of mitochondrial integrity, a crucial aspect of cellular function. In addition, TBB induced apoptosis-like cell death through the activation of caspases 3/7. These findings highlight the great potential of TMBP and TBB compounds as promising candidates for future studies, thus consolidating

their position as additional components in the development of new anticancer drug prototypes.

Key-words: Lung Cancer; Phenolic Compounds; Sesquiterpene Lactona; PI3K/AKT; Oxidative Stress.

LISTA DE ILUSTRAÇÕES

LISTA DE ABREVIATURAS E SIGLAS

ATP	Adenosina trifosfato
CAT	Catalase
CCG	Carcinoma de Células Grandes
CDDP	cisplatina
CTR1	Proteína transpostadora de cobre 1
DNA	Ácido desoxirribonucleico
eNOS	Óxido Nítrico Sintase endotelial
EMT	Transição epitélio-mesenquimal
FDA	*Food and Drug Administration*
GSH	Glutationa reduzida
GSSG	Glutationa dissulfeto
GSH-Px	Glutationa Peroxidase
HMG	Proteína do grupo de alta mobilidade
HNO_2	Ácido nitroso
HOCl	Hipocloreto
H_2O_2	Peróxido de hidrogênio
IARC	*International Agency for Research on Cancer*
IFN	Interferon
IKKα	IκB-Quinase -alfa
IL	Interleucina
iNOS	Óxido Nítrico Sintase induzível
LDH	Lactato Desidrogenase
LPS	Lipopolissacarídeo
LS	Lactona Sesquiterpênica
MAPK	Proteína quinase ativada por mitógeno
MMP	Metaloproteinase de matriz
MMP2/9	Metaloproteinase 2/9
MMR	Proteínas de reparo de incompatibilidade
NADPH	Fosfato de dinucleotídeo de nicotinamida e adenina
NBR	Norma Brasileira
NER	Reparo por excisão de nucleotídeos
NF-κB	Fator Nuclear-*κappa* B

nNOS	Óxido Nítrico Sintase neuronal
NO•	Óxido Nítrico
NO_2-	Dióxido de nitrogênio
NOS	Óxido Nítrico Sintase
NSCLC	*Non-Small Cell Lung Cancer*
N_2O_3	Trióxido de dinitrogênio
$O_2^{\bullet -}$	Ânion superóxido
•OH	Hidroxila
OMS	Organização Mundial da Saúde
$ONOO^-$	Peroxinitrito
OXPHOS	Fosforilação oxidativa
PI3K	Fosfoinositídeo 3-quinase
RNS	Espécies reativas de nitrogênio
ROS	Espécies reativas de oxigênio
SCLC	*Small Cell Lung Cancer*
SOD	Superóxido dismutase
TBB	Trilobolido-6-O-isobutirato
TLR	Receptor toll-like
TMBP	3,3',5,5'-tetrametoxibifenil-4,4'-diol
TNF	Fator de Necrose Tumoral
VEGF	Fator de crescimento do endotélio vascular

SUMÁRIO

1. INTRODUÇÃO

1.1 ASPECTOS GERAIS DO CÂNCER

A origem das células cancerígenas envolve um conjunto complexo de eventos genéticos, moleculares e celulares. O câncer inicia quando uma única célula normal sofre uma série de mutações genéticas que a tornam anormal e desencadeiam o crescimento descontrolado (STRATTON; CAMPBELL; FUTREAL, 2009). Essas células aberrantes têm a capacidade de invadir tecidos e órgãos circundantes, podendo se espalhar para outras partes do corpo, em um processo chamado metástase. A causa fundamental do câncer reside em mutações genéticas que ocorrem no DNA. Tais mutações podem ser adquiridas ao longo da vida devido a diversos fatores, como exposição a substâncias carcinogênicas (tabaco, radiações ionizantes e produtos químicos tóxicos), fatores genéticos herdados e erros que podem ocorrer durante a replicação do DNA. Além disso, podem afetar os mecanismos de controle de crescimento celular e inibir a capacidade das células se autorregularem, o que resulta em um crescimento descontrolado. As células cancerígenas também podem ignorar os sinais do sistema imunológico que normalmente reconhecem e eliminam células anormais (HANAHAN; WEINBERG, 2011; DE VISSER; JOYCE, 2023).

A carcinogênese é um processo intricado que pode ser subdividido em quatro estágios cruciais: iniciação, promoção, conversão maligna e progressão tumoral. No estágio inicial, agentes carcinogênicos ou moléculas iniciadoras entram em contato com as células e provocam alterações irreversíveis no material genético, resultando em mutações genéticas. Estas mutações são causadas pela ação direta dos agentes iniciadores, e elas representam o ponto de partida para o desenvolvimento do câncer. Os agentes promotores entram em ação no estágio de promoção, estimulando a proliferação das células mutadas. Esse estímulo provoca um aumento significativo na taxa de crescimento celular, resultando em um maior número de células com mutações genéticas. Isso cria um ambiente propício para a progressão do câncer, principalmente com o acúmulo de mutações nas células. A conversão maligna marca o terceiro estágio, no qual as células pré-neoplásicas que acumularam várias mutações genéticas distintas e diversificadas sofrem uma transformação em células malignas. Essa transformação envolve uma série complexa de eventos moleculares que conferem às células a capacidade de se comportarem de maneira maligna e invasiva. Finalmente, a progressão tumoral engloba a expressão

do fenótipo maligno adquirido, bem como a tendência dessas células malignas em adquirirem características ainda mais agressivas ao longo do tempo. Esse processo é acompanhado pelo desenvolvimento de características invasivas, o que permite que as células tumorais secretem proteases que facilitam a disseminação através da corrente sanguínea e a invasão de novos tecidos (HAHN; WEINBERG, 2002; PIRETTO et al., 2019).

Figura 1: Processo de desenvolvimento/carcinogênese do câncer.

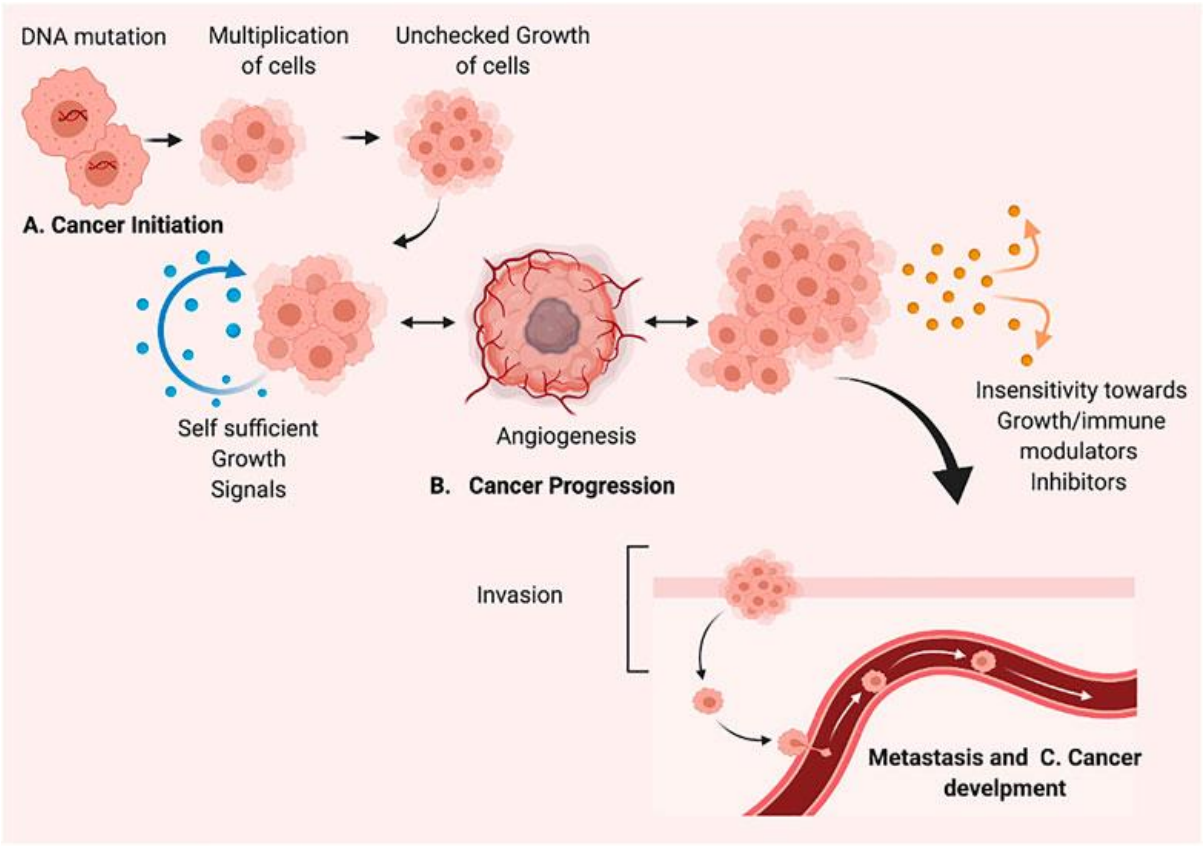

Fonte: CHAUDHRY et al. (2022), criado com BioRender.com. (A) iniciação, (B) progressão, (C) metástase e desenvolvimento do câncer.

O câncer é uma das quatros doenças com a maior taxa de mortalidade, considerado um dos principais problemas de saúde pública (SUNG et al., 2021). De acordo com dados da IARC (International Agency for Research on Cancer), em 2020 os cânceres de maior incidência foram de mama (4,7 milhões) e pulmão (2,2 milhões) (**Figura 2A**). Em relação às taxas de mortalidade, o câncer de pulmão levou à morte de 1,8 milhões de pessoas por ano, e o câncer de mama 1,3 milhões de mortes, ficando em primeiro e segundo lugar em mortalidade respectivamente (OMS,

2020) (**Figura 2B**).

Figura 2 – Número estimado de novos casos e de mortalidade em todo o mundo, considerando ambos os sexos e todas as faixas etárias.

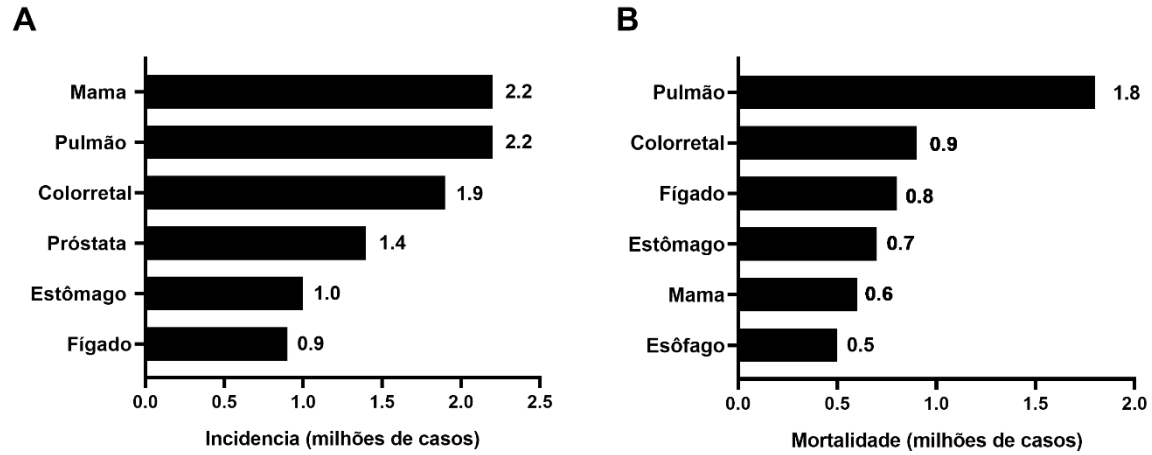

Fonte: Adaptado de OMS (2020).

1.2 CÂNCER DE PULMÃO

A classificação dos tumores pulmonares segue a diretriz da Organização Mundial da Saúde (OMS) de 2015. Este sistema de classificação se baseia na imuno-histoquímica e na análise microscópica para orientar o tratamento e estabelecer um prognóstico. Existem duas categorias principais de câncer de pulmão: carcinoma de células pequenas (*Small Cell Lung Cancer* - SCLC) e carcinoma de células não pequenas *(Non-Small Cell Lung Cancer* - NSCLC). O SCLC é um subtipo altamente agressivo que afeta aproximadamente 13 a 15% da população com câncer de pulmão. Ele tem uma tendência significativa de se espalhar para outros órgãos. Por outro lado, o NSCLC é responsável por cerca de 85% dos casos de câncer de pulmão e tem menor probabilidade de metástase, embora seja menos responsivo a terapias citotóxicas. O NSCLC inclui subtipos como o adenocarcinoma, o carcinoma de células escamosas e o carcinoma de grandes células, cada um com características morfológicas distintas. Em resumo, a classificação dos tumores pulmonares de acordo com a OMS considera o tipo histológico, morfologia macro e microscópica, e ajuda a orientar o tratamento e a prever o prognóstico de pacientes com câncer de pulmão (CLARK; ALSUBAIT, 2022; DUMA; SANTANA-DAVILA; MOLINA, 2019; GAZDAR, 2010; TRAVIS, 2011).

O adenocarcinoma, representando cerca de 40% dos casos de câncer

de pulmão, forma estruturas glandulares e se origina nos bronquíolos, avançando nos alvéolos; por isso, geralmente estão localizados na região periférica do pulmão e penetram em vasos linfáticos, por onde podem chegar à pleura e linfonodos hilares e formar metástases. Sintomas locais muitas vezes são ausentes ou aparecem tardiamente, e este tipo de câncer não está fortemente associado ao tabagismo (ZAMBONI, 2002; BALDOTTO et al., 2016; DUMA; SANTANA-DAVILA; MOLINA, 2019; SIDDIQUI; VAQAR; SIDDIQUI, 2023).

O carcinoma de células escamosas (ou epidermóide) abrange 25 a 30% dos casos de câncer de pulmão. Ele geralmente se desenvolve nos brônquios centrais e tem crescimento endobrônquico. A presença de pérolas de queratina é uma característica histológica marcante, tornando-o facilmente identificável, especialmente em tumores maiores. Os sintomas, como tosse e hemoptise, costumam aparecer precocemente, permitindo um diagnóstico nas fases iniciais, mas possa ocorrer disseminação para linfonodos regionais (TRAVIS, 2011; ZAPPA; MOUSA, 2016; DUMA; SANTANA-DAVILA; MOLINA, 2019; SIDDIQUI; VAQAR; SIDDIQUI, 2023).

Por fim, o carcinoma de células grandes (CCG) é o mais raro dos tipos de NSCLC, representando de 5% a 10% dos casos. Este subtipo é caracterizado pela falta de características morfológicas específicas dos outros carcinomas e, muitas vezes, é diagnosticado por exclusão de outras possibilidades. Os CCGs tendem a ter um prognóstico desfavorável devido à sua agressividade e rápida disseminação. Histologicamente, eles são compostos por células grandes com citoplasma moderado e nucléolos proeminentes, podendo ocorrer em qualquer parte do pulmão (ROSKOSKI, 2017; DUMA; SANTANA-DAVILA; MOLINA, 2019; SIDDIQUI; VAQAR; SIDDIQUI, 2023).

O principal fator de risco para o desenvolvimento do câncer de pulmão é o tabagismo, que é responsável por, aproximadamente, 6 milhões de mortes anuais no mundo, e aproximadamente 147 mil mortes no Brasil, incluindo o câncer (INCA, 2018). Além disso, outros fatores estão associados com a evolução desta doença, dentre eles, os fatores genéticos e ambientais, como exposição à compostos químicos como o asbesto, arsênico, cádmio, hidrocarbonetos, gás mostarda, entre outros, ainda mais quando associados ao hábito de fumar (SUN; SCHILLER; GAZDAR, 2007; DELA CRUZ; TANOUE; MATTHAY, 2011; SIDDIQUI; VAQAR; SIDDIQUI, 2023).

O câncer de pulmão é reconhecido como um dos tipos mais agressivos de câncer, com uma presença significativa em todo o mundo (FERLAY et

al., 2013). No Brasil, no ano de 2020, os tipos de câncer mais comuns relatados incluíram próstata (com 97.278 novos casos), mama (com 88.492 novos casos), colorretal (com 55.102 novos casos), pulmão (com 40.409 novos casos), tireoide (com 30.607 novos casos), estômago (com 20.139 novos casos) e colo do útero (com 17.743 novos casos) (**Figura 3**) (OMS, 2020).

Figura 3: Número estimado de novos casos de câncer em 2020 no Brasil, para ambos os sexos e todas as idades.

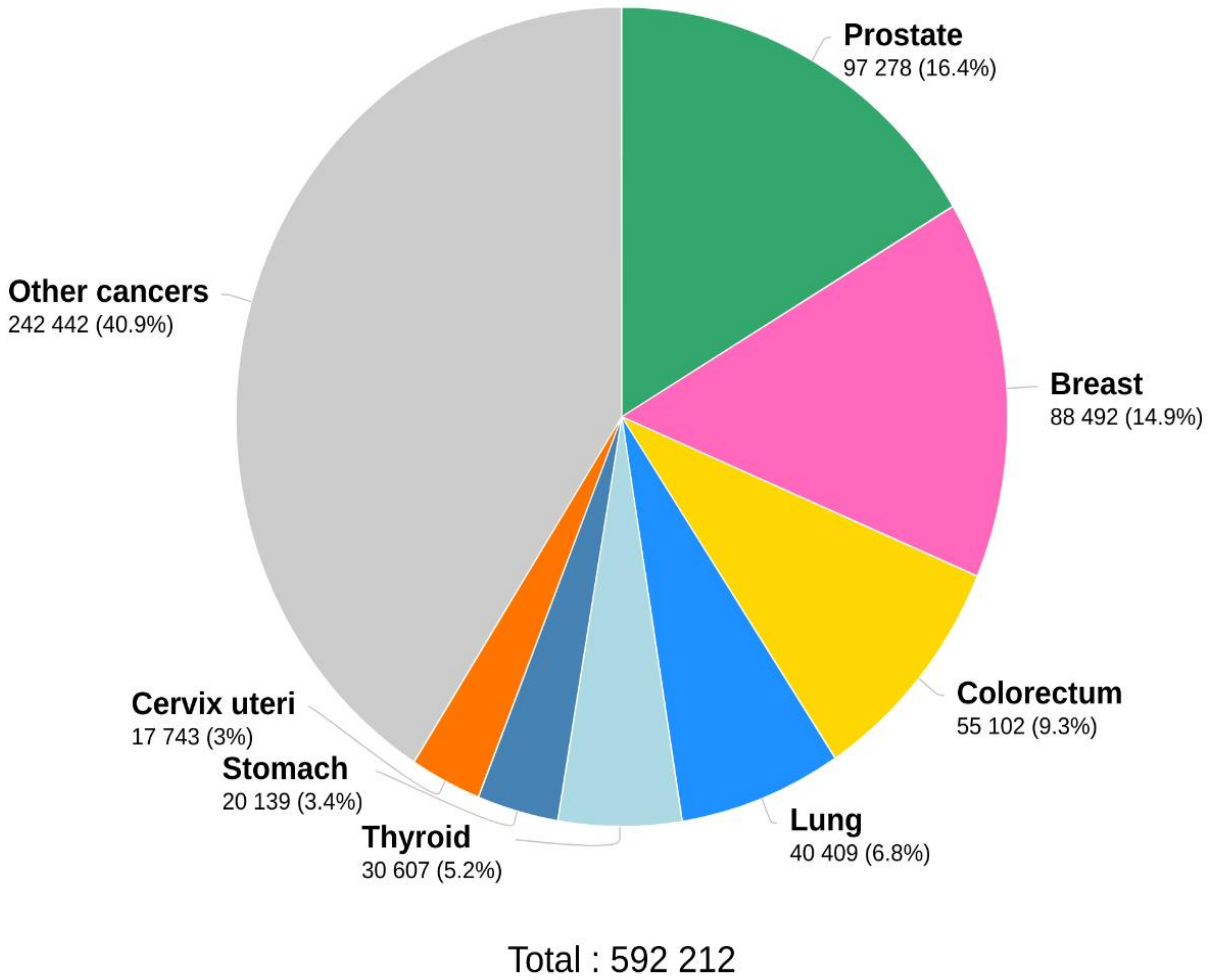

Fonte: Adaptado de OMS (2020).

Quanto às estimativas de mortalidade para o mesmo ano, o câncer de pulmão permaneceu no topo da lista, com 35.160 óbitos, seguido por câncer colorretal (26.170 óbitos), câncer de mama (20.725 óbitos), câncer de próstata (18.345 óbitos), câncer de estômago (15.783 óbitos), câncer de pâncreas (12.911 óbitos) e câncer de fígado (12.139 óbitos) (**Figura 4**) (0MS, 2020).

Figura 4: Número estimado de óbitos em 2020 no Brasil, para ambos os sexos e todas as idades.

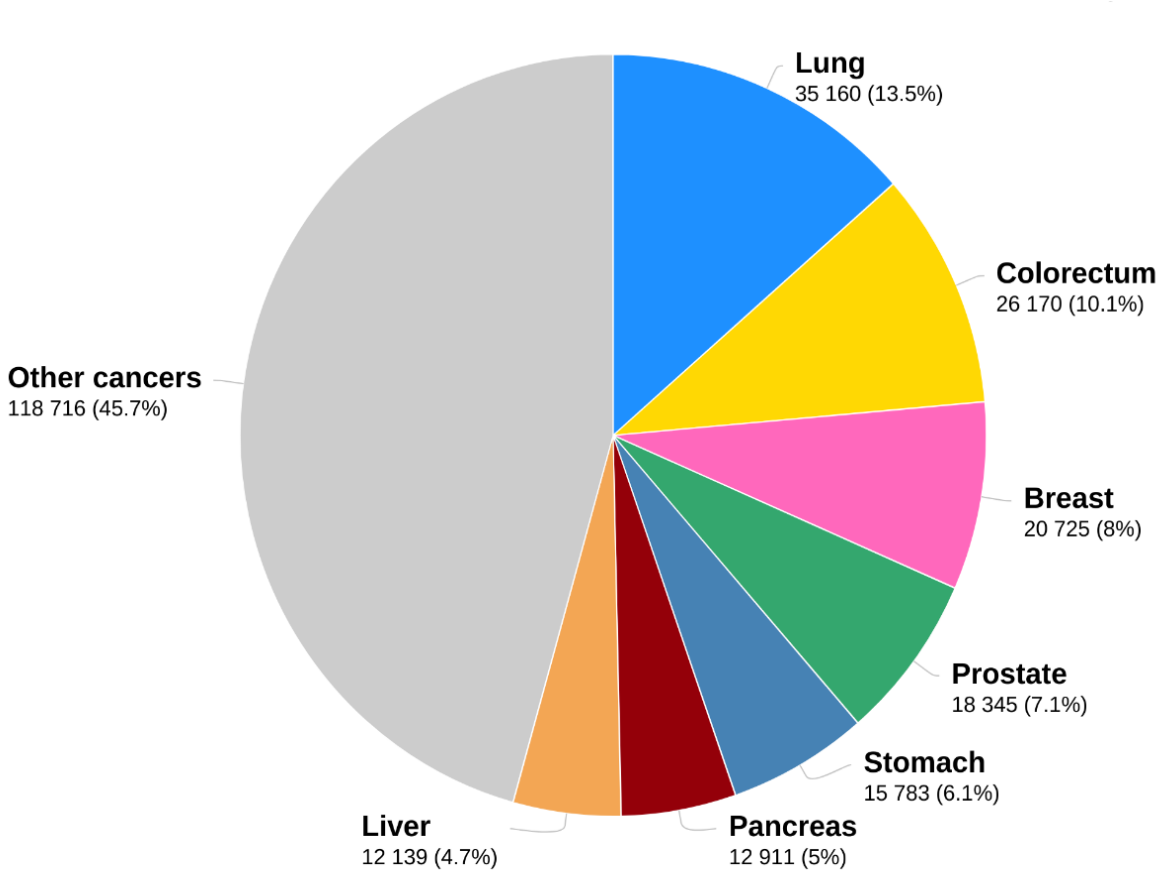

Fonte: Adaptado de OMS (2020).

1.3 PATOGÊNESE DO CÂNCER DE PULMÃO NSCLC

A patogênese do NSCLC envolve uma interação complexa de fatores genéticos, ambientais e moleculares que levam ao desenvolvimento de células cancerígenas nos pulmões. Tais fenômenos resultam na autossuficiência em sinais de crescimento, insensibilidade aos sinais antiproliferativos, evasão de apoptose, potencial replicativo ilimitado devido à ativação da telomerase, invasão tecidual e disseminação em locais distantes (PANOV, 2005; SINGH; KATHIRESAN, 2014). A interferência entre o estresse oxidativo, o estresse metabólico e as principais vias de sinalização, como PI3K (fosfoinositídeo 3-quinase), Akt (proteína quinase B), mTOR (proteína alvo da rifampicina em mamíferos) e NF-κB (fator nuclear-*kappa* B) desempenham um papel significativo na patogênese do câncer de pulmão (WENG et

al., 2019; SANAEI et al., 2022). A seguir será apresentada uma visão geral de como esses fatores se interconectam no contexto do desenvolvimento do câncer de pulmão.

1.3.1 VIA DE SINALIZAÇÃO PI3K/AKT/MTOR E NF-ΚB

A via de sinalização PI3K/Akt/mTOR desempenha papéis cruciais na regulação de processos celulares, incluindo sobrevivência, proliferação, crescimento e metabolismo. Essa via é frequentemente hiperativada em células cancerígenas, contribuindo para a angiogênese, metastátase e resistência a terapias (WENG et al., 2019) A proteína PI3K, classificada em classes I, II e III, é um dímero pertencente à família de lipídios-quinases, e é responsável por fosforilar o grupo 3'-OH dos fosfolipídios do inositol. PI3Ks de classe I consistem em subunidades catalíticas e adaptadoras/reguladoras que formam heterodímeros. PI3Ks de classe II incluem a subclasse IB, ativadas por receptores associados a proteínas G, e as isoformas catalíticas que não possuem subunidades reguladoras e são ativadas por receptores com atividade de tirosina quinase. Enquanto PI3Ks de classe III (PIK3C3) desempenham papel na regulação da fagocitose e autofagia de macrófagos, interagindo com um complexo proteico composto por uma subunidade reguladora e uma subunidade catalítica. Akt é um membro da família da proteína quinase AGC (PKA/PKG/PKC) e consiste em três homólogos (Akt1, Akt2 e Akt3). O mTOR é uma proteína quinase pertencente à família de quinases relacionadas à PI3K, encontrado em complexos como o mTORC1 (composto por mTOR, Raptor, mLST8 e PRAS40) e o mTORC2 (composto por mTOR, Rictor, Sin1 e mLST8) (PORTA; PAGLINO; MOSCA, 2014; ERSAHIN; TUNCBAG; CETIN-ATALAY, 2015; HE et al., 2021).

Os eixos PI3K/Akt e mTOR estão interconectados de tal forma que podem ser considerados como uma única via. A hiperatividade dessa via está associada ao aparecimento e desenvolvimento de tumores (FANG et al., 2020). Alterações nos componentes desse eixo podem contribuir para a progressão do câncer de pulmão, promover a metástase tumoral e desencadear uma série de processos celulares, como sobrevivência, proliferação, migração, metástase, angiogênese, metabolismo celular, senescência celular, integridade genômica e auto-renovação de células-tronco. A Akt está envolvida em processos como apoptose, proliferação, transcrição e migração. Ela desempenha um papel crucial na regulação da progressão do ciclo celular, impedindo a transição da fase G1 para S, entre outros processos (TAN, 2020). Além disso, a via de sinalização PI3K/Akt/mTOR pode afetar

negativamente proteínas epiteliais, como a E-caderina, e positivamente proteínas mesenquimais, como N-caderina, vimentina e β-catenina, através da inibição do homólogo de fosfatase tensina (PTEN). Essas alterações são responsáveis pela indução da transição epitélio-mesenquimal (do inglês, *epithelial-mesenchymal transition*, EMT) (SANAEI et al., 2022), um processo biológico que desempenha papel crítico no desenvolvimento do câncer, pois envolve a transformação de células epiteliais (forte adesão célula a célula e natureza relativamente estacionária) em células semelhantes a mesenquimais (frouxamente conectadas, mais móveis e invasivas), sendo um passo crucial na disseminação metastática do câncer (PÉGLION; ETIENNE-MANNEVILLE, 2012; BUSH et al., 2019; JANISZEWSKA; PRIMI; IZARD, 2020).

A interação entre a via PI3K-Akt-mTOR e o fator de transcrição NF-κB é reconhecida por contribuir para a sobrevivência e proliferação das células de câncer de pulmão (CHEN et al., 2011; WENG et al., 2019). O NF-κB é um fator de transcrição crucial que desempenha um papel fundamental em respostas imunológicas, inflamações, adesão celular, diferenciação, proliferação e apoptose (JOMOVA et al., 2023). Ele existe em várias formas, incluindo NF-κB/p105, NF-κB2/p100, RelA/p65, RelB e c-Rel, que podem formar heterodímeros ou homodímeros e se ligar a sequências consenso de DNA (XIA; SHEN; VERMA, 2014). Sua ativação descontrolada está associada a várias condições patológicas, incluindo câncer. Essa ativação pode ocorrer por meio de vias canônicas e não canônicas, desencadeadas por diferentes estímulos (JOMOVA et al., 2023; REYNAERT et al., 2006).

O NF-κB desempenha um papel crítico na prevenção da apoptose, induzindo a expressão de proteínas antiapoptóticas e suprimindo a apoptose mediada pelo estresse celular através da remoção de espécies reativas de oxigênio (do inglês, *reactive oxygen species* - ROS) e do aumento da expressão da superóxido dismutase de manganês (MnSOD). Assim, o NF-kB inibe a via mitocondrial (intrínseca) e do receptor de morte (extrínseca). Além disso, ele pode regular negativamente a ativação apoptótica de c-Jun N-Terminal quinase (JNK) e antagonizar a ação de p53. A via PI3K/Akt também está envolvida na ativação do NF-κB de maneira dependente de IκB kinase α (IKKα), contribuindo para a sobrevivência das células de câncer de pulmão (WENG et al., 2019; SANAEI et al., 2022). Além disso, alguns fatores de crescimento, como o fator de crescimento epidérmico (EGF), podem ativar o NF-κB independente de IKK, favorecendo o crescimento de células de adenocarcinoma pulmonar de

células não pequenas (CHEN et al., 2011).

1.3.2 ESTRESSE OXIDATIVO

As espécies reativas de oxigênio (ROS) e as espécies reativas de nitrogênio (*reactive nitrogen species* - RNS), conhecidas como RONS, são moléculas altamente reativas que contêm oxigênio e nitrogênio, respectivamente. Elas são produzidas naturalmente no organismo como subprodutos do metabolismo celular e têm papéis importantes em processos biológicos normais, como sinalização celular e resposta imunológica (LIOU; STORZ, 2010; KALUDERCIC; GIORGIO, 2016).

A maioria dos RONS contém elétrons desemparelhados e são denominados radicais livres. Em mamíferos, enzimas especializadas, como NADPH-oxidase, mieloperoxidase e óxido nítrico sintase (do inglês, *nitric oxide sintase* - NOS), desempenham um papel fundamental na geração controlada de RONS no ambiente intra e extracelular, como parte do sistema imunológico inato para combater bactérias. No entanto, a produção excessiva de RONS da origem ao estresse oxidativo, o que pode contribuir para a indução de danos às estruturas biológicas do hospedeiro (LIOU; STORZ, 2010; KALUDERCIC; GIORGIO, 2016).

As ROS podem ser divididas em duas categorias distintas: radicais livres de oxigênio e ROS não radicais. Entre os radicais livres de oxigênio, destacam-se: ânion superóxido ($O_2^{\bullet -}$), hidroxila (•OH), peróxido de hidrogênio (H_2O_2), hipocloreto (HOCl) e compostos carbonílicos altamente reativos derivados de lipídios ou carboidratos. Destes, os radicais superóxido, peróxido de hidrogênio e hidroxila são particularmente estudados em relação ao câncer. As RNS, por sua vez, incluem: óxido nítrico (do inglês, *nitric oxide* - NO•), dióxido de nitrogênio (NO_2^-), peroxinitrito ($ONOO^-$), trióxido de dinitrogênio (N_2O_3) e ácido nitroso (HNO_2), que também contribuem para o estresse oxidativo (WEIDINGER; KOZLOV, 2015; CANTON et al., 2021).

Várias fontes intracelulares de ROS/RNS foram identificadas e estão associadas a diversas patologias. Essas fontes incluem NADPH oxidases, xantina oxidase, óxido nítrico sintase desacoplada (NOS) e mitocôndrias, que em condições patológicas podem contribuir para danos oxidativos em células e tecidos. Em concentrações baixas, RONS desempenham um papel crucial como mediadores regulatórios em processos de sinalização. No entanto, em concentrações moderadas ou elevadas, podem ser prejudiciais para os organismos vivos, inativando moléculas

celulares importantes. Além disso, o aumento excessivo dessas espécies reativas, quando induzido por quimioterápicos, pode resultar na interrupção do ciclo celular, senescência ou morte de células tumorais (MIJATOVIĆ et al., 2020; CANTON et al., 2021).

Espécies reativas de oxigênio são produzidas durante o metabolismo celular aeróbio normal. Cerca de 85–90% do oxigênio (O_2) consumido é metabolizado nas mitocôndrias pela cadeia de transporte de elétrons e os 10–15% restantes são utilizados por diversas enzimas oxidases e oxigenases e por reações químicas de oxidação direta. O oxigênio é reduzido a ânion superóxido ($O_2^{\bullet-}$) por diferentes mecanismos celulares. O superóxido ($O_2^{\bullet-}$) produzido por diversas fontes atua como espécie reativa primária. $O_2^{\bullet-}$ reage rapidamente com o óxido nítrico (NO•) para produzir peroxinitrito ($ONOO^-$) ou é catalisado pela superóxido dismutase (SOD) para produzir peróxido de hidrogênio (H_2O_2). O H_2O_2 pode ser neutralizado pela catalase ou glutationa peroxidase (GSH). No entanto, na presença de íons de metais de transição, como ferro (Fe^{2+}) e cobre (Cu^+), radicais livres hidroxila (OH•) altamente tóxicos podem ser produzidos a partir de H_2O_2 (reação de Fenton). As ROS podem atuar como um segundo mensageiro para ativar o fator nuclear kappa-B (NF-κB), que orquestra um espectro de expressão gênica envolvida na resposta inflamatória e na transcrição de citocinas pró-inflamatórias (COSTA et al., 2018; FUJII; HOMMA; OSAKI, 2022; ANDRÉS et al., 2023) (**Figura 5**).

Figura 5: Vias de ação do $O_2^{\bullet-}$ e $ONOO^-$.

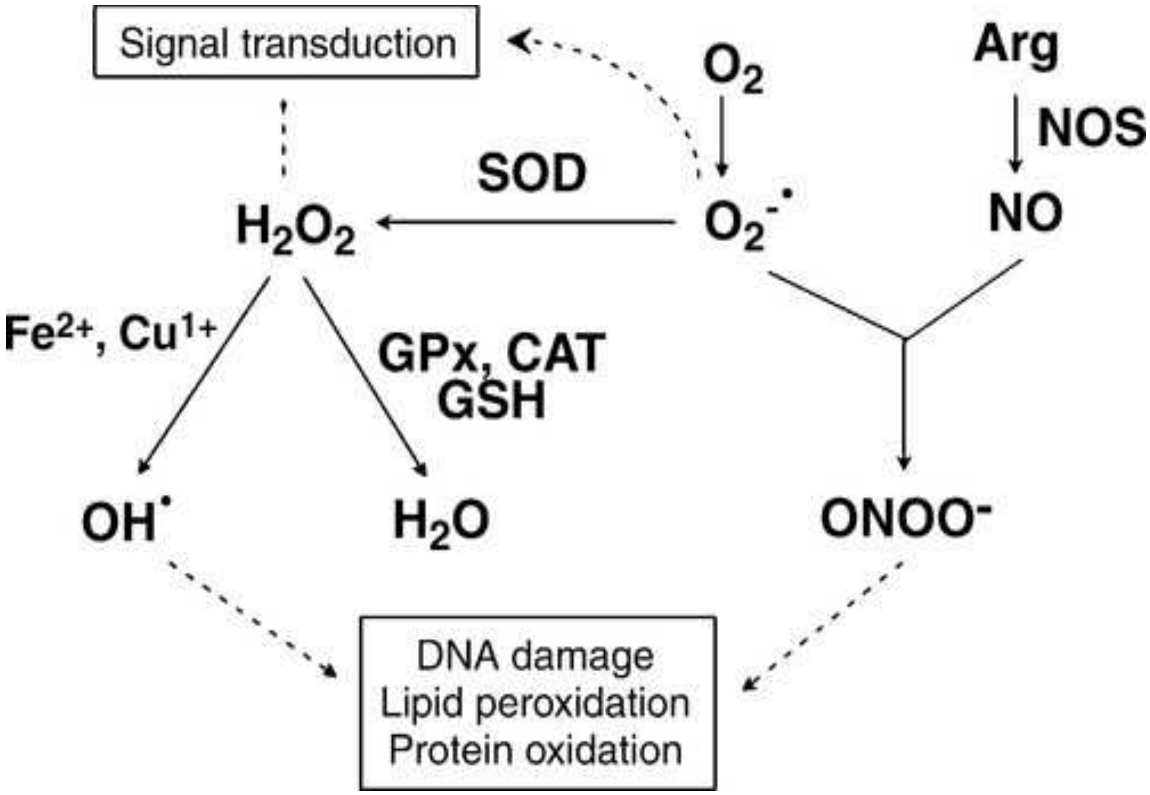

Fonte: BUETLER; KRAUSKOPF; RUEGG (2004).

O óxido nítrico é uma molécula gasosa altamente reativa de vida curta, desempenhando um papel fundamental na regulação de diversos processos fisiológicos e fisiopatológicos. Isso inclui funções vasculares, como angiogênese, controle do fluxo sanguíneo, permeabilidade vascular, interação entre leucócitos e células endoteliais, agregação plaquetária e fluxo microlinfático. Além disso, o NO desempenha um papel importante em funções neurológicas, como neurotransmissão e desenvolvimento do sistema nervoso. Em concentrações elevadas, o NO também tem funções citotóxicas, como a indução de citostase e citólise (FUKUMURA; KASHIWAGI; JAIN, 2006). A produção de NO é mediada por uma família de enzimas chamadas NOS, que incluem três isoformas: NOS neuronal (nNOS/NOS1), NOS endotelial (eNOS/NOS3) e NOS induzível (iNOS/NOS2). A expressão da iNOS é regulada por fatores pró-inflamatórios, como interferon-gama (IFN-γ), interleucina-1β (IL-1β), fator de necrose tumoral-alfa (TNF-α), prostaglandinas, lipopolissacarídeos (LPS) e/ou hipóxia. A produção de NO ocorre por meio da conversão de L-arginina em citrulina, utilizando fosfato de dinucleotídeo de nicotinamida e adenina (NADPH) como cofator (KASHFI; KANNIKAL; NATH, 2021; HUANG et al., 2023).

O NO e seus metabólitos, como nitrito, nitrato, S-nitrosotióis,

nitrosaminas e peroxinitrito, têm papéis importantes nos efeitos citotóxicos e/ou genotóxicos. Eles induzem o estresse oxidativo e nitrosativo, resultando em danos ao DNA, incluindo desaminação nitrosativa de bases de ácidos nucleicos, alquilação e quebra da cadeia de DNA. Além disso, o NO pode inibir enzimas responsáveis pelo reparo do DNA, como alquiltransferase e DNA ligase. Portanto, vários estudos indicaram que o NO pode desencadear e/ou promover o desenvolvimento de tumores (FUKUMURA; KASHIWAGI; JAIN, 2006).

Taxas elevadas de ROS também foram detectadas em quase todos os tipos de câncer, induzindo o desenvolvimento e progressão do tumor. No entanto, as células tumorais também expressam níveis aumentados de proteínas antioxidantes, a fim de desintoxicar ROS, sugerindo que um delicado equilíbrio dos níveis intracelulares é necessário para a função das células cancerígenas (LI et al., 2023).

A homeostase redox celular é um processo essencial e dinâmico que garante o equilíbrio entre as reações de redução e oxidação dentro das células (isto é, ocorre transferência de elétrons de um doador (“agente redutor”) para um aceitador (“agente oxidante”) e regula uma infinidade de respostas e eventos biológicos, incluindo metabolismo, morte celular, diferenciação e desenvolvimento, respostas imunes, ritmo circadiano (TRETTER et al., 2021; LE GAL; SCHMIDT; SAYIN, 2021), manutenção da sobrevivência e função normal das células, sendo estabelecido um equilíbrio entre produção e eliminação de RONS (LENNICKE; COCHEMÉ, 2021; LI et al., 2023). As defesas antioxidantes incluem moléculas enzimáticas e não-enzimáticas, que exercem efeito protetor contra os danos oxidativos, com destaque para a superóxido dismutase e glutationa (BECKER; INDRA, 2023). A superóxido dismutase (SOD) é uma metaloenzima responsável por catalisar a dismutação de duas moléculas de ânion superóxido em peróxido de hidrogênio e oxigênio molecular. Nos mamíferos, existem três formas distintas das quais requerem presença de metal para sua ativação: SOD1 (Cu/ZnSOD) presente no citoplasma; SOD2 (MnSOD) mitocondrial; e SOD3 (Cu/ZnSOD) extracelular. SOD1 é a principal forma intracelular, representando cerca de 80% de SOD total (JOMOVA et al., 2023). A glutationa (GSH), por sua vez, consiste em um antioxidante não-enzimático, composta por aminoácidos (glutamina, cisteína e glicina), responsável pela desintoxicação de radicais livres e xenobióticos. Para realizar essa função, as glutationas peroxidases (GSH-Px) reduzem o peróxido de hidrogênio em água, convertendo GSH em glutationa

dissulfeto (GSSG) (AHMADI; SHADBOORESTAN, 2016).

Embora a perda de GSH, ou uma diminuição na relação glutationa/dissulfeto de glutationa (GSH/GSSG), leve a um aumento da suscetibilidade ao estresse oxidativo e à carcinogênese, níveis elevados de GSH aumentam a capacidade antioxidante de muitas células cancerígenas, aumentando sua resistência ao estresse oxidativo (TRAVERSO et al., 2013). Notavelmente, a inibição desses sistemas antioxidantes induz morte das células tumorais, demonstrando a importância dos sistemas antioxidantes em favorecer a progressão do tumor.

1.3.3 METABOLISMO ENERGÉTICO DA CÉLULA TUMORAL

Tanto células saudáveis como células tumorais contam com as mesmas maquinarias enzimáticas para manter a homeostase celular. Na maioria das células de mamíferos, a glicose é a principal fonte de combustível. A glicose passa por um processo metabólico chamado glicólise, que envolve uma série de reações em várias etapas, culminando na produção de piruvato. Em condições normais de oxigênio, a maior parte desse piruvato é encaminhada para as mitocôndrias, onde passa pelo Ciclo de Krebs, um processo de oxidação que resulta na geração de ATP para suprir as necessidades energéticas da célula (HSU; SABATINI, 2008). Nas células tumorais, as mutações genéticas e as alterações nas interações entre as moléculas estão estreitamente ligadas a modificações complexas no metabolismo energético celular. Isso resulta em uma reprogramação intricada das vias metabólicas que envolvem a glicose, lipídeos e aminoácidos. Essas transformações metabólicas beneficiam o crescimento, a sobrevivência, a capacidade invasiva e o avanço do tumor (PAYEN et al., 2016).

O fenômeno metabólico em questão, denominado "*Efeito Warburg*", é uma notável característica observada em células tumorais que tem sido objeto de extensa pesquisa (LIN et al., 2020). Este fenômeno se manifesta como um aumento substancial na taxa de glicólise aeróbica nas células cancerosas, mesmo quando há presença adequada de oxigênio, uma situação que normalmente estimula o uso de processos metabólicos mais eficientes, como a fosforilação oxidativa (OXPHOS) (LIBERTI; LOCASALE, 2016). A glicólise aeróbica persistente em células tumorais é notável porque contrasta com o comportamento metabólico das células normais, que normalmente utilizam a OXPHOS como principal via para gerar energia na presença de oxigênio adequado (LIN et al., 2020; PAYEN et al., 2015).

Neste contexto, o lactato desempenha um papel fundamental. Durante a glicólise aeróbica, que é o processo metabólico onde a glicose é convertida em piruvato na presença de oxigênio, o piruvato normalmente entra na cadeia de transporte de elétrons e é oxidado na mitocôndria para produzir energia na forma de ATP (KENNEDY et al., 2013). No entanto, nas células tumorais que exibem o *Efeito Warburg*, há uma mudança notável nesse processo. Nas células tumorais afetadas pelo *Efeito Warburg*, o piruvato gerado a partir da glicólise aeróbica não é completamente direcionado para a OXPHOS. Em vez disso, uma parte significativa do piruvato é convertida em lactato por meio da enzima lactato desidrogenase (LDH), mesmo na presença de oxigênio suficiente. Esse processo é conhecido como a fermentação do piruvato para lactato (MARTINEZ-OUTSCHOORN et al., 2016)

A acumulação de lactato nas células tumorais e no ambiente circundante é uma característica distintiva do *Efeito Warburg*. Isso ocorre porque a glicólise aeróbica é um processo menos eficiente em termos de produção de ATP em comparação com a OXPHOS, mas fornece uma vantagem metabólica para as células cancerosas ao permitir uma produção mais rápida de ATP e intermediários metabólicos que podem ser usados para a biossíntese de macromoléculas necessárias para o rápido crescimento e proliferação das células tumorais. A acumulação de lactato também tem implicações no ambiente tumoral, criando um ambiente ácido que pode promover a invasão e metástase das células cancerosas, além de desencadear respostas imunossupressoras (AKRAM, 2013; VAZQUEZ et al., 2010).

A compreensão detalhada do *Efeito Warburg* e suas implicações nas células tumorais é de grande importância na pesquisa sobre câncer, uma vez que essa adaptação metabólica singular é vista como uma estratégia central para atender às demandas bioenergéticas e biosintéticas das células de câncer, contribuindo para a sua proliferação descontrolada. A investigação contínua desse fenômeno metabólico tem o potencial de levar a abordagens terapêuticas inovadoras no tratamento do câncer.

1.3.4 Principais Tipos de Morte Celular

A morte celular é um processo biológico fundamental que ocorre tanto em situações normais quanto patológicas. No contexto do câncer, as células conseguem evitar os mecanismos indutores de morte celular e promover o

crescimento descontrolado, bem como, manter a sobrevivência dessas células aberrantes. Existem vários tipos de morte celular, cada um com características e mecanismos distintos (**Figura 6**).

Figura 6: Tipos de morte celular e suas características gerais.

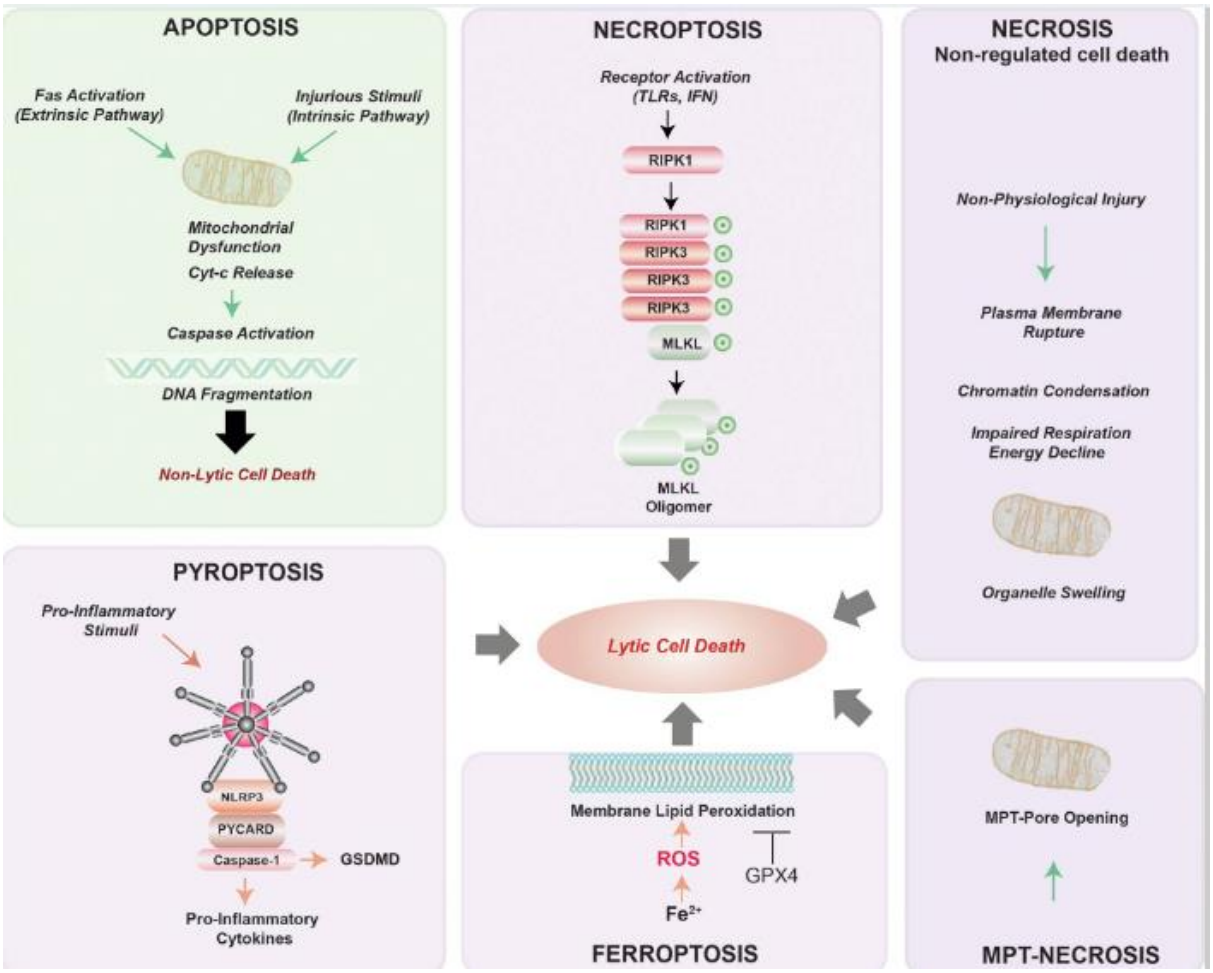

Fonte: CHOI et al. (2019).

1.3.4.1 AUTOFAGIA

A autofagia é um mecanismo intracelular de degradação no qual proteínas e organelas são encapsuladas em vesículas especializadas e posteriormente decompostas por enzimas lisossomais. Esse processo tem como objetivo a reciclagem de componentes celulares e a provisão de nutrientes essenciais para a célula. Em situações normais, a autofagia ocorre em níveis basais, desempenhando um papel fundamental na manutenção da homeostase celular. No entanto, em resposta ao estresse celular, como a falta de nutrientes, hipóxia, estresse

no retículo endoplasmático, estresse oxidativo ou exposição a substâncias tóxicas, a autofagia é ativada como uma via pró-sobrevivência, impedindo a morte celular (YUN; LEE, 2018; MULCAHY LEVY; THORBURN, 2020; LIM; MOHAMAD HANIF; CHIN, 2021).

Existem três tipos principais de autofagia que resultam na degradação lisossomal: Macroautofagia (ou simplesmente autofagia): caracterizada pela formação de autofagossomos, que são vacúolos de membrana dupla capazes de capturar proteínas citoplasmáticas, mitocôndrias, retículo endoplasmático e ribossomos. Esses autofagossomos, uma vez fundidos com lisossomos, formam os autofagolisossomos, onde ocorre a degradação das substâncias encapsuladas. Os produtos de degradação resultantes, como aminoácidos, nucleotídeos, ácidos graxos e açúcares, são reciclados para sustentar o metabolismo celular. Microautofagia: nesse tipo, o material citoplasmático é diretamente incorporado pelo lisossomo, sem a formação de vesículas de membrana dupla. Autofagia mediada por chaperonas: neste caso, proteínas específicas são translocadas através da membrana lisossomal e subsequentemente desdobradas e degradadas no interior do lisossomo (YUN; LEE, 2018; LIM; MOHAMAD HANIF; CHIN, 2021; MULCAHY LEVY; THORBURN, 2020).

A influência da autofagia no desenvolvimento de tumores ainda não está completamente esclarecida, pois pode desempenhar papéis contraditórios. Por um lado, a autofagia pode promover a sobrevivência das células tumorais, fornecendo nutrientes essenciais durante o estresse e permitindo a resistência à quimioterapia. Por outro lado, a autofagia pode suprimir o desenvolvimento de tumores, eliminando células de câncer que não podem passar pelo processo apoptótico. Além disso, em alguns casos, bloquear a autofagia pode ser necessário para manter o fenótipo maligno de certas células de câncer. Em resumo, a autofagia desempenha um papel complexo no contexto do câncer, fornecendo uma vantagem de sobrevivência às células tumorais em algumas situações, enquanto suprime o desenvolvimento tumoral em outras (YUN; LEE, 2018; LIM; MOHAMAD HANIF; CHIN, 2021; MULCAHY LEVY; THORBURN, 2020).

1.3.4.2 MORTE CELULAR PROGRAMADA - APOPTOSE

A morte celular pode ocorrer através de um processo ativo e regulado, conhecido como morte celular programada, ou de um curso passivo e descontrolado.

Devido às dramáticas diferenças morfológicas desses dois tipos de morte celular, eles foram originalmente denominados em apoptose e necrose, respectivamente.

A apoptose ou morte celular programada é um processo fisiológico que promove de maneira eficaz a remoção de células em excesso ou danificadas, sem a geração de resposta inflamatória, garantindo assim a homeostase do tecido. A apoptose é o principal tipo de morte celular que ocorre quando o dano ao DNA é irreparável e pode ser ativada de duas maneiras, pela via intrínseca ou mitocondrial e pela via extrínseca ou do receptor de morte. A via intrínseca é desencadeada pela perda do potencial de membrana mitocondrial, pelo seu rompimento decorrentes de danos no DNA causados por agentes citotóxicos, privação de fator de crescimento e privação de citocinas o que resulta na liberação do citocromo C no citoplasma. A via extrínseca é mediada por receptores transmembranares, chamados de receptores de morte, que são membros da superfamília do gene do receptor do fator de necrose tumoral (TNF) produzidos por células T citotóxicas do sistema imunológico em resposta a células danificadas ou infectadas. Os caminhos convergem nas caspases executoras (PFEFFER; SINGH, 2018; CARNEIRO; EL-DEIRY, 2020; CHAUDHRY et al., 2022) (**Figura 7**).

Figura 7: Vias de apoptose.

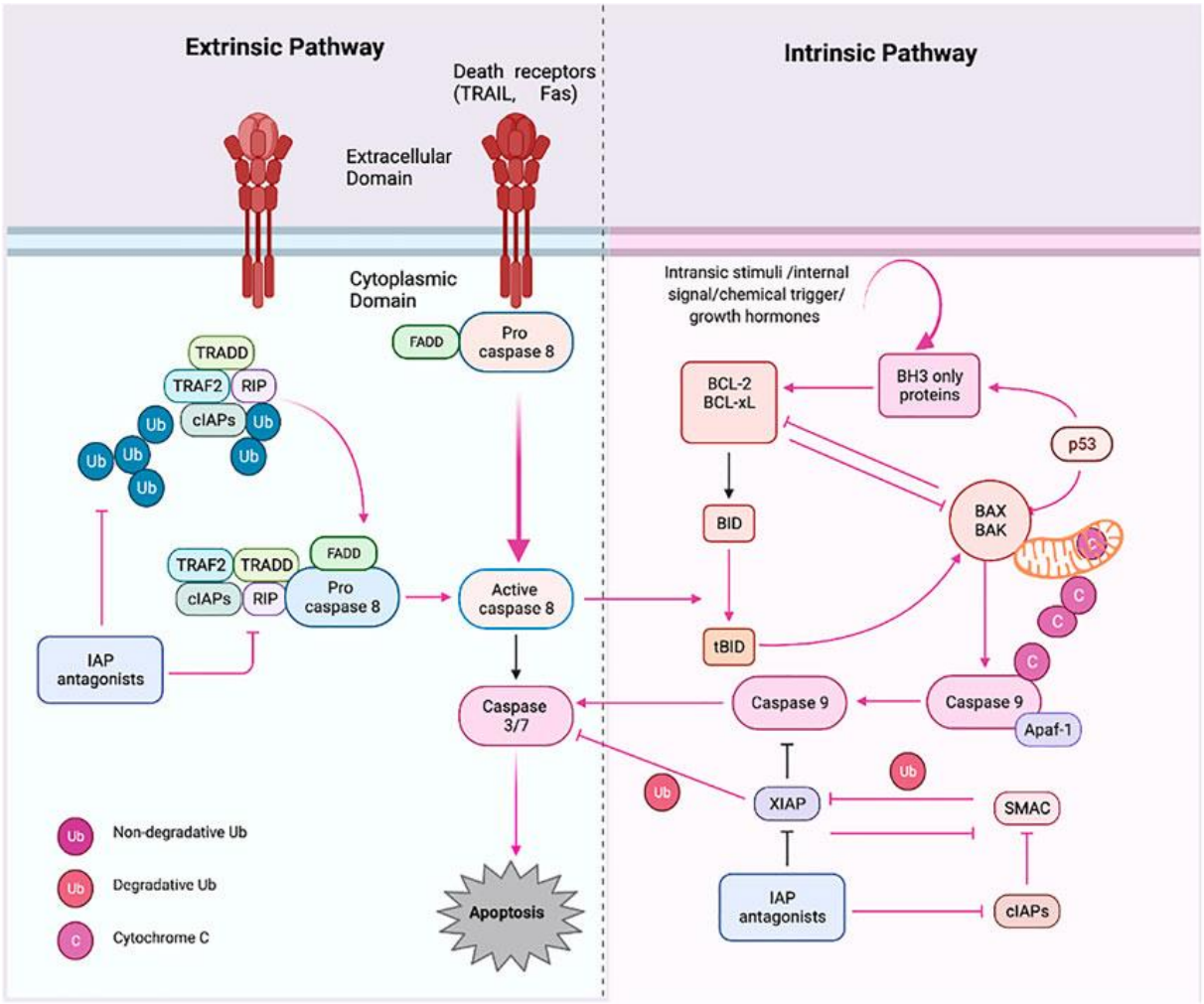

Fonte: CHAUDHRY et al. (2022), criado com BioRender.com. A apoptose tem duas vias principais conhecidas como i) via extrínseca e ii) intrínseca. Primeiro, estímulos externos ou moléculas ligantes ativam a transdução, incluindo receptores de morte, levando à ativação da caspase 3/7 ou 8. Via intrínseca; através da inserção de moléculas pró-apoptóticas BAX (proteína) na membrana mitocondrial resulta na geração de citocromo c, formando um apoptossomo, que desencadeia ainda mais as cascatas apoptóticas começando com a ativação pró-apoptótica da caspase 9 e ou então da caspase 3.

Assim que a apoptose é sinalizada, mudanças começam a ocorrer dentro da célula. Estas alterações incluem a ativação de caspases que clivam componentes celulares necessários para a função celular normal, tais como proteínas do citoesqueleto e nucleares. Como resultado da atividade das caspases, as células apoptóticas começam a encolher e sofrem alterações na membrana plasmática que sinalizam a resposta dos macrófagos. A apoptose é realizada por caspases (proteases específicas da cisteína aspartil), que são uma classe de proteínas cisteínas que clivam proteínas alvo. A atividade da caspase protease é essencial para o sucesso da

apoptose, pois clivam centenas de várias proteínas. Existem quatro caspases iniciadoras (caspase-2, -8, -9, 10) e três caspases executoras (caspase-3, -6, -7). As caspases executoras clivam as proteínas alvo, o que eventualmente leva à morte da célula. As vias são altamente reguladas, de modo que a apoptose só ocorrerá se for sinalizada. A via intrínseca, em particular, é regulada pela família de proteínas do linfoma-2 de células B (BCL-2), que inclui proteínas efetoras pró-apoptóticas, proteínas pró-apoptóticas BH3 e proteínas BCL-2 anti-apoptóticas. As proteínas antiapoptóticas BCL-2 inibem a apoptose através da inibição das proteínas BCL-2 pró-apoptóticas, proteína X associada a BCL-2 (BAX) e antagonista homólogo BCL-2 (BAK). As proteínas BH3 inibem as proteínas antiapoptóticas BCL-2 (PFEFFER; SINGH, 2018; CARNEIRO; EL-DEIRY, 2020; CHAUDHRY et al., 2022).

O termo apoptose descreve um processo de morte celular, cujas alterações incluem arredondamento da célula, redução do volume celular (picnose), formação de bolhas na membrana plasmática (*blebbing*), perda de adesão celular, condensação nuclear e, por fim, fagocitose por macrófagos residentes sem desencadear inflamação. As alterações moleculares observadas neste processo correspondem à exposição de fosftidilserina, fragmentação oligonucleossomal de DNA, ativação de caspases, perda do potencial de membrana mitocondrial com manutenção da integridade da membrana plasmática (PFEFFER; SINGH, 2018; CARNEIRO; EL-DEIRY, 2020; CHAUDHRY et al., 2022).

A desregulação da apoptose é um fenômeno encontrado em uma ampla variedade de doenças. Evidências acumuladas mostraram que a expressão anormal de alguns fatores regulatórios da apoptose pode levar ao câncer, indicando as intrincadas relações entre apoptose e câncer, como por exemplo, a molécula Bcl-2, a qual é super expressa em muitos tipos de células cancerígenas e o seu aumento ainda conduz a resistência a fármacos quimioterapêuticos e terapia de radiação (PFEFFER; SINGH, 2018; CARNEIRO; EL-DEIRY, 2020; CHAUDHRY et al., 2022). Portanto, a regulação da apoptose padrão poderia beneficiar o tratamento e a prevenção do câncer.

1.3.4.3 MORTE CELULAR PROGRAMADA – PIROPTOSE

A piroptose, uma forma de morte celular programada, é uma via recentemente identificada de morte celular que é estimulada por uma série de infecções microbianas (por exemplo, *Salmonella*, *Francisella* e *Legionella*) e estímulos

não infecciosos, incluindo fatores do hospedeiro produzidos durante o enfarte do miocárdio. É um processo inflamatório altamente regulado que desempenha um papel crucial na defesa do organismo contra infecções. Quando as células imunológicas detectam sinais de infecção, elas podem desencadear piroptose nas células infectadas para eliminar o patógeno (BERGSBAKEN; FINK; COOKSON, 2009; TAN et al., 2021; ZHENG et al., 2021; YU et al., 2021).

A piroptose é morfológica e mecanicamente distinta de outras formas de morte celular. O início da piroptose começa com o reconhecimento de uma ameaça, que pode ser um patógeno intracelular (por exemplo, bactérias ou vírus) ou sinais de estresse celular. Vários receptores de reconhecimento de padrões (RRPs) na superfície ou dentro da célula, incluindo receptores do tipo *Toll* (TLRs) e receptores do tipo Nod (NLRs), podem detectar a presença da ameaça. Em resposta à ameaça, RRPs específicos podem ativar um complexo proteico denominado inflamassoma. Uma vez ativado o inflamassoma, ele leva à ativação da caspase-1, uma enzima protease mediadora chave na via da piroptose. A caspase-1, cliva as proteínas gasdermina, particularmente gasdermina-D (GSDMD). As gasderminas ativadas sofrem uma mudança conformacional, expondo seu domínio N-terminal, formando poros na membrana celular. Esses poros permitem que íons e fluidos entrem na célula e perturbem o equilíbrio osmótico, levando ao inchaço celular e, por fim, à ruptura da membrana. Esta ruptura leva à liberação de conteúdos celulares, incluindo citocinas pró-inflamatórias, como interleucina-1 beta (IL-1β) e interleucina-18 (IL-18), no ambiente extracelular. Essas citocinas ativam respostas imunológicas e atraem células do sistema imune para o local da infecção ou dano celular. Este processo ajuda a conter a infecção (BERGSBAKEN; FINK; COOKSON, 2009; TAN et al., 2021; ZHENG et al., 2021; YU et al., 2021).

Este processo contrasta com a apoptose, onde as células encolhem e se fragmentam em corpos apoptóticos que são silenciosamente engolidos por células vizinhas ou fagócitos.

1.3.4.4 MORTE CELULAR PROGRAMADA - NECROPTOSE

A necroptose é uma forma de morte celular programada que compartilha características tanto com a apoptose quanto com a necrose (morte celular não programada). É um processo altamente regulado que pode ser iniciado sob

condições específicas e desempenha um papel em vários contextos fisiológicos e patológicos (DHURIYA; SHARMA, 2018; CHOI et al., 2019).

A necroptose é iniciada quando as células recebem sinais que normalmente desencadeariam a apoptose, mas a apoptose é inibida ou bloqueada. Isto pode ocorrer em resposta a certos receptores de morte, infecções virais ou estresse celular. O processo começa com a ativação de receptores de superfície celular, como os receptores do fator de necrose tumoral (TNF). Esses receptores podem ativar uma cascata de sinalização que inclui proteínas como a proteína quinase 1 de interação com o receptor (RIPK1) e a proteína quinase 3 de interação com o receptor (RIPK3). O complexo de sinalização do receptor ativado forma uma estrutura conhecida como necrossoma, que inclui RIPK1 e RIPK3. O necrossoma é um dos principais impulsionadores da necroptose (DHURIYA; SHARMA, 2018; CHOI et al., 2019).

Dentro do necrossoma, o RIPK3 fosforila a pseudoquinase semelhante ao domínio da quinase de linhagem mista (MLKL), uma molécula efetora chave na necroptose. O MLKL ativado e fosforilado transloca-se para a membrana celular e forma poros, perturbando a integridade da membrana plasmática. Isso leva à perda da integridade da membrana, fazendo com que a célula inche e se rompa. À medida que ocorre o rompimento, o conteúdo celular, incluindo moléculas pró-inflamatórias e padrões moleculares associados a danos (DAMPs), é liberado no espaço extracelular, o que pode resultar na ativação de respostas imunológicas e contribuir para a inflamação no tecido circundante (DHURIYA; SHARMA, 2018; CHOI et al., 2019).

1.3.4.5 MORTE CELULAR NÃO-PROGRAMADA - NECROSE

O processo de morte celular por necrose ocorre em resposta a muitos tipos de danos, como trauma, infarto, toxinas, e, portanto, é normalmente o resultado de um processo patológico. Por este motivo, a necrose foi considerada morte celular quase "acidental", um processo aleatório e descontrolado (ELMORE, 2007; JABOIN; HWANG; LU, 2009; LIU et al., 2017).

O processo necrótico por muitos anos era anteriormente considerado uma morte celular catastrófica e desordenada, caracterizado por integridade da membrana plasmática comprometida, inchaço das organelas celulares, degradação aleatória do DNA e liberação descontrolada de moléculas inflamatórias. Estudos realizados na última década descobriram que a necrose pode ocorrer de forma

regulada e inclui vários mecanismos de morte celular conhecidos como necroptose, ocitose, ferroptose, NETose, pironecrose e piroptose. Esses mecanismos de morte celular têm sido empregados para explicar uma variedade de necroses observadas *in vivo* em diversas situações patológicas. Ainda assim, se a necrose tumoral é regulada através destes mecanismos e como a necrose se desenvolve no desenvolvimento do tumor permanecem em grande parte obscuros (LIU; JIAO, 2020; YEE; LI, 2021).

As principais alterações morfológicas que ocorrem no processo de necrose incluem inchaço celular, formação de vacúolos citoplasmáticos, retículo endoplasmático distendido, formação de bolhas citoplasmáticas, mitocôndrias condensadas, inchadas ou rompidas, desagregação e desprendimento dos ribossomos, membranas de organelas rompidas, lisossomas inchados e rompidos, e, finalmente, a ruptura da membrana celular. Essa perda de integridade da membrana celular resulta na liberação do conteúdo citoplasmático no tecido circundante, enviando sinais quimiotáticos com eventual recrutamento de células inflamatórias. Além disso, a inflamação local subsequente induzida pela necrose pode promover o crescimento do tumor e correlaciona-se com mau prognóstico em tumores sólidos (KARSCH-BLUMAN et al., 2019).

Em resumo, o estresse oxidativo, o estresse metabólico e a desregulação das vias de sinalização como PI3K/AKT e NF-κB são processos interligados que contribuem para a patogênese do câncer de pulmão. O estresse oxidativo pode levar a danos no DNA e à disfunção mitocondrial, enquanto o metabolismo alterado, particularmente o *efeito Warburg*, fornece às células cancerígenas a energia e os suprimentos necessários para o crescimento descontrolado. A via PI3K/AKT é frequentemente hiperativada no câncer de pulmão e desempenha um papel fundamental na regulação do metabolismo, sobrevivência e proliferação celular. O NF-κB, associado à inflamação e à sobrevivência celular, também interage com essas vias, promovendo ainda mais o desenvolvimento e progressão do câncer de pulmão. A evasão ou escape da morte celular proporciona as células de câncer capacidade de resistir ou evitar os mecanismos normais de morte celular que normalmente eliminariam células danificadas ou prejudiciais do corpo, contribuindo para o crescimento descontrolado e a sobrevivência das células cancerígenas. A compreensão dessas interações complexas pode fornecer insights sobre potenciais alvos terapêuticos para o tratamento do câncer de pulmão.

1.4 TRATAMENTO

O câncer de pulmão de células não pequenas é considerado uma doença heterogênea. Em vista disso, seu tratamento deve ser realizado de acordo com a condição clínica do paciente (*performance status*), estágio da doença, tipo histológico e perfil molecular. De maneira geral, o NSCLC pode ser classificado em ressecável, localmente avançado e avançado, desta forma, o tratamento pode envolver cirurgia, radiação e quimioterapia, separados ou em combinação, dos quais visam a remoção ou destruição das células tumorais, sem afetar células normais. Em tumores ressecáveis, a ressecção cirúrgica é considerada a opção mais eficaz, no entanto, em tumores de estágio avançado e irressecáveis, é necessária combinação de radiação e quimioterapia (CHAFT et al., 2021). Recentemente, a imunoterapia tem sido amplamente avaliada, envolvendo inibidores de checkpoints imunológicos anti-antígeno 4 de linfócito T citotóxico (anti-CTLA-4) e anti-proteína de morte celular programada 1 (anti-PD-1) (STEVEN; FISHER; ROBINSON, 2016; ONOI et al., 2020).

O quimioterápico de primeira escolha para NSCLC consiste na cisplatina (*cis*-diaminodicloroplatina-II) (CDDP), composto organometálico a base de platina. A CDDP liga-se ao DNA genômico (gDNA) ou mitocondrial (mtDNA) através da formação de adutos, e consequentemente, induz distorção da dupla hélice e bloqueio da replicação e transcrição, interferindo nos mecanismos de reparo e levando a morte celular (RANASINGHE; MATHAI; ZULLI, 2022). Inicialmente, o influxo de CDDP nas células ocorre através de difusão passiva ou por meio da proteína transportadora de cobre (CTR1). Dentro das células, ocorre processo de adequação da cisplatina, no qual grupos de cloreto são substituídos por moléculas de água, sendo capaz de reagir com componentes de membrana, citoplasmáticos e DNA.

Compostos à base de platina hidratados, como a cisplatina, são conhecidos por sua capacidade de reagir com o átomo de nitrogênio na posição 7 (N7) das purinas, que são uma das duas principais classes de bases nitrogenadas encontradas no DNA (a outra classe é a das pirimidinas). As purinas incluem adenina e guanina, que são componentes essenciais das moléculas de DNA. A cisplatina, portanto, quando presente no ambiente celular, pode formar ligações covalentes com o átomo N7 das purinas no DNA e induzir ligações cruzadas intracadeias, entre duas purinas adjacentes (1,2 ou 1,3), ou formar ligações intercadeias, entre duas bases de fitas opostas de DNA. A ligação CDDP-DNA pode desencadear mecanismos de reparo por excisão de nucleotídeos (NER, do inglês, *nucleotide excision repair*)

permitindo a sobrevivência da célula, no entanto, proteínas HMG (do inglês, *high mobility group*) são capazes de proteger do processo de reparo, induzindo parada do ciclo celular. Além do dano ao DNA, a citotoxicidade da cisplatina pode ser induzida através de estresse oxidativo, regulação positiva de p53, ativação de proteína quinase ativada por mitógeno (MAPK), e consequente morte por apoptose (DASARI; BERNARD TCHOUNWOU, 2014; GHOSH, 2019).

Os danos induzidos pela cisplatina nas células cancerígenas podem, no entanto, desencadear mecanismos de quimiorresistência, como é o caso de células não pequenas de câncer pulmão, das quais ativam processos que removem ou reparam as lesões do DNA. Assim, a ligação cisplatina-DNA ativa vias de reparo NER, levando ao reconhecimento, desenrolamento e remoção de adutos, ou ainda pode ocorrer correção de bases mal pareadas através da ativação de proteínas de reparo de incompatibilidade (MMR, do inglês, *mismatch repair*) (ROCHA et al., 2018). Além disso, uma vez que o influxo de cisplatina depende de transportadores, a redução da expressão de CTR1 ou rápida degradação pode resultar em sua menor disponibilidade intracelular. A superexpressão de transportadores da família ABC (MRP2) também pode favorecer a quimiorresistência, aumentando a liberação de cisplatina das células (AMABLE, 2016). A CDDP em sua forma adequada é capaz de reagir com diversas proteínas, incluindo a enzima GSH, que pode servir como sistema de desintoxicação, removendo a cisplatina intracelular. Por fim, sabe-se que a exposição contínua a cisplatina também é capaz de promover anormalidades nas diferentes vias ativadas, induzindo capacidade antiapoptótica e quimiorresistência, assim, a inativação da via MAPK, por exemplo, pode favorecer a sobrevivência celular (CHEN; CHANG, 2019).

A quimioterapia a base de CDDP também é reconhecida por induzir uma série de efeitos adversos. Dentre os principais efeitos consiste a nefrotoxicidade, desencadeando lesão renal aguda e perda de função, devido ao seu acúmulo em células tubulares, inflamação e lesão vascular. A ototoxicidade é outro efeito bem conhecido induzido por cisplatina, no qual leva a perda auditiva neurossensorial bilateral, progressiva e irreversível, muitas vezes associada a vertigem e zumbido. Isso ocorre devido ao estresse oxidativo, inflamação e morte celular das células presentes no ouvido interno (GHOSH, 2019).

1.5 Produtos Naturais Como Alternativa Terapêutica para o Câncer de Pulmão

Ao longo da história, os produtos naturais desempenharam um papel dominante no tratamento de doenças humanas. Por exemplo, a lendária descoberta da penicilina por Alexander Fleming, em 1928, transformou a existência global, pois antes da sua introdução não existia tratamento eficaz para diversas infecções. Outro medicamento, o ácido salicílico, que foi derivado de uma planta medicinal, deu origem ao ácido acetilsalicílico (AAS; conhecido como aspirina) em 1897, através do trabalho de Felix Hoffman. O AAS foi considerado uma "droga milagrosa" por suas notáveis propriedades medicinais (SNEADER, 2000; MINER; HOFFHINES, 2007; AMERICAN CHEMICAL SOCIETY, 2023).

Atualmente, os produtos naturais constituem uma grande parte dos agentes farmacêuticos atuais e são amplamente reconhecidos como fontes abundantes de compostos bioativos com potencial terapêutico. Nos últimos anos, tem havido esforços significativos para isolar novos produtos naturais de microrganismos e plantas terrestres e aquáticas a fim de avaliar suas propriedades biológicas em várias doenças, incluindo o câncer (ATANASOV et al., 2021; HASHEM et al., 2022; HUANG; LU; DING, 2021). Pesquisas recentes revelaram que 32% de todos os medicamentos de moléculas pequenas aprovados entre janeiro de 1981 e setembro de 2019 eram produtos naturais e seus derivados (NEWMAN; CRAGG, 2020).

Uma das fontes mais importantes de compostos biologicamente ativos é o reino vegetal. Atualmente, existem mais de 350.000 espécies de plantas vasculares registradas no mundo, e novas espécies são adicionadas a cada ano.

As plantas podem ser usadas terapeuticamente em diversas formas, como chá, onde várias partes das plantas, incluindo folhas, flores, caules e raízes, são mergulhadas em água quente para criar infusões que podem ser consumidas como bebidas para aliviar doenças comuns, como problemas digestivos, estresse, insônia e até mesmo por fornecer efeitos antioxidantes e anti-inflamatórios; corantes, os quais podem ser frequentemente derivados de raízes, folhas ou frutos de certas plantas e têm sido usados para diversas aplicações terapêuticas e cosméticas, como no caso da cúrcuma, um corante amarelo-laranja, usada na medicina por suas propriedades anti-inflamatórias e antioxidantes e henna, usada na coloração capilar, esmaltes e maquiagens; e extratos, onde as plantas são processadas para extrair compostos bioativos específicos (BRUDZYŃSKA; SIONKOWSKA; GRISEL, 2021; SINGH, Tripti

et al., 2023). Além disso, seus compostos ativos podem ser isolados e utilizados como medicamentos ou como precursores de drogas sintéticas e semissintéticas. Existe uma grande lista de fitoquímicos (ou seja, compostos químicos produzidos por plantas) com atividade terapêutica, incluindo alcaloides, óleos essenciais, flavonoides, carotenoides, terpenos e compostos fenólicos. Esses compostos têm sido objeto de investigação extensa devido à sua segurança, à acessibilidade, à aplicabilidade e à redução da citotoxicidade (HASHEM et al., 2022).

De maneira geral, esses compostos podem ser usados para quimioprevenção e quimioterapia, pois atingem várias vias de sinalização, impactando assim a atividade molecular das células, interferindo na iniciação, desenvolvimento e progressão do câncer e modulando diversos mecanismos. Entre os mecanismos principais encontrados, tem-se a supressão da proliferação celular, regulação do ciclo e interferência em diversas vias de sinalização tumorigênica, como fosfoinositídeo 3-quinase (PI3K), metaloproteinase de matriz (MMP), MAPK/ERK conhecida como a via Ras-Raf-MEK-ERK, via do receptor toll-like (TLR) e via AKT. Além disso, os produtos naturais podem estimular mecanismos de reparo do DNA através da ação dos produtos dos genes p21, p27, p51 e/ou p53, como as proteínas Bax, Bak e Bid, que causam a síntese de enzimas protetoras, como as caspases 3, 7, 8, 9, 10, 12 e modula enzimas antioxidantes como GST, GSH e GPx, bem como apoptose, angiogênese e metástase (NAEEM et al., 2022). Consequentemente, eles podem ser usados como potenciais adjuvantes na terapia do câncer (**Figure 8**).

Figura 8: Importância dos produtos naturais na inibição das várias vias de sinalização que servem como impulsionadores da carcinogênese.

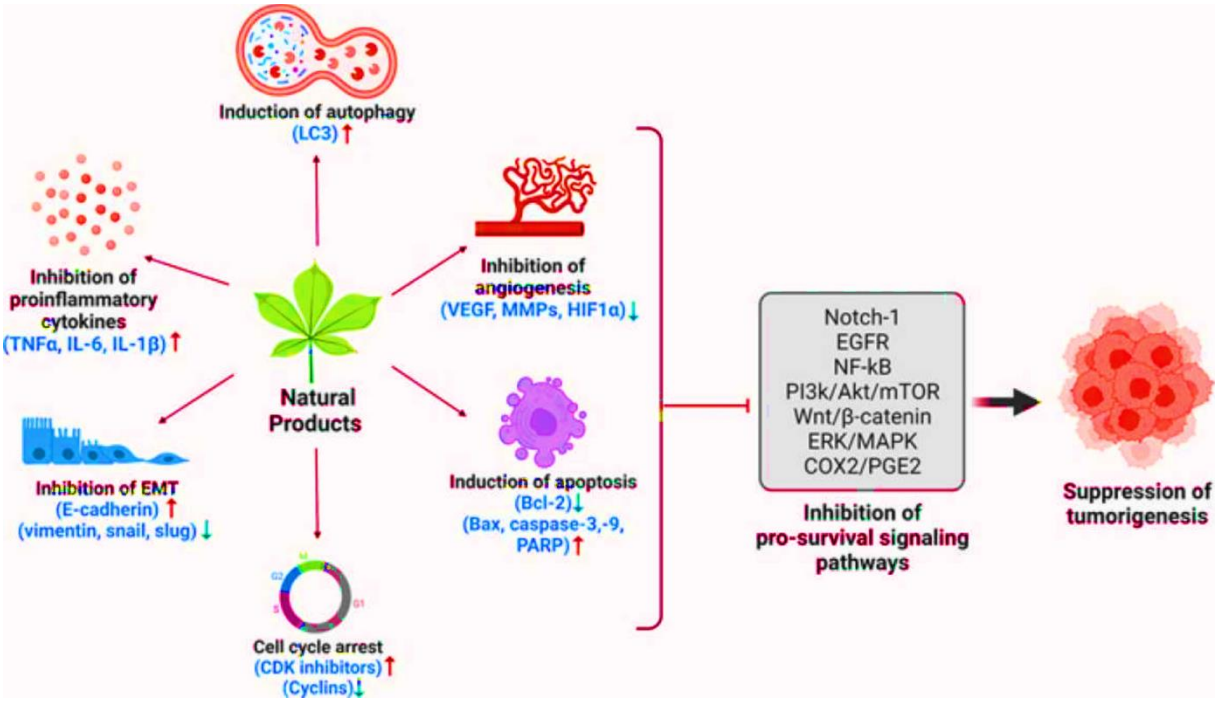

Fonte: HASHEM et al. (2022).

De acordo com a Food and Drug Administration (FDA), foram aprovados cerca de 300 medicamentos quimioterápicos para o tratamento do câncer, incluindo taxol, vinca e seus derivados, análogos de platina, 5-fluorouracil, bevacizumabe, erlotinibe, nivolumabe, ipilimumabe, sunitinibe e olaparibe, com outras combinações diferentes de medicamentos quimioterápicos (PATRIDGE et al., 2016). No entanto, a maioria deles é altamente tóxica e induz resistência, o que acaba resultando em recorrência tumoral e metástase, limitando suas atividades anticancerígenas devido ao desenvolvimento de resistência adaptativa por células tumorais direcionadas e toxicidades não específicas para células normais (NAEEM et al., 2022). Portanto, são necessárias alternativas melhores, mais seguras e mais eficazes para ter uma atividade anticancerígena mais proeminente e superar a quimiorresistência encontrada no câncer de pulmão.

1.5.1 3,3',5,5'-TETRAMETOXIBIFENIL-4,4'-DIOL (TMBP)

Compostos fenólicos são encontrados naturalmente em plantas, mas a obtenção de compostos dessa classe também pode ser alcançada por diferentes metodologias de sínteses. A biocatálise é uma metodologia baseada no uso de enzimas para a transformação estrutural de moléculas. Neste processo ocorre a síntese de moléculas estruturalmente diversas através da utilização de lacases.

As lacases são enzimas polifenol oxidases, que podem ser obtidas a partir de fungos, plantas, insetos e bactérias (CANNATELLI; RAGAUSKAS, 2017; WAN; DU; MIYAKOSHI, 2008). Estas enzimas oxidam uma extensa variedade de compostos fenólicos, promovendo a formação de derivados que podem apresentar propriedades bioativas potencializadas em relação aos substratos de origem (CANNATELLI; RAGAUSKAS, 2017; MOGHARABI; FARAMARZI, 2014). A oxidação do ácido ferúlico catalisada por lacase levou a formação de derivados fenólicos com maior atividade antioxidanteade (ADELAKUN et al., 2012). Na oxidação do 2,6-dimetoxifenol catalisada por lacases, o composto bifenólico formado, TMBP, apresentou potencial antioxidante superior ao substrato (ADELAKUN et al., 2012; SCHIRMANN et al., 2019).

Os compostos fenólicos têm sido extensivamente estudados quanto às suas atividades biológicas, inclusive como agentes anticâncer (ABOTALEB et al., 2020). Nesse sentido, os compostos bifenílicos, constituídos por dois anéis de benzeno unidos ligados através de suas posições 1,1′, são considerados um importante intermediário na química orgânica que constitui a porção estrutural de muitos compostos apresentando diversas atividades farmacológicas, como antiinflamatória, diurética, anti-diabética e antimicrobiana (JAIN; GIDE; KANKATE, 2017).

O bifenil, 3,3',5,5'-tetrametoxibifenil-4,4'-diol (TMBP), é um composto fenólico, que foi obtido através da oxidação do 2,6-dimetoxifenol (do inglês, *2,6-DMP*) utilizando a enzima lacase produzida pelo fungo ascomicetos *Botryosphaeria rhodina* MAMB-05 (SCHIRMANN et al., 2018, 2019). Do ponto de vista estrutural, o TMBP é composto por dois anéis aromáticos, duas hidroxilas e quatro grupos metoxilas (RIZWANUL FATTAH et al., 2014), conferindo à molécula propriedades antioxidantes (**Figura 9**) (FOTI et al., 2005; RICE-EVANS; MILLER; PAGANGA, 1996; SCHIRMANN et al., 2018, 2019; SOARES, 2002). O TMBP foi descrito como um antioxidante com potencial para inibir processos oxidativos e influência estabilizadora no biodiesel de soja (FOTI et al., 2005; SCHIRMANN et al., 2018, 2019).

Figura 9: Estrutura química bidimensional do 3,3’,5,5’-tetrametoxibifenil-4,4’-diol (TMBP).

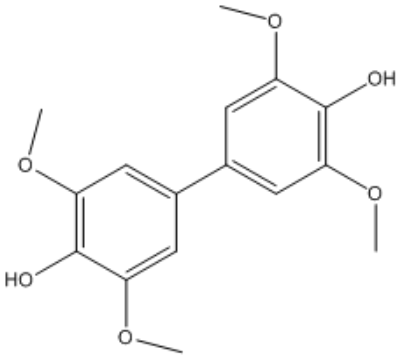

Fonte: O próprio autor.

No estudo realisado por nosso grupo de pesquisa foi relatado que o tratamento com TMBP sobre a linhagem celular A549 de câncer de pulmão foi capaz de reduzir a viabilidade celular, por ação citotóxica e promover a redução do tamanho celular. Posteriormente, descobrimos que o tratamento com TMBP aumentou ROS, causando despolarização mitocondrial e aumento de gotículas lipídicas. O tratamento também foi capaz de promover a parada do ciclo celular na fase G2/M e induzir a morte por apoptose direta. Além disso, o tratamento com TMBP sobre as células primárias, como macrófagos peritoneais e eritrócitos de ovelhas não causou toxicidade. Assim, este estudo revelou que o TMBP poderia ser um candidato promissor para o desenvolvimento de medicamentos antitumorais direcionados ao câncer de pulmão (Concato et al. 2020).

No trabalho de Schirmann et al. (2023), os autores mostraram pela primeira vez a atividade biológica do TMBP contra as formas promastigotas e amastigotas de *L. amazonensis* utilizando diferentes abordagens experimentais. O tratamento com TMBP inibiu a proliferação e induziu a morte de formas promastigotas gerando ERO e disfunção mitocondrial. Nas amastigotas intracelulares, o TMBP reduziu a porcentagem de macrófagos infectados, sendo 62,7 vezes mais seletivo ao parasita. O TMBP não hemolisou eritrócitos de ovelhas; indicativo de baixa citotoxicidade. Além disso, análise de docking molecular em dois alvos enzimáticos de *L. amazonensis*: tripanotiona redutase (TR) e leishmanolisina (Gp63), sugeriram que o grupo hidroxila poderia ser um grupo farmacofórico devido à sua afinidade de ligação por ligações de hidrogênio com resíduos no sítio ativo de ambas as enzimas. O TMBP foi mais seletivo ao alvo Gp63 do que o TR. Dessa forma, torna-se promissor para atuar como agente anti-*Leishmania*.

Os efeitos antiproliferativos e indutores de apoptose de outro composto bifenílico, viz., 2,4,3',4'-tetrametoxibifenil, também relataram apoptose agindo através de uma via mitocondrial/caspase em células MGC-803 de câncer gástrico humano (SUI et al., 2014).

1.5.2 TRILOBOLIDO-6-*O*-ISOBUTIRATO (TBB)

As lactonas sesquiterpênicas (LS) são um grupo grande e diversificado de produtos naturais presentes em mais de 100 famílias de plantas. Entre eles o maior número de SLs é derivado da família Compositae (Asteraceae), com mais de 3.000 estruturas relatadas. Uma das plantas medicinais importantes desta família, é a *Sphagneticola trilobata* (L.) J.F. Pruski (HUANG; JIANG; OOI, 2003; ZHANG et al., 2016).

S. trilobata, também conhecida popularmente como “pseudo-arnica”, “margaridão”, “pingo-de-ouro”, “picão-da-praia” ou apenas “Wedelia”, pertence à família de plantas Asteraceae e tem sido um recurso medicinal tradicional na Índia, China, Caribe e Américas Central e do Sul (MARDINA et al., 2020). Apesar da sua classificação como erva daninha invasora, esta planta medicinal destaca-se pela sua elevada diversidade molecular e pela sua diversificada atividade biológica que engloba antibacteriana (SHANKAR; THOMAS, 2014), antifúngica (HUSAIN; SRIVASTAVA, 2018), antiplasmodial (SRAVYA et al., 2011), atividades antidiabética, hepatoprotetora, antipirético-analgésica e anticancerígena (MARDINA et al., 2020).

Os principais constituintes químicos de *S. trilobata* são os diterpenos ent-kaurano, lactonas sesquiterpênicas eudesmane e triterpenos (HUI et al., 2019). Investigações recentes demonstraram o potencial terapêutico das lactonas sesquiterpênicas (SLs), especialmente no domínio da pesquisa do câncer (DHYANI et al., 2022; DONG; QIAN; LI, 2022; SHOAIB et al., 2017). Entre estes está o trilobolido-6-*O*-isobutirato (TBB), fórmula molecular $C_{23}H_{32}O_9$ (**Figura 10**), uma notável lactona sesquiterpênica natural extraída de *S. trilobata* (Bohlmann et al., 1981). O TBB é construído a partir da fusão de dois anéis ciclohexano e um anel de lactona. Este último anel contém oxigênio com função carbonila, e é o grupo mais responsável por efeitos biológicos, como tratamento de tumor, e redução da pressão arterial em humanos (FERREIRA et al., 1994; HUANG; JIANG; OOI, 2003).

Figura 10. Representação bidimensional da estrutura química do trilobolido-6-*O*-isobutirato (TBB).

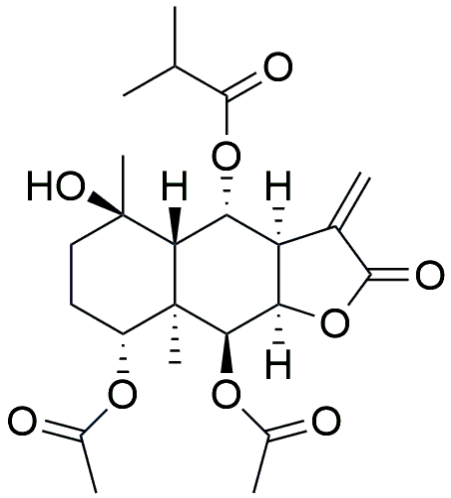

Fonte: O próprio autor.

A lipofilicidade também foi considerada um aspecto importante na atividade das LS, potencialmente devido à maior permeabilidade da membrana, permitindo que os sesquiterpenos atinjam células e núcleos onde exercem seus principais efeitos. Outras funções biológicas de grande relevância, como antimicrobiana, anti-herbicidas, antioxidante, antimalárica, imunomodulador e até mesmo anti-metástase são também descritas (CHADWICK et al., 2013; GHANTOUS et al., 2010; MERFORT, 2011; TOPPO et al., 2013)

No trabalho de Guzman et al., (2005) observaram que as LS partenolídeo induziu apoptose em células estaminais e progenitoras de leucemia mielóide aguda humana. Uma das principais razões para isto é que LS tem preferência por Fe (II), o qual é sequestrado em altas concentrações em células cancerígenas e o partenolídeo é clivado a oxidantes citotóxicos em contato com Fe (II) que danificam as células tumorais próximas. Além disso, foi constatado que o partenolídeo sensibiliza as células tumorais a medicamentos contra o câncer, como tamoxifeno paclitaxel, além do TNF e, consequentemente, promove a morte celular quando aplicado em níveis baixos o suficiente para não ser tóxico (CHADWICK et al., 2013; REN; YU; KINGHORN, 2016.)

LS ainda possuem a capacidade de inibir a expressão de NF-κB, proteína que medeia a resposta imune em humanos, controlando a resposta de outros efetores, como citocinas, moléculas inflamatórias e moléculas de adesão celular, além de regular mais de 150 genes inflamatórios, sendo alguns responsáveis pela proliferação celular (CHADWICK et al., 2013; GHANTOUS et al., 2010; MERFORT,

2011)

Em relação ao TBB, uma recente investigação *in vitro* utilizando TBB, isolado de *S. trilobata,* contra as linhagens de células tumorais de hepatocarcinoma humano: HuH7, HepG2, SK-Hep1 e Bel7402, descobriu-se que o tratamento inibiu o crescimento e a formação de colônias em um tempo- e forma dependente da concentração. O tratamento com TBB exibiu efeitos inibitórios sobre a migração, invasão e glicólise, culminando em última análise na paragem do ciclo celular na fase G2 / M, disfunção mitocondrial e morte celular induzida por apoptose. Além disso, o TBB também foi capaz de regular a expressão de genes essenciais associados à proliferação, migração e metástase como PCNA (antígeno nuclear de células em proliferação), Ki67, Ciclina B1, Ciclina E, Bax, Bcl2, MMP2/9 (metaloproteinase 2/9) e PGK1 (fosfoglicerato quinase 1), principalmente através da inibição dos transdutores de interleucina-6/sinal e ativadores da via de sinalização da transcrição-3 (IL-6/STAT3). A eficácia *in vivo* dos atributos anticancerígenos do TBB foi validada através de experimentação com um modelo de tumor xenoenxertado em camundongos nus BALB/c machos, onde o TBB foi eficaz na eliminação do crescimento tumoral (peso e volume) sem causar toxicidade aos animais experimentais (ZHOU et al., 2021).

1.6 MODELO EXPERIMENTAL *IN VITRO*

Um modelo experimental *in vitro* refere-se a um ambiente controlado e artificial onde experimentos são conduzidos usando células, tecidos ou componentes biológicos isolados fora de seu contexto natural, normalmente em um ambiente de laboratório. O termo "*in vitro*" significa "*em vidro*" em latim, refletindo o uso histórico de recipientes de vidro para tais experimentos (KATT et al., 2016; COSTA et al., 2020; MARTINEZ-PACHECO; O'DRISCOLL, 2021).

Os modelos *in vitro* são representações simplificadas de processos biológicos em comparação com modelos *in vivo* (em um organismo vivo). Os pesquisadores podem isolar elementos específicos e focar em aspectos específicos de um sistema biológico, como sinalização celular, expressão genética ou testes de drogas. Neste modelo experimental, as variáveis externas são minimizadas ou controladas, podem ser facilmente reproduzidos, aumentando a confiabilidade e validade dos resultados. Além disso, são comumente usados em pesquisas farmacêuticas para testar a segurança e eficácia de novos medicamentos ou terapias,

o que permite a triagem inicial antes de avançar para estudos *in vivo* de maior complexidade, além de ser crucial na investigação do câncer para decifrar mecanismos moleculares de eventos-chave, como crescimento tumoral, metástase, resistência a medicamentos e aspectos de evasão imunológica (KATT et al., 2016; COSTA et al., 2020; MARTINEZ-PACHECO; O'DRISCOLL, 2021).

No entanto, este modelo experimental possui algumas desvantagens. Apresentam limitações por não replicarem totalmente a complexidade dos sistemas biológicos nos organismos vivos e os resultados precisam ser validados em modelos *in vivo* para garantir a sua relevância para situações da vida real (KATT et al., 2016; COSTA et al., 2020; MARTINEZ-PACHECO; O'DRISCOLL, 2021).

2 JUSTIFICATIVA

A atual quimioterapia para o câncer não é satisfatória devido à alta toxicidade dos fármacos utilizados, tais como toxicidade gastrointestinal, nefrotoxicidade, neurotoxicidade, ototoxicidade, hipersensibilidade e mielossupressão. Além disso, os pacientes continuam a apresentar recorrência da doença e resistência aos medicamentos durante o curso da terapia à base de platina, o que reduz a eficácia do tratamento do NSCLC. Sabendo da importância desta doença e de suas complicações anatomofisiológicas, a busca por novas alternativas para o tratamento do câncer é necessária.

Uma série de estudos tem demonstrado o efeito anticâncer de compostos isolados naturais e sintéticos e seus múltiplos mecanismos de ação em experimentos *in vitro* e *in vivo*. Esses compostos são capazes de atuar nas células tumorais através de vias importantes relacionadas a proliferação, invasão, metástase e de morte celular.

Esses achados nos encorajaram a investigar o potencial anticâncer do bifenil TMBP e da lactona sesquiterpênica TBB, por diferentes mecanismos de ação, sobre linhagens tumorais de câncer de pulmão (A549 e NCI-H460) que ainda não foram relatados na literatura.

3 OBJETIVOS

3.1 Objetivo Geral

Avaliar *in vitro* a atividade antiproliferativa dos compostos 3,3',5,5'-tetrametoxibifenil-4,4'-diol (TMBP) e trilobolido-6-*O*-isobutirato (TBB) sobre as

linhagens tumorais de câncer de pulmão, A549 (adenocarcinoma pulmonar) e NCI-H460 (carcinoma de células grandes), bem como elucidar os principais mecanismos de ação e propriedades metabólicas envolvidas.

3.1.1 Objetivos específicos

- Efetuar o estudo *in silico* da estrutura de TBB quanto às regras de Lipinski e Veber e das propriedades de ADME;
- Avaliar *in vitro* a viabilidade do TBB sobre as linhagens epiteliais, monocitos e macrófagos alveolares;
- Avaliar *in vitro* a viabilidade hemolítica do TMBP em eritrócitos extraídos de carneiro;
- Determinar as concentrações de TBB e TMBP capazes de inibir o crescimento das linhagens tumorais A549 e NCI-H460;
- Determinar a concentração inibitória (IC_{50}) das linhagens normais e tumorais de TBB e TMBP e índice de seletividade tumoral para TBB;
- Analisar os aspectos morfológicos das células tumorais após o tratamento com TBB e TMBP;
- Avaliar parâmetros relacionados ao perfil redox e metabólico das células tumorais após o tratamento com TBB e TMBP;
- Avaliar se o tratamento com TBB e TMBP alteram a capacidade migratória das células tumorais;
- Analisar se o TMBP é capaz de interferir na regulação do ciclo celular e caracterizar os mecanismos de morte envolvidos durante a ação dos tratamentos com TBB e TMBP sob as células tumorais;
- Analisar as proteínas PI3K, AKT, Pakt, ARG-1, iNOS, NF-Kb, pNF-Kb e Nrf2 após o tratamento com TMBP;

REFERÊNCIAS

ABOTALEB, M. et al. Therapeutic Potential of Plant Phenolic Acids in the Treatment of Cancer. **Biomolecules**, v. 10, n. 2, 1 fev. 2020.

ADELAKUN, O. E. et al. Laccase-catalyzed dimerization of ferulic acid amplifies antioxidant activity. **Journal of Molecular Catalysis B: Enzymatic**, v. 74, n. 1–2, p. 29–35, jan. 2012.

AHMADI, A.; SHADBOORESTAN, A. Oxidative stress and cancer; the role of hesperidin, a citrus natural bioflavonoid, as a cancer chemoprotective agent. **Nutrition and cancer**, v. 68, n. 1, p. 29–39, 2 jan. 2016.

AKRAM, M. Mini-review on glycolysis and cancer. **Journal of Cancer Education**, v. 28, n. 3, p. 454–457, 1 set. 2013.

AMABLE, L. Cisplatin resistance and opportunities for precision medicine. **Pharmacological research**, v. 106, p. 27–36, 1 abr. 2016.

AMERICAN CHEMICAL SOCIETY. **Discovery and Development of Penicillin**. Disponível em: <https://www.acs.org/education/whatischemistry/landmarks/flemingpenicillin.html>. Acesso em: 16 out. 2023.

ANDRÉS, C. M. C. et al. Superoxide Anion Chemistry—Its Role at the Core of the Innate Immunity. **International Journal of Molecular Sciences**, v. 24, n. 3, 1 fev. 2023.

ATANASOV, A. G. et al. Natural products in drug discovery: advances and opportunities. **Nature Reviews Drug Discovery**, v. 20, n. 3, p. 200–216, 28 jan. 2021.

BALDOTTO, C. et al. Mutações drivers em câncer de pulmão não-pequenas células (CPNPC). **Pulmão RJ**, v. 25, n. 2, p. 23–28, 2016.

BECKER, A. L.; INDRA, A. K. Oxidative Stress in Melanoma: Beneficial Antioxidant and Pro-Oxidant Therapeutic Strategies. **Cancers**, v. 15, n. 11, 1 jun. 2023.

BERGSBAKEN, T.; FINK, S.L.; COOKSON, B.T. Pyroptosis: host cell death and inflammation. **Nature reviews. Microbiology**, v. 7, n. 2, p. 99–109, 2009.

BRUDZYŃSKA, P.; SIONKOWSKA, A.; GRISEL, M. Plant-Derived Colorants for Food, Cosmetic and Textile Industries: A Review. **Materials**, v. 14, n. 13, 1 jul. 2021.

BUETLER, T. M.; KRAUSKOPF, A.; RUEGG, U. T. Role of superoxide as a signaling molecule. **News in Physiological Sciences**, v. 19, n. 3, p. 120–123, jun. 2004.

CANNATELLI, M. D.; RAGAUSKAS, A. J. Two Decades of Laccases: Advancing Sustainability in the Chemical Industry. **Chemical record,** v. 17, n. 1, p. 122–140, 1 jan. 2017.

CANTON, M. et al. Reactive Oxygen Species in Macrophages: Sources and Targets. **Frontiers in Immunology**, v. 12, p. 734229, 30 set. 2021.

CARNEIRO, B. A.; EL-DEIRY, W. S. Targeting apoptosis in cancer therapy. **Nature reviews. Clinical oncology**, v. 17, n. 7, p. 395–417, 1 jul. 2020.

CHADWICK, M. et al. Sesquiterpenoids Lactones: Benefits to Plants and People. **International Journal of Molecular Sciences**, v. 14, n. 6, p. 12780, jun. 2013.

CHAUDHRY, G. E. S. et al. Cancer and apoptosis: The apoptotic activity of plant and marine natural products and their potential as targeted cancer therapeutics. **Frontiers in Pharmacology**, v. 13, p. 842376, 10 ago. 2022.

CHAFT, J.E. et al. Evolution of systemic therapy for stages I-III non-metastatic non-small-cell lung cancer. **Nature reviews. Clinical oncology**, v. 18, n. 9, p. 547–557, 1 set. 2021.

CHEN, W. et al. NF-kappaB in lung cancer, a carcinogenesis mediator and a prevention and therapy target. **Frontiers in bioscience**, v. 16, n. 3, p. 1172–1185, 1 jan. 2011.

CHEN, S.H.; CHANG, J.Y. New Insights into Mechanisms of Cisplatin Resistance: From Tumor Cell to Microenvironment. **International journal of molecular sciences**, v. 20, n. 17, 1 set. 2019.

CHOI, M. E. et al. Necroptosis: a crucial pathogenic mediator of human disease. **JCI insight**, v. 4, n. 15, 8 ago. 2019.

CLARK, S. B.; ALSUBAIT, S. Non–Small Cell Lung Cancer. **StatPearls**, 5 set. 2022.

CONCATO, V. M. et al. 3,3′,5,5′-tetramethoxybiphenyl-4,4′diol induces cell cycle arrest in G2/M phase and apoptosis in human non-small cell lung cancer A549 cells. **Chemico-Biological Interactions**, v. 326, n. March, p. 109133, 2020.

COSTA, N. T. et al. Influence of disease-modifying antirheumatic drugs on oxidative and nitrosative stress in patients with rheumatoid arthritis. **Inflammopharmacology**, v. 26, n. 5, p. 1151–1164, 1 out. 2018.

COSTA, E. et al. Experimental Models as Refined Translational Tools for Breast Cancer Research. **Scientia Pharmaceutica**, v. 88, n. 3, p. 32, 31 jul. 2020.

DASARI, S.; BERNARD TCHOUNWOU, P. Cisplatin in cancer therapy: molecular mechanisms of action. **European journal of pharmacology**, v. 740, p. 364, 10 out. 2014.

DE VISSER, K. E.; JOYCE, J. A. The evolving tumor microenvironment: From cancer initiation to metastatic outgrowth. **Cancer cell**, v. 41, n. 3, p. 374–403, 13 mar. 2023.

DELA CRUZ, C. S.; TANOUE, L. T.; MATTHAY, R. A. Lung Cancer: Epidemiology, Etiology, and Prevention. **Clinics in Chest Medicine**, v. 32, n. 4, p. 605–644, dez. 2011.

DHYANI, P. et al. Sesquiterpenoid lactones as potential anti-cancer agents: an update on molecular mechanisms and recent studies. **Cancer Cell International**, v. 22, n. 1, p. 1–18, 7 out. 2022.

DHURIYA, Y. K.; SHARMA, D. Necroptosis: a regulated inflammatory mode of cell death. **Journal of Neuroinflammation**, v. 15, n. 1, p. 1–9, 6 jul. 2018.

DONG, Y.; QIAN, X.; LI, J. Sesquiterpene Lactones and Cancer: New Insight into Antitumor and Anti-inflammatory Effects of Parthenolide-Derived Dimethylaminomicheliolide and Micheliolide. **Computational and Mathematical Methods in Medicine**, v. 2022, 2022.

DUMA, N.; SANTANA-DAVILA, R.; MOLINA, J. R. Non-Small Cell Lung Cancer: Epidemiology, Screening, Diagnosis, and Treatment. **Mayo Clinic proceedings**, v. 94, n. 8, p. 1623–1640, 1 ago. 2019.

ELMORE, S. Apoptosis: A Review of Programmed Cell Death. **Toxicologic Pathology**. v. 35, n. 4, p. 495-516, 25 jun. 2007

ERSAHIN, T.; TUNCBAG, N.; CETIN-ATALAY, R. The PI3K/AKT/mTOR interactive pathway. **Molecular BioSystems**, v. 11, n. 7, p. 1946–1954, 16 jun. 2015.

FANG, W. et al. PI3K-AKT-mTOR pathway alterations in advanced NSCLC patients after progression on EGFR-TKI and clinical response to EGFR-TKI plus everolimus combination therapy. **Translational Lung Cancer Research**, v. 9, n. 4, p. 1258–1267, 1 ago. 2020.

FERREIRA, D. et al. Eudesmanolide Lactones From *Wedelia Paludosa*. **Natural Product Letters**, v. 4, n. 1, p. 1–7, 1 fev. 1994.

FOTI, P. et al. Comparison between daidzein and genistein antioxidant activity in primary and cancer lymphocytes. **Archives of Biochemistry and Biophysics**, v. 433, n. 2, p. 421–427, 15 jan. 2005.

FUJII, J.; HOMMA, T.; OSAKI, T. Superoxide Radicals in the Execution of Cell Death. **Antioxidants**, v. 11, n. 3, p. 501, 4 mar. 2022.

FUKUMURA, D.; KASHIWAGI, S.; JAIN, R. K. The role of nitric oxide in tumour progression. **Nature Reviews Cancer**, v. 6, n. 7, p. 521–534, jul. 2006.

GAZDAR, A. F. Should we continue to use the term non-small-cell lung cancer? **Annals of Oncology**, v. 21, n. Suppl 7, p. vii225, out. 2010.

GHANTOUS, A. et al. What made sesquiterpene lactones reach cancer clinical trials? **Drug discovery today**, v. 15, n. 15–16, p. 668–678, ago. 2010.

GHOSH, Sumit. Cisplatin: The first metal based anticancer drug. **Bioorganic chemistry**, v. 88, 1 jul. 2019.

GUZMAN, M. L. et al. The sesquiterpene lactone parthenolide induces apoptosis of human acute myelogenous leukemia stem and progenitor cells. **Blood**, v. 105, n. 11, p. 4163, 6 jun. 2005.

HAHN, W. C.; WEINBERG, R. A. Modelling the molecular circuitry of cancer. **Nature reviews. Cancer**, v. 2, n. 5, p. 331–341, 2002.

HANAHAN, D.; WEINBERG, R. A. Hallmarks of Cancer: The Next Generation. **Cell**, v. 144, n. 5, p. 646–674, 4 mar. 2011.

HASHEM, S. et al. Targeting cancer signaling pathways by natural products: Exploring promising anti-cancer agents. **Biomedicine & Pharmacotherapy**, v. 150, p. 113054–113054, 30 abr. 2022.

HE, Y. et al. Targeting PI3K/Akt signal transduction for cancer therapy. **Signal Transduction and Targeted Therapy**, v. 6, n. 1, p. 1–17, 16 dez. 2021.

HSU, P. P.; SABATINI, D. M. Cancer cell metabolism: Warburg and beyond. **Cell**, v. 134, n. 5, p. 703–707, 5 set. 2008.

HUANG, M.; LU, J. J.; DING, J. Natural Products in Cancer Therapy: Past, Present and Future. **Natural products and bioprospecting**, v. 11, n. 1, p. 5–13, 1 fev. 2021.

HUANG, X. S.; JIANG, R. W.; OOI, V. E. C. Trilobolide-6-O-isobutyrate, a eudesmanolide from Wedelia trilobata. **Acta Crystallographica Section E: Structure Reports Online**, v. 59, n. 6, jun. 2003.

HUANG, Y. et al. Nitric oxide and thyroid carcinoma: A review. **Frontiers in Endocrinology**, v. 13, p. 1050656, 9 jan. 2023.

HUI, Y. et al. Chemical Constituents of the Flowers of *Wedelia trilobata*. **Chemistry of Natural Compounds**, v. 55, n. 1, p. 160–163, 15 jan. 2019.

HUSAIN, N.; SRIVASTAVA, D. K. Phytochemical Analysis of Leaf of Wedeliatrilobata, Achyranthesaspera and Chrysanthemum from the Twin–City (Durg & Bhilai), Chhattisgarh, India: A Comparative Study. **International Journal of Advanced Biological and Biomedical Research**, v. 6, n. 2, p. 116–120, 1 jun. 2018.

INCA. Instituto Nacional de Câncer José Alencar Gomes da Silva. **Câncer de pulmão – Estatísticas**, 2018. Disponível em: <http://www1.inca.gov.br/estimativa/2018/>. Acesso em: 01/10/2023.

JAIN, Z. J.; GIDE, P. S.; KANKATE, R. S. Biphenyls and their derivatives as synthetically and pharmacologically important aromatic structural moieties. **Arabian Journal of Chemistry**, v. 10, p. S2051–S2066, 1 maio 2017.

JABOIN, J. J.; HWANG, M.; LU, B. Autophagy in lung cancer. **Methods in enzymology**, v. 453, n. C, p. 287–304, 2009.

JANISZEWSKA, M.; PRIMI, M. C.; IZARD, T. Cell adhesion in cancer: Beyond the migration of single cells. **The Journal of biological chemistry**, v. 295, n. 8, p. 2495–2505, 21 fev. 2020.

JOMOVA, K. et al. Reactive oxygen species, toxicity, oxidative stress, and antioxidants: chronic diseases and aging. **Archives of Toxicology**, v. 97, n. 10, p. 2499–2574, 19 ago. 2023.

KALUDERCIC, N.; GIORGIO, V. The dual function of reactive oxygen/nitrogen species in bioenergetics and cell death: The role of ATP synthase. **Oxidative Medicine and Cellular Longevity**, v. 2016, 2016.

KARSCH-BLUMAN, A. et al. Tissue necrosis and its role in cancer progression. **Oncogene**, v. 38, n. 11, p. 1920–1935, 14 mar. 2019.

KASHFI, K.; KANNIKAL, J.; NATH, N. Macrophage Reprogramming and Cancer Therapeutics: Role of iNOS-Derived NO. **Cells**, v. 10, n. 11, 1 nov. 2021.

KATT, M. E. et al. *In Vitro* Tumor Models: Advantages, Disadvantages, Variables, and Selecting the Right Platform. **Frontiers in bioengineering and biotechnology**, v. 4, n. FEB, 12 fev. 2016.

KENNEDY, K. M. et al. Catabolism of Exogenous Lactate Reveals It as a Legitimate Metabolic Substrate in Breast Cancer. **PLoS ONE**, v. 8, n. 9, 12 set. 2013.

LENNICKE, C.; COCHEMÉ, H. M. Redox metabolism: ROS as specific molecular regulators of cell signaling and function. **Molecular cell**, v. 81, n. 18, p. 3691–3707, 16 set. 2021.

LE GAL, K.; SCHMIDT, E. E.; SAYIN, V. I. Cellular Redox Homeostasis. **Antioxidants**, v. 10, n. 9, 1 set. 2021.

LI, Y. et al. Modulation of redox homeostasis: A strategy to overcome cancer drug resistance. **Frontiers in Pharmacology**, v. 14, 2023.

LIBERTI, M. V.; LOCASALE, J. W. The Warburg Effect: How Does it Benefit Cancer Cells? **Trends in biochemical sciences**, v. 41, n. 3, p. 211, 1 mar. 2016.

LIM, S. M.; MOHAMAD HANIF, E. A.; CHIN, S. F. Is targeting autophagy mechanism in cancer a good approach? The possible double-edge sword effect. **Cell & Bioscience**, v. 11, n. 1, p. 1–13, 20 mar. 2021.

LIN, X. et al. Glucose Metabolism on Tumor Plasticity, Diagnosis, and Treatment. **Frontiers in Oncology**, v. 10, p. 317, 6 mar. 2020.

LIOU, G. Y.; STORZ, P. Reactive oxygen species in cancer. **Free radical research**, v. 44, n. 5, p. 479–496, 2010.

LIU, Z. G.; JIAO, D. Necroptosis, tumor necrosis and tumorigenesis. **Cell Stress**, v. 4, n. 1, p. 1, 1 jan. 2020.

LIU, G. et al. Role of Autophagy and Apoptosis in Non-Small-Cell Lung Cancer. **International journal of molecular sciences**, v. 18, n. 2, 10 fev. 2017.

MARDINA, V. et al. Antioxidant and cytotoxic activities of the ethyl acetate extract of Sphagneticola trilobata (L.) J.F. Pruski on MCF-7 breast cancer cell. **Journal of Advanced Pharmaceutical Technology & Research**, v. 11, n. 3, p. 123, 2020a.

MARTINEZ-OUTSCHOORN, U. E. et al. Cancer metabolism: a therapeutic perspective. **Nature Reviews Clinical Oncology 2016 14:1**, v. 14, n. 1, p. 11–31, 4 maio 2016.

MARTINEZ-PACHECO, S.; O'DRISCOLL, L.. Pre-Clinical In Vitro Models Used in Cancer Research: Results of a Worldwide Survey. **Cancers**, v. 13, n. 23, 1 dez. 2021.

MERFORT, I. Perspectives on sesquiterpene lactones in inflammation and cancer. **Current drug targets**, v. 12, n. 11, p. 1560–1573, 7 nov. 2011.

MIJATOVIĆ, S. et al. The Double-Faced Role of Nitric Oxide and Reactive Oxygen Species in Solid Tumors. **Antioxidants**, v. 9, n. 5, 1 maio 2020.

MINER, J.; HOFFHINES, A. The Discovery of Aspirin's Antithrombotic Effects. **Texas Heart Institute Journal**, v. 34, n. 2, p. 179, 2007.

MOGHARABI, M.; FARAMARZI, M. A. Laccase and Laccase-Mediated Systems in the Synthesis of Organic Compounds. **Advanced Synthesis & Catalysis**, v. 356, n. 5, p. 897–927, 24 mar. 2014.

MULCAHY LEVY, J. M.; THORBURN, A. Autophagy in cancer: moving from understanding mechanism to improving therapy responses in patients. **Cell death and differentiation**, v. 27, n. 3, p. 843–857, 1 mar. 2020.

NAEEM, A. et al. Natural Products as Anticancer Agents: Current Status and Future Perspectives. **Molecules,** v. 27, n. 23, 1 dez. 2022.

NEWMAN, D. J.; CRAGG, G. M. Natural Products as Sources of New Drugs over the Nearly Four Decades from 01/1981 to 09/2019. **Journal of natural products**, v. 83, n. 3, p. 770–803, 27 mar. 2020.

ONOI, K. et al. Immune Checkpoint Inhibitors for Lung Cancer Treatment: A Review. **Journal of Clinical Medicine**, v. 9, n. 5, 1 maio 2020.

PANOV, S. Z. Molecular biology of the lung cancer. **Radiology and Oncology**, v. 39, n. 3, 1 set. 2005.

PATRIDGE, E. et al. An analysis of FDA-approved drugs: natural products and their derivatives. **Drug discovery today**, v. 21, n. 2, p. 204–207, 2016.

PAYEN, V. L. et al. Metabolic changes associated with tumor metastasis, part 1: tumor pH, glycolysis and the pentose phosphate pathway. **Cellular and Molecular Life Sciences**, v. 73, n. 7, p. 1333–1348, 1 dez. 2015.

PAYEN, V. L. et al. Metabolic changes associated with tumor metastasis, part 1: tumor pH, glycolysis and the pentose phosphate pathway. **Cellular and molecular life sciences: CMLS**, v. 73, n. 7, p. 1333–1348, 1 abr. 2016.

PÉGLION, F.; ETIENNE-MANNEVILLE, S. N-cadherin expression level as a critical indicator of invasion in non-epithelial tumors. **Cell Adhesion & Migration**, v. 6, n. 4, p. 327, 7 jul. 2012.

PFEFFER, C. M.; SINGH, A. T. K. Apoptosis: A Target for Anticancer Therapy. **International journal of molecular sciences**, v. 19, n. 2, 2 fev. 2018.

PIRETTO, E. et al. Effects of mutations and immunogenicity on outcomes of anti-cancer therapies for secondary lesions. **Mathematical biosciences**, v. 315, 1 set. 2019.

PORTA, C.; PAGLINO, C.; MOSCA, A. Targeting PI3K/Akt/mTOR signaling in cancer. **Frontiers in Oncology**, v. 4 APR, p. 67531, 14 abr. 2014.

RANASINGHE, R.; MATHAI, M. L.; ZULLI, A. Cisplatin for cancer therapy and overcoming

chemoresistance. **Heliyon**, v. 8, n. 9, 1 set. 2022.

REN, Y.; YU, J.; KINGHORN, A. D. Development of Anticancer Agents from Plant-derived Sesquiterpene Lactones. **Current medicinal chemistry**, v. 23, n. 23, p. 2397, 11 maio 2016.

REYNAERT, N. L. et al. Dynamic redox control of NF-κB through glutaredoxin-regulated S-glutathionylation of inhibitory κB kinase β. **Proceedings of the National Academy of Sciences**, v. 103, n. 35, p. 13086–13091, 29 ago. 2006.

RICE-EVANS, C. A.; MILLER, N. J.; PAGANGA, G. Structure-antioxidant activity relationships of flavonoids and phenolic acids. **Free Radical Biology and Medicine**, v. 20, n. 7, p. 933–956, 1996.

RIZWANUL FATTAH, I.M. et al. Effect of antioxidants on oxidation stability of biodiesel derived from vegetable and animal based feedstocks. **Renewable and Sustainable Energy Reviews**, v. 30, p. 356–370, fev. 2014.

ROCHA, C. R. R. et al. DNA repair pathways and cisplatin resistance: an intimate relationship. **Clinics**, v. 73, n. suppl 1, 2018.

ROSKOSKI, R. Anaplastic lymphoma kinase (ALK) inhibitors in the treatment of ALK-driven lung cancers. **Pharmacological Research**, v. 117, p. 343–356, 1 mar. 2017.

SANAEI, M. J. et al. The PI3K/Akt/mTOR pathway in lung cancer; oncogenic alterations, therapeutic opportunities, challenges, and a glance at the application of nanoparticles. **Translational Oncology**, v. 18, p. 101364, 1 abr. 2022.

SCHIRMANN, J. G. et al. Selective control for the laccase-catalyzed synthesis of dimers from 2,6-dimethoxyphenol: Optimization of 3,3',5,5'-tetramethoxy-biphenyl-4,4'-diol synthesis using factorial design, and evaluation of its antioxidant action in biodiesel. **Applied Catalysis A: General**, v. 555, p. 88–97, 5 abr. 2018.

SCHIRMANN, J. G. et al. 3,3″,5,5″-Tetramethoxybiphenyl-4,4″-diol: A new antioxidant enhancing oxidative stability of soybean biodiesel. **Fuel**, v. 237, p. 593–596, 1 fev. 2019.

SCHIRMANN, J. G. et al. In-vitro biological evaluation of 3,3',5,5'-tetramethoxy-biphenyl-4,4'-diol and molecular docking studies on trypanothione reductase and Gp63 from *Leishmania amazonensis* demonstrated anti-*leishmania* potential. **Scientific reports**, v. 13, n. 1, 1 dez. 2023.

SHANKAR, R.; THOMAS, T. ANTIBACTERIAL ACTIVITY OF FLOWER HEADS OF WEDELIA TRILOBATA (L.) A. S. HITCHC. **Journal of Biological & Scientific Opinion**, v. 2, n. 6, p. 409–412, 22 dez. 2014.

SHOAIB, M. et al. Sesquiterpene lactone! a promising antioxidant, anticancer and moderate antinociceptive agent from *Artemisia macrocephala* jacquem. **BMC Complementary and Alternative Medicine**, v. 17, n. 1, p. 1–11, 7 jan. 2017.

SIDDIQUI, F.; VAQAR, S.; SIDDIQUI, A. H. Lung Cancer. **Cambridge Handbook of Psychology, Health and Medicine, Second Edition**, p. 605–606, 8 maio 2023.

SINGH, C. R.; KATHIRESAN, K. Molecular understanding of lung cancers-A review. **Asian Pacific journal of tropical biomedicine**, v. 4, n. Suppl 1, p. 35–41, maio 2014.

SINGH, T. et al. Natural bio-colorant and pigments: Sources and applications in food processing. **Journal of Agriculture and Food Research**, v. 12, p. 100628, 1 jun. 2023.

SNEADER, W. The discovery of aspirin: a reappraisal. **BMJ,** v. 321, n. 7276, p. 1591–1594, 23 dez. 2000.

STEVEN, A.; FISHER, S. A.; ROBINSON, B. W. Immunotherapy for lung cancer. **Respirology**, v. 21, n. 5, p. 821–833, 1 jul. 2016.

SOARES, S. E. Phenolic acids as antioxidants. **Revista de Nutricao**, v. 15, n. 1, p. 71–81, 2002.

SRAVYA, N. S. et al. Antimicrobial, antioxidant and in vitro anti-inflammatory activity and phytochemical screening of water extract of *Wedelia trilobata* (L.) Hitchc. **Journal of Medicinal Plants Research**, v. 5, n. 24, p. 5718–5729, 2011.

STRATTON, M. R.; CAMPBELL, P. J.; FUTREAL, P. A. The cancer genome. **Nature**, v. 458, n. 7239, p. 719–724, 9 abr. 2009.

SUI, X. et al. 2,4,3′,4′-tetramethoxy-biphenyl induces apoptosis in MGC-803 cells through a mitochondrial/caspase pathway. **Bangladesh Journal of Pharmacology,** v. 9, n. 2, p. 235–243, 3 jun. 2014.

SUN, S.; SCHILLER, J. H.; GAZDAR, A. F. Lung cancer in never smokers — a different disease. **Nature Reviews Cancer**, v. 7, n. 10, p. 778–790, 1 out. 2007.

SUNG, H. et al. Global Cancer Statistics 2020: GLOBOCAN Estimates of Incidence and Mortality Worldwide for 36 Cancers in 185 Countries. **CA: a cancer journal for clinicians**, v. 71, n. 3, p. 209–249, maio 2021.

TAN, A. C. Targeting the PI3K/Akt/mTOR pathway in non-small cell lung cancer (NSCLC). **Thoracic cancer**, v. 11, n. 3, p. 511–518, 1 mar. 2020.

TAN, Y. et al. Pyroptosis: a new paradigm of cell death for fighting against cancer. **Journal of Experimental & Clinical Cancer Research**, v. 40, n. 1, p. 1–15, 3 maio 2021.

TRAVIS, W. D. Pathology of lung cancer. **Clinics in chest medicine**, v. 32, n. 4, p. 669–692, dez. 2011.

TRAVERSO, N. et al. Role of Glutathione in Cancer Progression and Chemoresistance. **Oxidative Medicine and Cellular Longevity**, v. 2013, 2013.

TRETTER, V. et al. Understanding Cellular Redox Homeostasis: A Challenge for Precision Medicine. **International journal of molecular sciences**, v. 23, n. 1, 1 jan. 2021.

TOPPO, K. I. et al. ANTIMICROBIAL ACTIVITY OF SPHAGNETICOLA TRILOBATA (L.) PRUSKI, AGAINST SOME HUMAN PATHOGENIC BACTERIA AND FUNGI. 2013.

VAZQUEZ, A. et al. Catabolic efficiency of aerobic glycolysis: The Warburg effect revisited. **BMC Systems Biology**, v. 4, p. 58, 6 maio 2010.

WAN, Y.; DU, Y.; MIYAKOSHI, T. Enzymatic catalysis of 2,6-dimethoxyphenol by laccases and products characterization in organic solutions. **Science in China, Series B: Chemistry**, v. 51, n. 7, p. 669–676, jul. 2008.

WEIDINGER, A.; KOZLOV, A. V. Biological Activities of Reactive Oxygen and Nitrogen Species: Oxidative Stress versus Signal Transduction. **Biomolecules**, v. 5, n. 2, p. 472–484, 15 abr. 2015.

WENG, M. C. et al. Apoptosis induction and AKT/NF-κB inactivation are associated with regroafenib-inhibited tumor progression in non-small cell lung cancer in vitro and in vivo. **Biomedicine & Pharmacotherapy**, v. 116, p. 109032, 1 ago. 2019.

WORLD HEALTH ORGANIZATION (WHO); International Association of Cancer Registries (IACR) (2020). **Cancer today**. Disponível em:<https://gco.iarc.fr/today/home> acesso em 01/10/2023.

XIA, Y.; SHEN, S.; VERMA, I. M. NF-κB, an active player in human cancers. **Cancer immunology research**, v. 2, n. 9, p. 823, 1 set. 2014.

YEE, P. P.; LI, W. Tumor necrosis: A synergistic consequence of metabolic stress and inflammation. **BioEssays: news and reviews in molecular, cellular and developmental biology**, v. 43, n. 7, 1 jul. 2021.

YU, P. et al. Pyroptosis: mechanisms and diseases. **Signal Transduction and Targeted Therapy**, v. 6, n. 1, p. 1–21, 29 mar. 2021.

YUN, C. W.; LEE, S. H. The Roles of Autophagy in Cancer. **International Journal of Molecular Sciences**, v. 19, n. 11, 5 nov. 2018.

ZAMBONI, M. Epidemiologia do câncer do pulmão. **Jornal de Pneumologia**, v. 28, n. 1, p. 41–47, jan. 2002.

ZAPPA, C.; MOUSA, S. A. Non-small cell lung cancer: current treatment and future advances. **Translational Lung Cancer Research**, v. 5, n. 3, p. 288–300, jun. 2016.

ZHANG, F. et al. Naringenin prevents TGF-β1 secretion from breast cancer and suppresses pulmonary metastasis by inhibiting PKC activation. **Breast Cancer Research**, v. 18, n. 1, p. 1–16, 1 abr. 2016.

ZHENG, X. et al. The Role and Mechanism of Pyroptosis and Potential Therapeutic Targets in Sepsis: A Review. **Frontiers in Immunology**, v. 12, p. 711939, 7 jul. 2021.

ZHOU, X. Q. et al. Trilobolide-6-O-isobutyrate suppresses hepatocellular carcinoma tumorigenesis through inhibition of IL-6/STAT3 signaling pathway. **Phytotherapy research : PTR**, v. 35, n. 10, p. 5741–5753, 1 out. 2021.

4 PRODUÇÃO CIENTÍFICA

4.1 Manuscrito: 3,3',5,5'-Tetramethoxybiphenyl-4,4'diol triggers oxidative stress, metabolic changes and apoptosis-like process by reducing the PI3K/AKT/NF-κB pathway in the NCI-H460 lung cancer cell line

Aceito na revista: *Biomedicine & pharmacological*

4.2 Manuscrito: Trilobolide-6-*O*-isobutyrate from *Sphagneticola trilobata* acts by inducing oxidative stress, metabolic changes and apoptosis-like processes by caspase 3/7 activation of human lung cancer cell lines

Aceito na revista: *Phytomedicine*

3,3',5,5'-Tetramethoxybiphenyl-4,4'diol triggers oxidative stress, metabolic changes, and apoptosis-like process by reducing the PI3K/AKT/NF-κB pathway in the NCI-H460 lung cancer cell line

Virginia Marcia Concato[a,*], Taylon Felipe Silva[a], Mariana Barbosa Detoni[a], Ellen Mayara Souza Cruz[a], Manoela Daiele Gonçalves[b], Bruna Taciane da Silva Bortoleti[a,c], Fernanda Tomiotto-Pellissier[a,c,d], Amanda Cristina Machado Carloto[a], Maria Beatriz Madureira[a], Ana Carolina Jacob Rodrigues[a,c], Jéseka Gabriela Schirmann[e], Aneli M. Barbosa-Dekker[e], Robert F. H. Dekker[f], Ivete Conchon-Costa[a], Carolina Panis[g], Danielle Lazarin-Bidóia[a], Milena Menegazzo Miranda-Sapla[a], Mario Sergio Mantovani[h], Wander Rogério Pavanelli[a]

Author information:

[a]Laboratory of Immunoparasitology of Neglected Diseases and Cancer, Department of Immunology, Parasitology and General Pathology, Center of Biological Sciences, State University of Londrina, PR, Brazil.

[b]Laboratory of Biotransformation and Phytochemical, Department of Chemistry, Center of Exact Sciences, State University of Londrina, PR, Brazil.

[c]Graduate Program in Biosciences and Biotechnology, Carlos Chagas Institute (ICC), Fiocruz, Curitiba, PR, Brazil.

[d]Department of Medical Pathology, Federal University of Paraná, Curitiba, PR, Brazil.

[e]Laboratory Research of Bioactive Molecules, Department of Chemistry, Center of Exact Sciences, State University of Londrina, PR, Brazil.

[f]Federal Technological University of Paraná, Graduate Program in Environmental Engineering, Campus Londrina, Londrina, PR, Brazil.

[g]Laboratory of Tumor Biology, State University of West Paraná, Unioeste, Francisco Beltrao, Brazil.

[h]Laboratory of Toxicological Genetics, Department of General Biology, Center of Biological Sciences, State University of Londrina, PR, Brazil.

[*] **Corresponding author:** Virginia Marcia Concato, Department of Immunology, Parasitology and General Pathology, Laboratory of Immunopathology of Neglected Diseases and Cancer, State University of Londrina – UEL. Rodovia Celso Garcia Cid Campus, CEP: 86057-970, Post Box 10.011. Londrina, PR.

Tel: +055 4333714539. *E*-mail: vir_93_@hotmail.com

Highlights

- TMBP treatment reduces cell viability and alters morphology in NCI-H460.
- The treatment reduces migratory capacity and N-cadherin and β-catenin proteins.
- TMBP treatment promotes oxidative and metabolic stress on lung cancer cell-line.
- TMBP induces the G2/M arrest phase, cell death, and reduces STAT-3 in NCI-H460.
- The treatment act in NCI-H460 decreases PI3K/AKT/ARG-1/NF-κB and increases iNOS.

Abstract

Lung cancer is one of the leading causes of cancer-related deaths in men and women worldwide. Current treatments have limited efficacy, cause significant side effects, and cells can develop drug resistance. New therapeutic strategies are needed to discover alternative anticancer agents with high efficacy and low-toxicity. TMBP, a biphenyl obtained by laccase-biotransformation of 2,6-dimethoxyphenol, possesses antitumor activity against A549 adenocarcinoma cells. Without causing damage to sheep erythrocytes and mouse peritoneal macrophages of BALB/c mice. In addition to being classified as a good oral drug according to *in-silico* studies. This study evaluated the *in-vitro* cytotoxic effect of TMBP on lung-cancer cell-line NCI-H460 and reports mechanisms on immunomodulation and cell death. TMBP treatment (12.5-200μM) inhibited cell proliferation at 24, 48, and 72 h. After 24-h treatment, TMBP at IC_{50} (154μM) induced various morphological and ultrastructural changes in NCI-H460, reduced migration and immunofluorescence staining of N-cadherin and β-catenin, induced increased reactive oxygen species and nitric oxide with reduced superoxide radical-anion, increased superoxide dismutase activity and reduced glutathione reductase. Treatment also caused metabolic stress, reduced glucose-uptake, intracellular lactate dehydrogenase and lactate levels, mitochondrial depolarization, increased lipid droplets, and autophagic vacuoles. TMBP induced cell-cycle arrest in the G2/M phase, death by apoptosis, increased caspase-3/7, and reduced STAT-3 immunofluorescence staining. The anticancer effect was accompanied by decreasing PI3K, AKT, ARG-1, and NF-κB levels, and increasing iNOS. These results suggest its potential as a candidate for use in future lung anticancer drug design studies.

Keywords: Treatment; Cancer; Cell Death; Redox Disruption;

Graphical Abstract

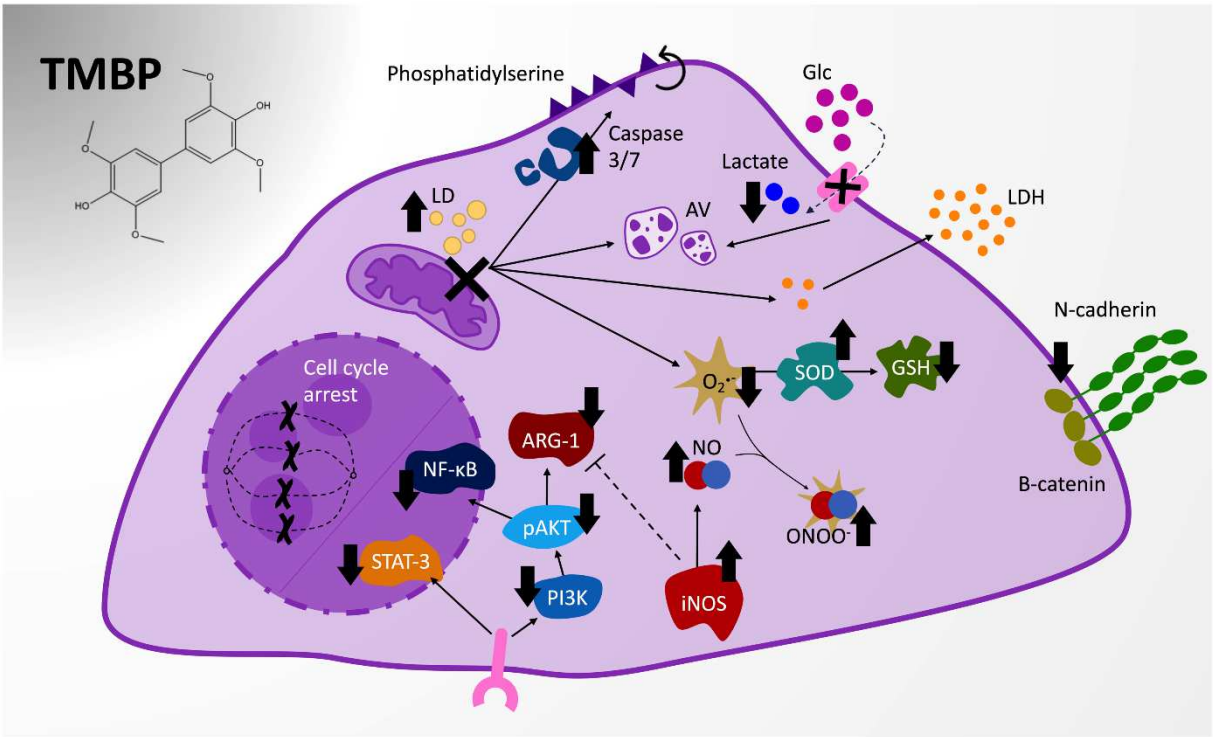

Schematic model of the lung anticancer effect of TMBP on the NCI-H460 large cell carcinoma cell line. Caption: TMBP, 3,3',5,5'-Tetramethoxybiphenyl-4,4'-Diol; ROS, Reactive oxygen species; NO, Nitric oxide; $O_2^{\cdot-}$, Superoxide anion radical; SOD, Superoxide dismutase; GSH, Reduced glutathione; Glc, Glucose; LDH, Lactate dehydrogenase; LD, Lipid droplets; LD, Lipid droplets; AV, Autophagic vacuoles; iNOS, Induzivel nitric oxide synthase; ARG-1, Arginase-1; PI3K, phosphatidylinositol-3-kinase; AKT, Protein kinase B, pAKT, Phosphoprotein kinase B; NF-κB, Nuclear factor *kappa* B; STAT-3, signal transducer and activator of transcription 3; $ONOO^-$, Peroxynitrite anion;

Abbreviations: LC, Lung Cancer; NSCLC- Non-small cell lung cancer; SCLC- Small cell lung cancer; TMBP, 3,3',5,5'-Tetramethoxybiphenyl-4,4'-Diol; 2,6-DMP, 2,6-Dimethoxyphenol; ROS, Reactive Oxygen Species; DMSO, Dimethyl sulfoxide; SEM, Scanning Electron Microscopy; TEM, Transmission Electron Microscopy; H_2DCFDA, 2',7'-dichlorofluorescein diacetate; MTT, 3-(4,5-dimethylthiazol-2-yl)-2,5-diphenyltetrazolium bromide; PBS, Phosphate-buffered saline; SBF, fetal bovine serum; Glc, Glucose; TMRE, tetramethylrhodamine-ethyl-ester; H_2O_2, Hydrogen peroxide; CCCP, Carbonylcyanide *m*-chlorophenylhydrazone; NAC, N-Acetylcysteine; NO, Nitric Oxide; L-NAME, NG-nitro-L-arginine methyl ester; $O_2^{\cdot-}$, Superoxide anion radical; SOD, Superoxide dismutase; GSH, Reduced Glutathione; LDH, Lactate dehydrogenase; $\Delta\psi m$, Mitochondrial membrane potential;

LD, Lipid droplets; NR, Nile red; MDC, monodansylcadaverine; CPT, Camptothecin; ELISA, Enzyme-linked immunosorbent assay; iNOS, Induzivel nitric oxide sintase; ARG-1, Arginase-1; PI3K, phosphatidylinositol-3-kinase; AKT, Protein kinase B, pAKT, Phospho Protein kinase B; NF-κB, Nuclear factor *kappa* B; p NF-κB, Phospho nuclear factor *kappa* B; NRF2, Erythroid-derived nuclear factor 2; KOH, Potassium hydroxide; Z-DEVD-AMC substrate, Fluorogenic substrate for caspase 3 e 7; Ac-DEVD-CHO inhibitor, Caspase-3 e 7 Inhibitor I, N-Ac-Asp-Glu-Val-Asp-CHO; RIPA, Radioimmunoprecipitation Assay; EDTA, Ethylenediaminetetraacetic acid; TME, tumor microenvironment; STAT-3, signal transducer and activator of transcription 3; EMT, epithelial-mesenchymal transition; OH^-, Hydroxyl radical; OXPHOS, Oxidative phosphorylation; CAT, catalase; PRDXs, Peroxiredoxins; GPXs, Glutathione peroxidases; $ONOO^-$, Peroxynitrite anion; RNS, Reactive Nitrogen Species;

1. Background

Lung cancer (LC), a heterogeneous disease, remains one of the leading causes of cancer-related mortalities worldwide, with an estimated 2.9 million cases by 2040 [1]. In addition, most patients have metastatic disease at the time of diagnosis [1]. Non-small cell lung cancer (NSCLC) accounts for more than 85% of all LCs and is common in both men and women [2]. Available chemotherapy for NSCLC has advanced significantly over the past decade, and platinum-based doublet therapy (e.g., cisplatin in combination with carboplatin) has been successfully implemented [3]. Several side effects, however, remain, including severe kidney problems, allergic reactions, decreased immunity to infection, gastrointestinal upset, bleeding, hearing loss, and also drug resistance, especially if the tumor recurs [4]. Because of the challenges in treating this disease, new therapeutic strategies are needed and should be developed.

Phenolic compounds are naturally present in plants and can be synthesized through various methods, including biocatalysis, which involves the use of enzymes for the transformation of molecular structures [5,6]. One of the advantages of synthesizing compounds through biocatalysis is that it can be part of a green process, as it employs fewer toxic methodologies. This has been highlighted in research conducted by [7–9]. 3,3',5,5'-Tetramethoxybiphenyl-4,4'-diol (TMBP), a biphenyl (**Figure suppl. 1**), was obtained by oxidation of 2,6-dimethoxyphenol (2,6-DMP) using laccase produced by the ascomyceteous fungus *Botryosphaeria rhodina* (MAMB-05) [7,8]. Biphenolic compounds have interesting chemical structures and many of these compounds play diverse biological roles [5,6], including fungicidal [10,11], bactericidal [12,13], anti-inflammatory [14,15], antioxidant [16], cell anti-

147 proliferation [17,18], and anti-tumor activity. In a recent study using TMBP on the A549 (lung
148 adenocarcinoma) tumor cell line, our group showed that treatment with TMBP reduced
149 viability, increased reactive oxygen species (ROS) production, induced mitochondrial
150 depolarization, was involved in cell cycle arrest in the G2/M phase, and death by direct
151 apoptosis, without causing toxicity in BALB/c mouse peritoneal macrophages and sheep
152 erythrocytes [19].

153 In this study, using different endpoints, TMBP was shown to reduce cell viability and
154 migratory potential, promote morphological and ultrastructural changes, followed by apoptosis
155 and autophagy. These phenomena were mediated by an oxidative burst and metabolic damage
156 through decreased levels of PI3K/pAKT/ARG-1/pNF-κB and an increase of the iNOS pathway
157 in NCI-H460 lung cancer cells.
158

159 **2. Material And Methods**
160

161 **2.1 TMBP**

162 The biphenyl 3,3',5,5'-tetramethoxybiphenyl-4,4'-diol (TMBP; $C_{16}H_{18}O_6$, MW 306) was
163 synthesized from 2,6-DMP using laccase from *Botryosphaeria rhodina* MAMB-05 under
164 conditions previously described [20]. The resulting yellow solid was identified by ^{1}H NMR
165 (CDCl3, 400 MHz) at δ 3.98 (s, 12H), 6.73 (s, 4H), 5.56 (s, 2H), purity 99%, and melting point
166 185-188 °C. A stock solution of TMBP was prepared in 1% dimethyl sulfoxide (DMSO)
167 (Sigma-Aldrich, St. Louis, MO, USA); the concentration of DMSO was kept at a maximum of
168 0.06% in all experiments.
169

170 **2.2 Cell culture**

171 The established NSCLC line, NCI-H460 (large cell carcinoma), from Frederick Ma
172 (National Cancer Institute, Bethesda, MD, USA) was kindly provided by the Toxicological
173 Genetics Laboratory-UEL. The cell was cultured in Roswell Park Memorial Institute (RPMI)
174 1640 culture medium (Life Technologies, Carlsbad, CA, USA) supplemented with 10% fetal
175 bovine serum (FBS) (GIBCO, Invitrogen, New York, USA), 100 U/mL penicillin and 100
176 µg/mL streptomycin (Santa Cruz Biotechnologies, Dallas, TX, USA), and incubated at 37 °C
177 under 5% CO_2.

178 **2.3 Cell viability assay**

179 NCI-H460 cells (10^4 cells/well) were treated with TMBP (range 12.5-100 μM) or
180 cisplatin (Cis) (50 μM), and cytotoxicity was assessed at 24, 48, and 72 h. MTT assays were
181 performed as previously described [19]. Briefly, the cells were washed, and MTT (0.33 mg/ml)
182 (Sigma-Aldrich) was added to the cells and then incubated for 3 h at 37 °C. The MTT product
183 formed (formazan crystals) was diluted with 100 μl of DMSO and measured
184 spectrophotometrically at 550 nm. The 50% inhibitory concentration (IC_{50}) curve was
185 calculated by logarithmic regression using GraphPad Prism 8 software for the above times. The
186 IC_{50} at 24 h was used for the remaining experiments. Micrographs of TMBP-treated IC_{50} cells
187 were taken using an EVOS Microscope FL Auto Cell imaging system (Thermo-Fisher
188 Scientific, Multiskan GO, Waltham, MA, USA) at 100× magnification.
189
190 **2.4 Morphological and ultrastructural analysis of NCI-H460 cells by scanning electron**
191 **microscopy (SEM) and transmission electron microscopy (TEM)**

192 Scanning electron microscopy (SEM) of the NCI-H460 cell line was performed to
193 analyze morphological changes in the cell surface topography [21]. Briefly, cells (10^6
194 cells/well) were treated with IC_{50}-TMBP for 24 h at 37 °C. They were then fixed with 2.5%
195 glutaraldehyde in 0.1 M sodium cacodylate buffer (pH 7.4) and allowed to adhere to poly-L-
196 lysine-coated coverslips for 60 min. The cells were then dehydrated through increasing
197 concentrations of ethanol (30-100%), subjected to critical point drying (Baltec SCD-030,
198 Balzers, Liechtenstein), and metallized with gold for visualization using a high-resolution FEI
199 SCIOS (Oregon, USA) double beam electron microscope (Thermo Fisher Scientific,
200 Massachusetts, United States).

201 To assess ultrastructural changes in the TMBP-treated cells by TEM (JEOL USA JEM
202 1400, Tokyo, Japan, transmission electron microscope), cells were treated and fixed similarly
203 as described above. The samples were then postfixed with 1% OsO_4, 0.8% potassium
204 ferrocyanide, and 10.0 mM $CaCl_2$ in 0.1 M sodium cacodylate buffer (pH 7.4) for 1 h at room
205 temperature and protected from light. The samples were then washed in 0.1 M sodium
206 cacodylate buffer and dehydrated in increasing concentrations of acetone (30-100%). The total
207 acetone content was gradually replaced by EPON™ epoxy resin (Electron Microscopy
208 Sciences, Hatfield, United States) by cell diffusion and polymerized at 60 °C for 72 h.
209 Nanoscale sections (60-70 nm) were sliced with an ultramicrotome (PowerTomer BMC -
210 Germany) and contrasted with 5% uranyl acetate and 2% lead citrate. Finally, the samples were

analyzed by TEM. The NCI-H460 cell line maintained in RPMI culture medium without TMBP treatment was used as a negative control.

2.5 Cell scratch assay

NCI-H460 cells (10^6 cells/well) were seeded into 6-well plates and incubated (37 °C, 5% CO_2) to confluence. We then created a 'scratch' in the monolayer by gently passing a 200 µL pipette tip over the bottom of each well. This passage created a discontinuity in the monolayer whose cells at the edge tended to migrate into the empty spaces. The cells were next treated with IC_{50}-TMBP, and photomicrographs (40× objective) were taken at different times (0, 12, and 24 h) using an EVOS FL Auto 2 microscope (Thermo Scientific, USA). Cell migration was assessed as the free area (region without cells) measured using Image-Pro plus program software (ImageJ), while the percentage decrease in the area was characterized by the cell migration index. Assays were performed in triplicate from each group tested.

2.6 Immunofluorescence (IF) staining

NCI-H460 cells (10^5 cells/well) were seeded in 24-well plates containing coverslips and treated with the 24 h IC_{50} value of TMBP at 37 °C. The assay was performed as described by Duplancic and Kero (2021) [22]. Briefly, background blocking was performed using Abcam Protein Block (ab64226; Abcam, UK) for 25 min after the antigen retrieval. The following primary and secondary antibodies used for IF staining (24 h at 4 °C) were from Santa Cruz Biotechnology (USA): N-cadherin (1:1000), β-catenin (1:500), and STAT-3 (1:1500). Secondary antibodies were used at dilution 1:2000: anti-mouse Texas red (RED) and anti-rabbit Alexa Fluor 488 (GREEN). Cell nuclei were stained with diamidino-2-phenylindole (DAPI, Sigma-Aldrich, USA). The slides were mounted with glycerol and kept protected from light under a fluorescence microscope for later observation. The intensity and localization of the immunoreactivity were analyzed with the Motic BA 410E fluorescence microscope and MOTICAM ProS5 Plus (40× objective lens). The merge of DAPI and Texas Red images was performed using the Image J software (NIH, USA).

2.6 Analysis of Reactive Oxygen Species (ROS)

ROS generation was assessed by the conversion of non-fluorescent H_2DCFDA to highly fluorescent 2',7'-dichlorofluorescein (DCF) by intracellular free radicals. Briefly, ROS scavenger (N-acetylcysteine – NAC, 5.0 M) was added, or not added, to the NCI-H460 cells 2 h before they received treatment with IC_{50} of TMBP, and were incubated for 24 h at 37 °C.

After this period, the cells were washed, and H_2DCFDA solution (10.0 M) was added and left in the dark for 45 min. Fluorescence intensity was quantified using a Glomax® spectrophotometer (Promega, USA) (excitation: 488 nm; and emission: 530 nm). Untreated cells were used as a negative control, and H_2O_2 (0.04%) was used as a positive control. Data were normalized and expressed in arbitrary units.

2.7 Determination of nitrite; an estimate of nitric oxide (NO) levels

NO levels were determined based on the Griess method. NCI-H460 cells (10^5 cells/well) were treated, or not, with the non-specific iNOS inhibitor (L-NAME, NG-nitro-L-arginine methyl ester, Sigma-Aldrich, USA) (25uM) for 1 h before treatment with IC_{50} of TMBP and incubated for 24 h. The supernatant of the samples was collected and analyzed according to Cataneo et al., (2019) [23]. Briefly, 60 µL of supernatant was added to 60 µL of Griess reagent (1% sulfanilamide and 0.1% N-(1-Naphthyl) ethylenediamine in 5% orthophosphoric acid (H3PO4)), incubated for 10 min, protected from light, at room temperature, and read on a plate reader (Thermo Scientific, Multiskan GO, USA) at 550 nm. For quantification, serial dilutions of $NaNO_2$ were used. Untreated cells were used as a negative control.

2.8 Resazurin assay

To assess whether cells treated with IC_{50} of TMBP would alter viability in the presence or absence of the inhibitors NAC and L-NAME, the resazurin assay was performed as follows. NCI-H460 cells (10^5 cells/well) were seeded in 24-well plates and incubated (24 h at 37 °C). After this period, NAC (5M) or L-NAME (50µM) was added 2 h and 1 h before, respectively, with or without IC_{50}-TMBP treatment and incubated (24 h at 37 °C). Resazurin (60 µM) was then added and left for 2 h, and the fluorescence intensity was quantified in a Glomax® spectrophotometer (520 nm excitation and 580nm emission). Data were normalized and expressed in arbitrary units.

2.9 Superoxide anion production

The production of superoxide anion radical ($O_2^{\bullet-}$) was determined by the reduction of the Redox dye nitro blue tetrazolium (1 mg/mL; NBT, Sigma-Aldrich). NCI-H460 cells (10^4 cells/well) were treated with IC_{50}-TMBP, incubated for 24 h, washed with PBS, and subsequently, 100 µL of NBT solution was added and incubated at 37 °C for 1 h. The supernatant was removed, and the formazan precipitate was then solubilized by adding 60 µL of 2.0 M KOH and 60 µL of DMSO. The optical density was measured spectrophotometrically

279 at 600 nm in a microplate reader (Multiskan GO Microplate Spectrophotometer, Thermo
280 Scientific, and Vantaa, Finland). Untreated cells were used as a negative control, and phorbol
281 myristate acetate (PMA) treatment was used as a positive control.
282
283 **2.10 Superoxide dismutase (SOD) activity**
284 SOD activity was determined based on the enzyme capacity to inhibit auto-oxidation of
285 pyrogallol, as described by Marklund and Marklund [24]. For the determination of SOD
286 activity, NCI-H460 cells (10^5 cells/well) were seeded, treated with the IC_{50} of TMBP, and
287 incubated for 24 h at 37 °C. Subsequently, the cells submitted a cycle of freezing at − 80 ◦C
288 and thawing at 37 ◦C for 30 min each. Total protein was determined on the cell lysate by the
289 Lowry method [25]. The data were normalized as mg protein/mL. Untreated cells were used as
290 a negative control.
291
292 **2.11 Reduced glutathione (GSH)**
293 Reduced L-glutathione (GSH) was measured to determine the intensity of oxidative
294 stress. NCI-H460 cells (10^5 cells/well) were seeded and treated with TMBP as described above.
295 After 24 h, GSH quantification was performed according to the method described by Rahman
296 et al., 2007 [26]. Concentrations were determined based on a standard curve constructed with
297 serial dilutions of GSH. Untreated cells were used as a negative control.
298
299 **2.12 Glucose assay**
300 To assess glucose uptake, NCI-H460 cells (10^5 cells/well) were seeded in 24-well plates,
301 treated with IC_{50} TMBP, and incubated for 24 h at 37 °C. The enzymatic-colorimetric glucose
302 assay was performed according to the manufacturer's kit instructions (Gold Analisa
303 Diagnostics, Minas Gerais, Brazil). Briefly, 1.0 µl aliquots of the supernatant from the treated
304 or standard samples were transferred to a 96-well plate, followed by the addition of 100 µl of
305 the glucose kit reagent, and the mixture incubated for 10 min at 37 °C. The reading was
306 performed in a preheated spectrophotometer (37 ºC) at 505 nm. Untreated cells were used as a
307 negative control.
308
309 **2.13 Lactate dehydrogenase (LDH) Activity**
310 To evaluate the LDH activity, NCI-H460 cells (10^6 cells/well) were seeded in 6-well
311 microplates and treated with IC_{50}-TMBP for 24 h at 37 °C. After this period, the cell supernatant

was collected to measure extracellular LDH. For the determination of intracellular LDH activity, the cells that had adhered to the multiplate wells were first washed twice with PBS, and water was added to perform 3 repetitions of freezing (-80 °C) and thawing in a heated waterbath, in order to lyze the cells. The intra- and extracellular LDH assays were performed according to the kit instructions (Gold Analisa Diagnóstico, Minas Gerais, Brazil). Untreated cells were used as a negative control.

2.14 Lactate analysis

For intracellular lactate measurement, cells were lyzed (as described above) and the procedures were followed according to the kit datasheet (Katal Biotecnológica, Belo Horizonte, MG, Brazil). Spectrophotometric reads (540 nm) were performed using a microplate reader (Thermo Scientific Multiskan). Untreated cells were used as a negative control.

2.15 Determination of mitochondrial membrane potential (ΔΨm)

We performed the analysis of mitochondrial membrane potential through tetramethylrhodamine-ethyl ester (TMRE; Sigma-Aldrich, USA). NCI-H460 cells (10^4 cells/well) were treated with IC_{50}-TMBP for 24 h at 37 °C. The assay was performed as described by Concato et al. (2020) [19]. Untreated cells were used as a negative control and carbonylcyanide *m*-chlorophenylhydrazone (CCCP) (100 µM) was used as a positive control. Data were normalized and expressed in arbitrary units.

2.16 Detection of lipid droplets (LD)

To determine LD accumulation, NCI-H460 cells (10^4 cells/well) were treated with IC_{50}-TMBP for 24 h at 37 °C and stained with 10 µg/mL Nile red (NR; Sigma-Aldrich, St. Louis, MO, USA) for 30 min. The assay was performed according to Concato et al. (2020) [19]. Untreated cells were used as a negative control, and PBS treatment was used as a positive control. Data were normalized and expressed in arbitrary units.

2.17 Determination of the formation of autophagic vacuoles

The formation of autophagic vacuoles was evaluated by staining with monodansylcadaverine (MDC; Sigma-Aldrich, St. Louis, MO, USA), according to Concato et al. (2020) [19]. Briefly, NCI-H460 cells (10^4 cells/well) were treated with IC_{50}-TMBP for 24 h at 37 °C and MDC was then added and left for 1 h. The fluorescence intensity was quantified

by spectrophotometry (Glomax, Promega, USA) (excitation 380 nm and emission 525 nm). Untreated cells were used as a negative control, and PBS treatment was used as a positive control. Data were normalized and expressed in arbitrary units.

2.18 Cell cycle analysis

NCI-H460 cells (10^6 cells/well) were treated with IC_{50}-TMBP for 24 h at 37 °C. The assay was performed as described by Concato et al. (2020) [19]. Briefly, the cell suspension was subjected to centrifugation at 1500 rpm for 5 min and the cell pellet resuspended in 300 µL of PBS. Subsequently, a solution containing 0.05% ribonuclease A (RNAse A) (Sigma, St. Louis, MO, USA) was added and incubated for 30 min at 37 °C. In the end, a solution of 0.1% sodium citrate and 1% Triton-X100 was added with 50 µg propidium iodide (PI) (Sigma, St. Louis, MO, USA) for 30 min. The fluorescence was estimated using a Muse Cell Analyzer (Merck Millipore), with 5000 events. The DNA content was analyzed, and the percentage of cells in different phases of the cycle (G1, S, and G2/M) were estimated according to the fluorescence intensity.

2.19 Cell death assay

NCI-H460 cells (10^6 cells/well) were treated with IC_{50}-TMBP for 24 h, and phosphatidylserine exposure was detected using Annexin-V FITC (Invitrogen, Eugene, USA), and cellular membrane integrity was detected with PI (0.50 µg/ ml) (Sigma, St. Louis, MO, USA). The assay was performed and described by Concato et al. (2020) [19].

2.20 Caspase-3/7 Assay

Caspase-3/7 protease activity was measured using the EnzChek™ Caspase-3/7 Assay Kit (Invitrogen™). Briefly, NCI-H460 cells (10^6 cells/well) were treated with IC_{50}-TMBP for 24 h, washed with PBS, and incubated at -80 °C for lysis. Lysis buffer (Triton X-100 in 1% PBS) was subsequently added and the solution was left for 30 min. This was followed by the addition of kit reagents (i.e., reaction buffer, dithiothreitol, and 5.0 mM Z-DEVD-AMC substrate) and incubated for 30 min. On completion of the reaction, the increase in fluorescence intensity, which is indicative of cleavage of the Z-DEVD-AMC substrate, was fluorometrically read (GloMax, Promega, USA) at excitation and emission wavelengths of 342 and 441 nm, respectively. The reactions were performed with and without the Ac-DEVD-CHO inhibitor (1 mM). Data were normalized and expressed in arbitrary units.

2.21 Protein Extraction and Enzyme-linked Immunosorbent Assay

NCI-H460 cells (10^6 cells/well) were plated and treated with IC_{50}-TMBP for 24 h, followed by washing with sterile PBS to remove non-adherent cells in the plate wells. The adhered cells were incubated with RIPA lysis buffer (150 mM sodium chloride, 1% triton X-100, 0.5% sodium deoxycholate, 0.1% sodium dodecyl sulfate, 5 mM EDTA, 50 mM Tris, pH 8.0) overnight at -80 °C. The cell lysate was collected and centrifuged at 13,000 × *g* for 20 min at 4 °C, the supernatant recovered and transferred to a new tube and the total protein concentration was quantified using NanoVue Plus reagent (Biochrom, USA). The protein concentration of all samples was normalized to 20 µg/mL, and a 100-µL aliquot was added in a 96-well ELISA plate for adsorption of proteins overnight at 4 °C. This was followed by adding a blocking buffer (ELISA/ELISPOT, eBioscience™, USA) and the plate was incubated for 1 h. The wells were then washed 3x with wash buffer (PBS in 0.5% Tween-20) and incubated with primary antibodies: anti-human PI3K, AKT, pAKT, arginase-1, NF-κB, pNF-κB, iNOS, and NRF2 (Santa Cruz Biotech, USA) for 2 h at room temperature. The wells were then washed (wash buffer) to remove unbound antibodies, followed by the addition of universal biotinylated secondary antibody (LSAB2 System-HRP, Dako, USA) and incubated for 1 h. The wells were then washed (wash buffer), followed by the addition of streptavidin-HRP (LSAB2 System-HRP, Dako, USA) and incubated for 1 h. After the incubation time, the wells were washed 5 times (wash buffer) and 100 µL of TMB substrate solution (eBioscience™, USA) was added, followed by incubation for 30 min, and then 100 µL of stop solution (0.5 M sulfuric acid) was added. The plate was read in a microplate reader at 450 nm (GloMax, Promega, USA).

2.22 Statistical analysis

Data are expressed as the mean ± standard error of the mean. Three independent experiments were performed, each with duplicate data sets, and analyzed with GraphPad Prism 8 statistical software (GraphPad Software, Inc., USA, 500.288). Significant differences between groups were determined through t-tests or one-way ANOVA followed by Tukey's test for multiple comparisons. A result was considered statistically significant if $p < 0.05$. Values were also categorized fallows: * ($p < 0.05$); ** ($p \leq 0.01$); *** ($p \leq 0.001$); **** ($p \leq 0.0001$).

3. Results

3.1 TMBP treatment reduces proliferative activity in NCI-H460 cell line

We first evaluated the cell viability after treatment with TMBP (12.5-200 µM) or cisplatin (CIS) (50 µM) for 24-72 h. The vehicle (DMSO) showed no toxic effect at any of the

times tested. At 24, 48, and 72 h, the concentrations of TMBP within the range 25-200 µM reduced the proliferation of the NCI-H460 cells ($p \leq 0.0001$), but the effects were more pronounced at 72 h. The concentration of 12.5 µM TMBP also affected cell viability which was reduced by 20% during this period (**Fig. 1A**). The IC_{50} was calculated for all the times tested (24, 48, and 72 h), resulting in the respective values of 152 µM (± 0.07), 73 µM (± 0.03), and 42 µM (± 0.03) (**Table 1**). The IC_{50} at 24 h was used for the following experiments, as previously described [19] and representative microscopic images showed morphological changes, such as rounding and apoptosis-like signs (white arrow) (**Fig. 1B**).

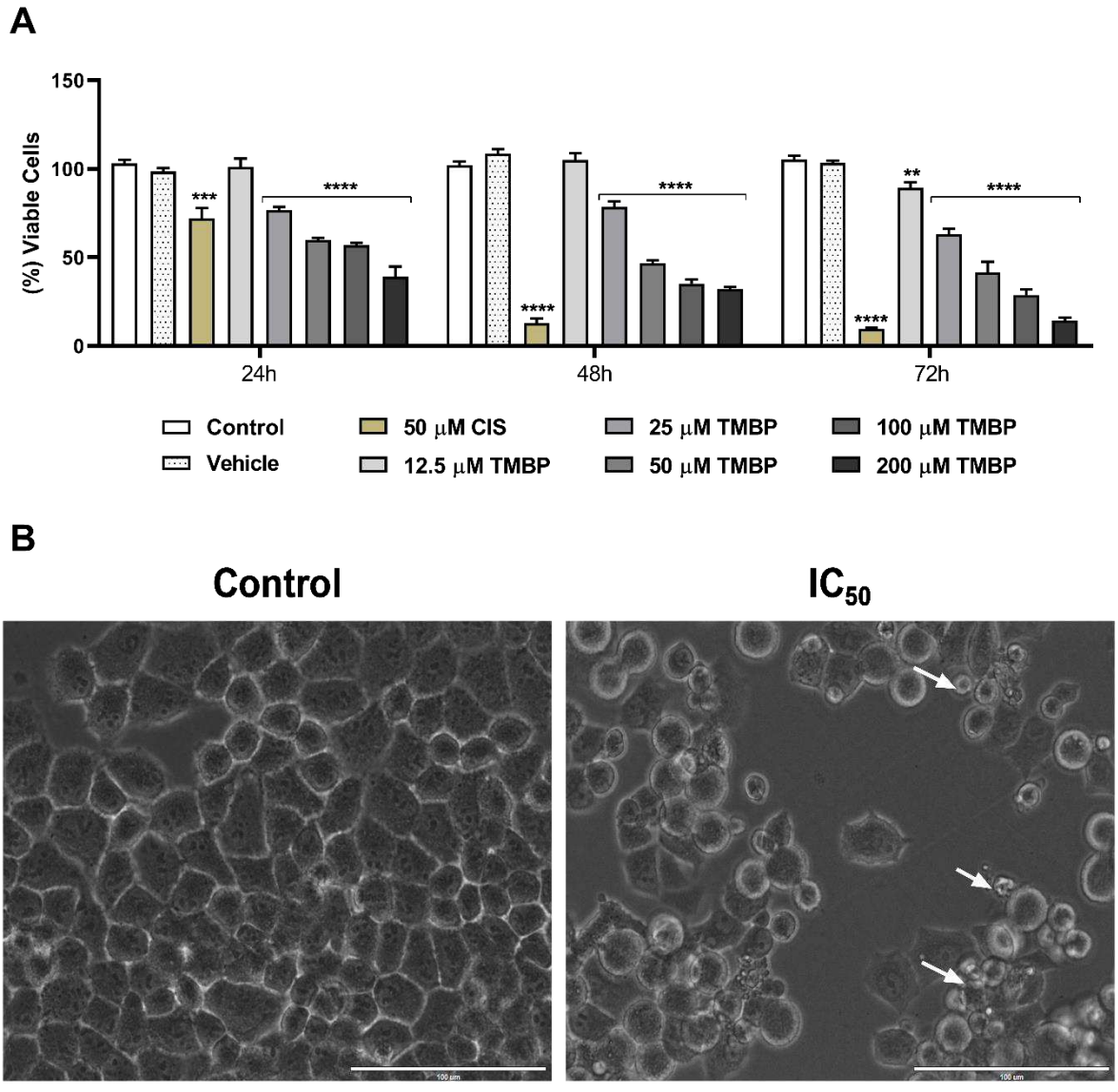

Figure 1: TMBP reduced the viability of the human cancer cell line NCI-H460 at different concentrations. NSCLC cells were treated with TMBP for 24, 48, and 72 h. The relative survival rate (**A**) was determined by the MTT test. After determining the half-maximal inhibitory concentration (IC_{50}) of TMBP, representative images were taken by light microscopy

(1000×) (**B**). Blebbing around the cells (white arrow). Values are expressed as mean ± SEM. Significant difference with $^{**}p \leq 0.01$, $^{***}p \leq 0.001$ and $^{****}p \leq 0.0001$ vs. control; vehicle (DMSO 0.06%); CIS, cisplatin. Scale bar = 100 µm.

Table 1: The half-maximal inhibitory concentration **(**IC_{50}) in lung cancer NCI-H460 cell line after TMBP treatment for 24-72 h.

	IC_{50} (± SEM)		
Cell Type	**24 h**	**48 h**	**72 h**
NCI-H460	152 µM (± 0.07)	73 µM (± 0.03)	42 µM (± 0.03)

IC_{50} – Half-maximal inhibitory concentration; SEM – standard error of the mean.

3.2 TMBP induces morphological changes in NCI-H460 cell line

SEM was used to determine the morphological changes induced by TMBP treatment in the NCI-H460 cell line. Untreated cells (**Fig. 2 A, B**) showed normal characteristics such as firm adherence to the substrate, intact cell membrane, presence of lamellipodia, filopodia, microvilli throughout the cell surface, and well-preserved structures. Cells treated with IC_{50}-TMBP, however, showed rounded shapes, reduction of lamellipodia, irregular cell surface, and absence and/or reduction of microvilli. TMBP treatment induced a reduction in cell surface blebbing, indicating the release of large oncosomes; a type of extracellular vesicle characteristic of cells with a more aggressive profile and metastatic potential (**Fig. 2 C-F**). Our data demonstrated that in addition to reducing proliferation, TMBP treatment was also able to alter the morphology of the cells, contributing to their inability to move and reducing malignancy.

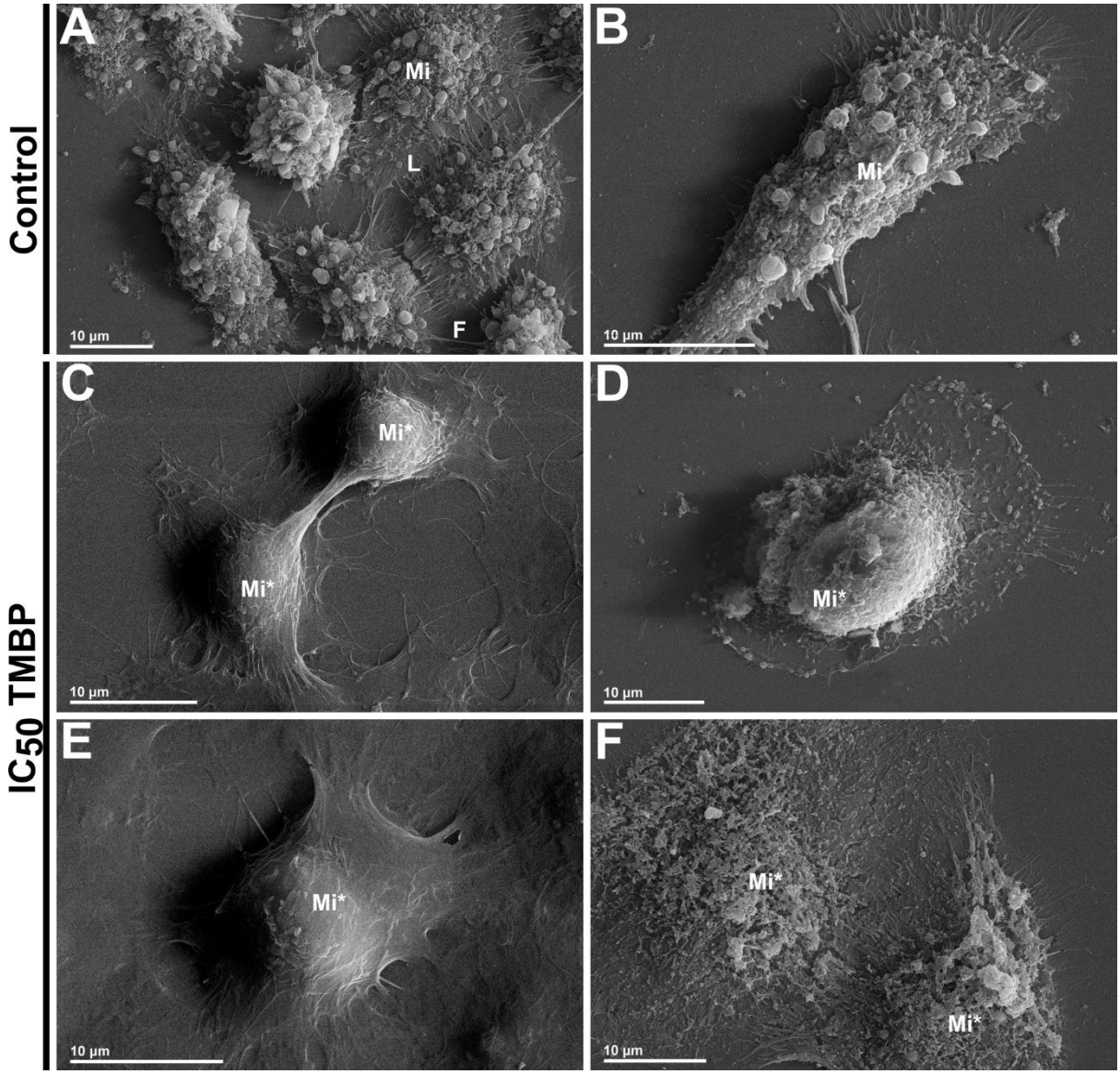

Figure 2: Effect of TMBP treatment on the morphology of NCI-H460 cells. Morphological changes were observed by scanning electron microscopy after treatment with TMBP for 24 h. (**A-B**) Control, untreated cells; (**C-F**) cells treated with IC_{50} of TMBP (152 µM). (Mi) microvilli, (Mi*) microvilli alterations, (L) lamellipodia and (F) filopodia. Scale bars = 10 µm (A-F).

3.3 TMBP treatment reduces migratory capacity and N-cadherin/β-catenin markers in the NCI-H460 cell line

The effect of IC_{50}-TMBP treatment on the migratory potential of NCI-H460 cells was assessed using the *in vitro* wound healing assay (**Fig. 3**). The filling of the scratched area by migrating cells was monitored at regular time intervals (0, 12, and 24 h) and illustrated by representative images (**Fig. 3A**). Quantitative analysis concerning the time traveled revealed

that in the control group, cells migrated to the wound site, however, those that received TMBP treatment showed an increase in the scratched area in comparison to time 0 h ($p < 0.0001 \pm 0.29$) (**Fig. 3 B-C**). Corroborating these data, after 24 h of treatment with IC_{50} of TMBP, we observed reduced levels of fluorescence intensity of β-catenin ($p < 0.0001 \pm 1.22$) and N-cadherin ($p < 0.0001 \pm 1.56$) compared to the untreated group (**Fig. 3 D-F**).

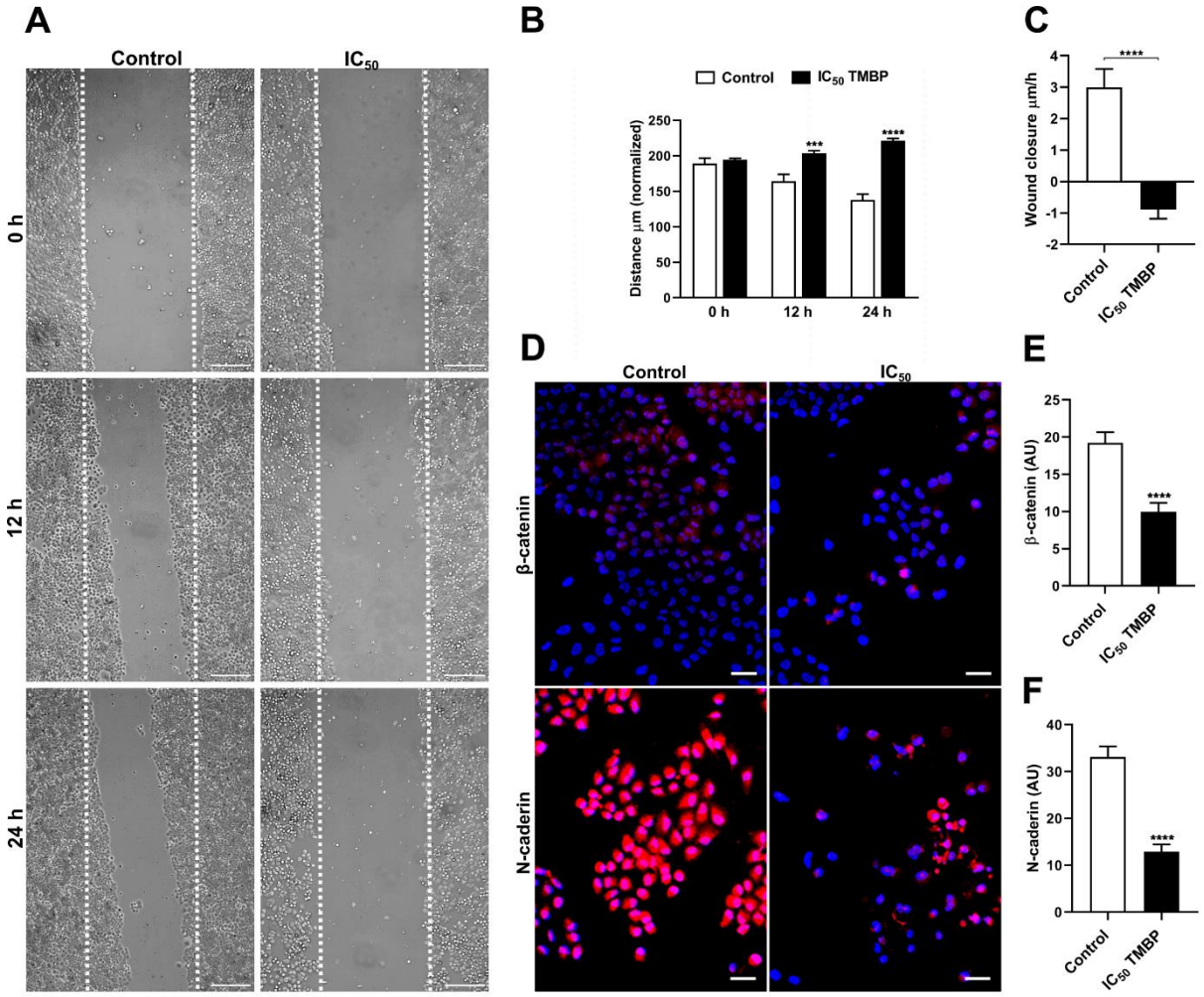

Figure 3: TMBP treatment inhibited NCI-H460 cell migration, with cell retraction and reduced N-cadherin and β-catenin staining. A scratch assay was performed to observe the effect of treatment on cell migration over time (0, 12 and 24 h) (**A**). The distance of the free surface of these treated cells (**B**) was quantified. The time taken by the cells to reach the wound site was also quantified (**C**). Immunofluorescence staining of TMBP-treated and control cells to show reduced β-caternin (red) and N-cadherin (red) presence after 24 h (**D**) (scale bar 2µm). (**E-F**) quantification of fluorescence intensity using Image J software. Values represent the mean ± SEM of three different experiments performed in triplicate. Significant difference versus control ***$p \leq 0.001$ and ****$p \leq 0.0001$. Scale bars = 200 µm (A) and 20 µm (D).

3.4 TMBP induces oxidative stress in the NCI-H460 cell line by a ROS/NO-dependent process

ROS production in TMBP-treated cells was analyzed by fluorescence. **Figure 4B** demonstrated that exposure of cells to TMBP resulted in a 2-fold increase in fluorescence intensity compared to the control ($p < 0.0001 \pm 0.09$). The antioxidant N-acetyl cysteine (NAC) was used to confirm the elevation of ROS. The addition of NAC effectively blocked TMBP-induced ROS in NCI-H460 cells and restored viability (**Fig. 4 A, B**). In the same way, when the levels of NO post-treatment with TMBP were evaluated, an increase of 80% ($p < 0.0001 \pm 0.041$) levels of this mediator was observed. The addition of L-NAME, a nitric oxide synthase (NOS) inhibitor, restored these levels and cell viability (**Fig. 4 A, C**).

Superoxide anion radical ($O_2^{\bullet -}$) is one of the most frequently generated ROS in the cell and can react with other molecules to form potent reactive species, such as peroxynitrite, or be dismutated by SOD to produce O_2 and H_2O_2 [27,28]. After treatment of the cells with TMBP, we observed reduced $O_2^{\bullet -}$ levels (**Fig. 4D**) and increased SOD activity (**Fig. 4E**). Furthermore, a reduction of the antioxidant GSH (**Fig. 4F**) (which is essential for ROS detoxification) was also observed. These results suggest that TMBP reduces NCI-H460 cell viability mediated by increasing levels of ROS/NO molecules.

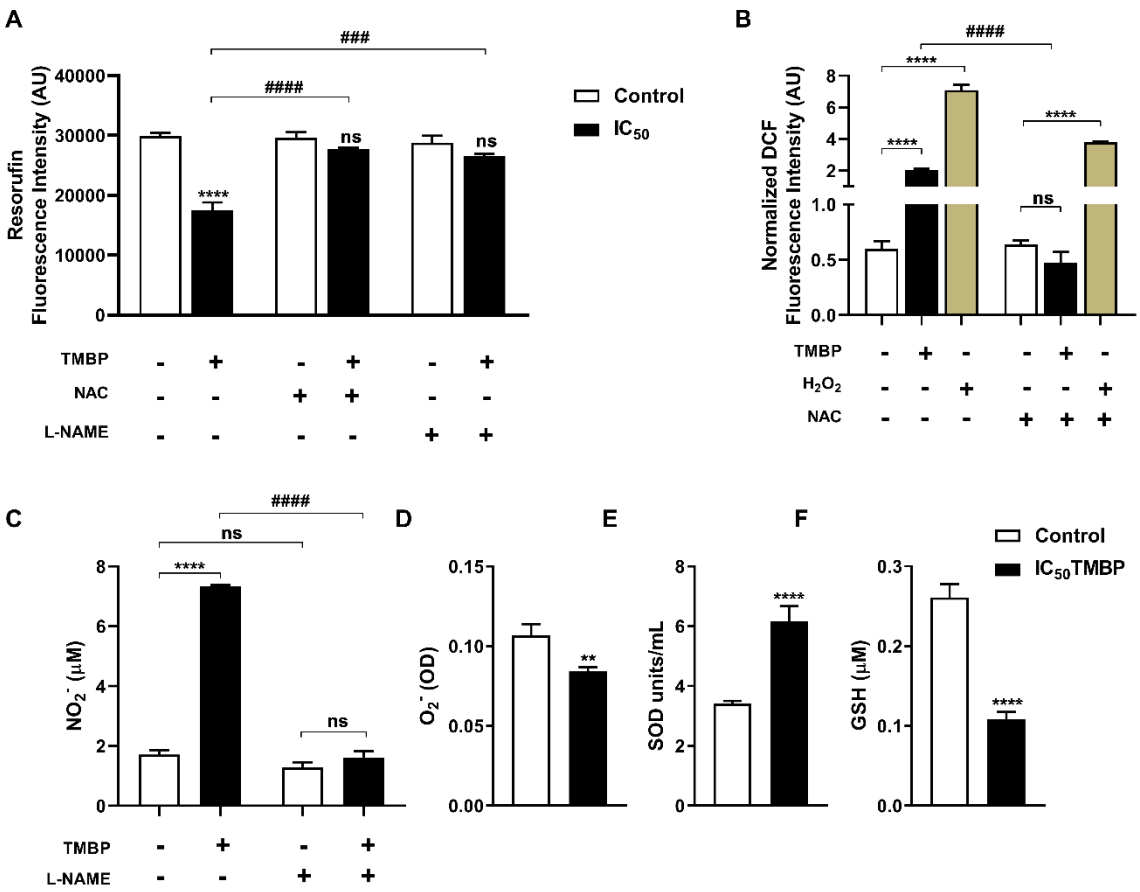

Figure 4: TMBP treatment induced oxidative stress in NCI-H460 cells. The viability of cells treated with IC_{50} of TMBP was assessed by resazurin in the presence or absence of NAC or L-NAME (**A**). ROS levels were assessed with H_2DCFDA in the presence or absence of NAC (**B**). Nitric oxide was determined after TMBP treatment in the presence or absence of L-NAME (**C**). Superoxide radical anion was determined using NBT (**D**). SOD and GSH activity were also determined after TMBP treatment (**E-F**). Data are expressed as mean ± SEM of 3 independent experiments performed in triplicate. ns not significant; ** ($p < 0.01$); **** ($p \leq 0.0001$) vs. control. ### ($p \leq 0.001$) and #### ($p \leq 0.0001$) treatment differences.

3.5 TMBP promotes metabolic changes in NCI-460

To assess cellular metabolism, we first examined glucose levels after TMBP treatment of NCI-H460 cells. We observed a reduction in glucose uptake compared to untreated cells ($p \leq 0.0001$) (**Fig. 5A**). When LDH (which is crucial for converting pyruvate to lactate and vice versa) enzyme activity was assessed, there was a significant 70% increase in extracellular levels and a 65% decrease in intracellular levels ($p > 0.0001$; both activities), indicating cellular damage (**Fig. 5 B-C**). The levels of lactate (a glucose metabolite of aerobic glycolysis) also

decreased compared to the control, with concentrations of 80 mg/dL in the control group and 10 mg/dL in the TMBP-treated groups ($p > 0.0001$) (**Fig. 5D**).

The mitochondrial membrane was examined in NCI-H460 cells after treatment with IC_{50} of TMBP. A decrease in TMRE fluorescence intensity was observed, indicating a loss of mitochondrial activity ($p \leq 0.01$) (**Fig. 5E**). Excess intracellular lipids can be stored in lipid droplets (LDs) to prevent lipotoxicity. During nutrient deprivation, fatty acids are released from LDs for energy production through mitochondrial β-oxidation and the Krebs cycle apoptosis (Cruz et al., 2020). In our results, TBMP treatment induced and increased the level of LD accumulation compared to the control ($p \leq 0.0001$) (**Fig. 5F**). In addition, we investigated whether treating cells with IC_{50} of TMBP would affect autophagy. We found that the treated group increased the fluorescence intensity, indicating the formation of autophagic vacuoles in NCI-H460 cells ($p \leq 0.0001$) (**Fig. 5G**).

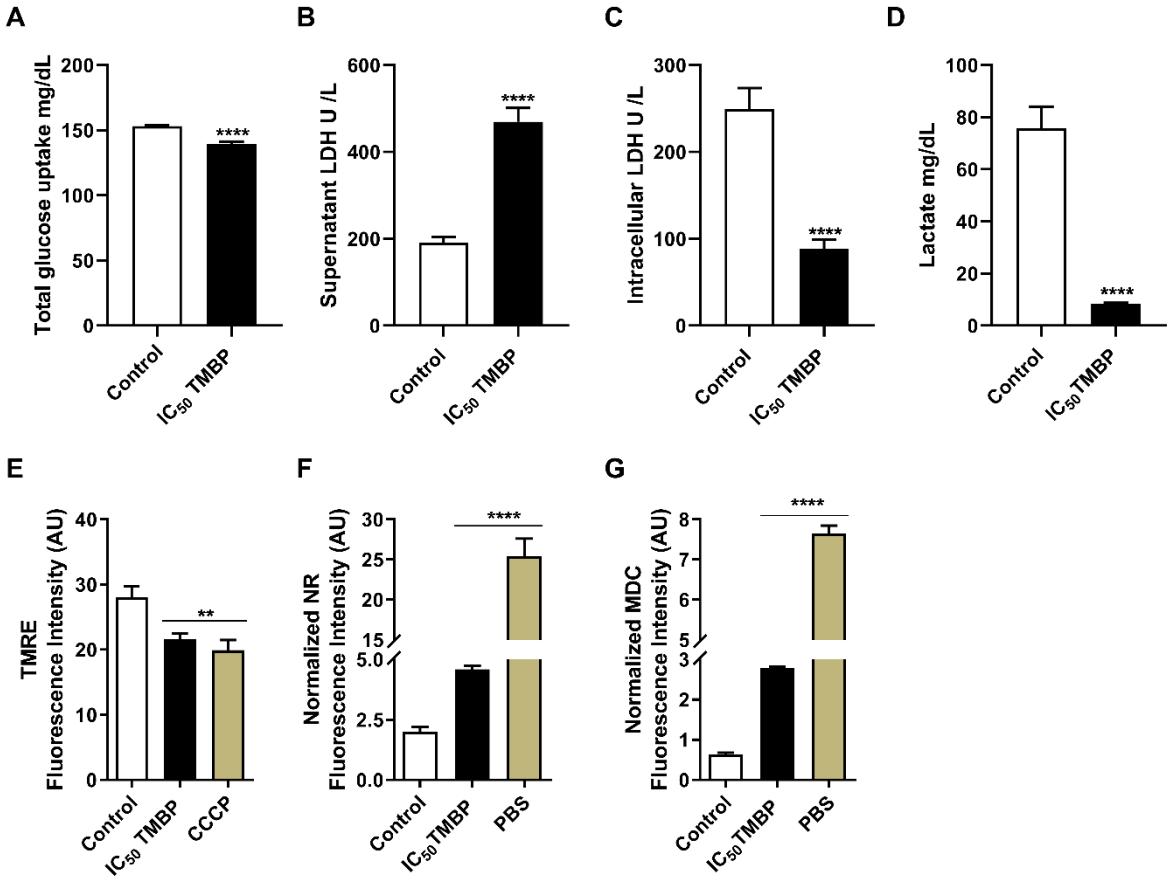

Figure 5: TMBP treatment induced metabolic stress in NCI-H460 cells. Cells were treated with TMBP for 24 h. (**A**) extracellular glucose uptake; (**B** and **C**) extracellular and intracellular LDH activity, respectively; and (**D**) intracellular lactate level. ΔΨm (**E**), lipid droplets (**F**), and autophagic vacuoles (**G**) were quantified by fluorescence. Data are expressed as mean ± SEM

525 of 3 independent experiments, each performed in triplicate. ** ($p < 0.01$); **** ($p \leq 0.0001$)
526 vs. control. CCCP, carbonylcyanide *m*-chlorophenylhydrazone; PBS, phosphate-buffered
527 saline
528
529 **3.6 TMBP induces structural changes in the NCI-H460 cell line**
530 Ultrastructural evaluation by TEM showed that the control group displayed a
531 homogeneous cytoplasm with regular organelles (mitochondria and endoplasmic reticulum)
532 and without the presence of vacuole-like structures, indicating cellular integrity (**Fig. 6 A-B**).
533 After TMBP treatment, changes in mitochondrial structures were observed, such as swelling
534 and enlargement of these organelles (m*) (**Fig. 6 C-E**). These changes were consistent with the
535 data presented above and indicated that mitochondria were damaged. In addition, an intense
536 accumulation of lipid storage droplets (*) and autophagic vacuoles (white arrow) were observed
537 (**Fig. 6 C, D, F**). Furthermore, the absence of microvilli, filopodia, and lamellopodia (black
538 arrowhead) were also observed (**Fig. 6 D-F**).

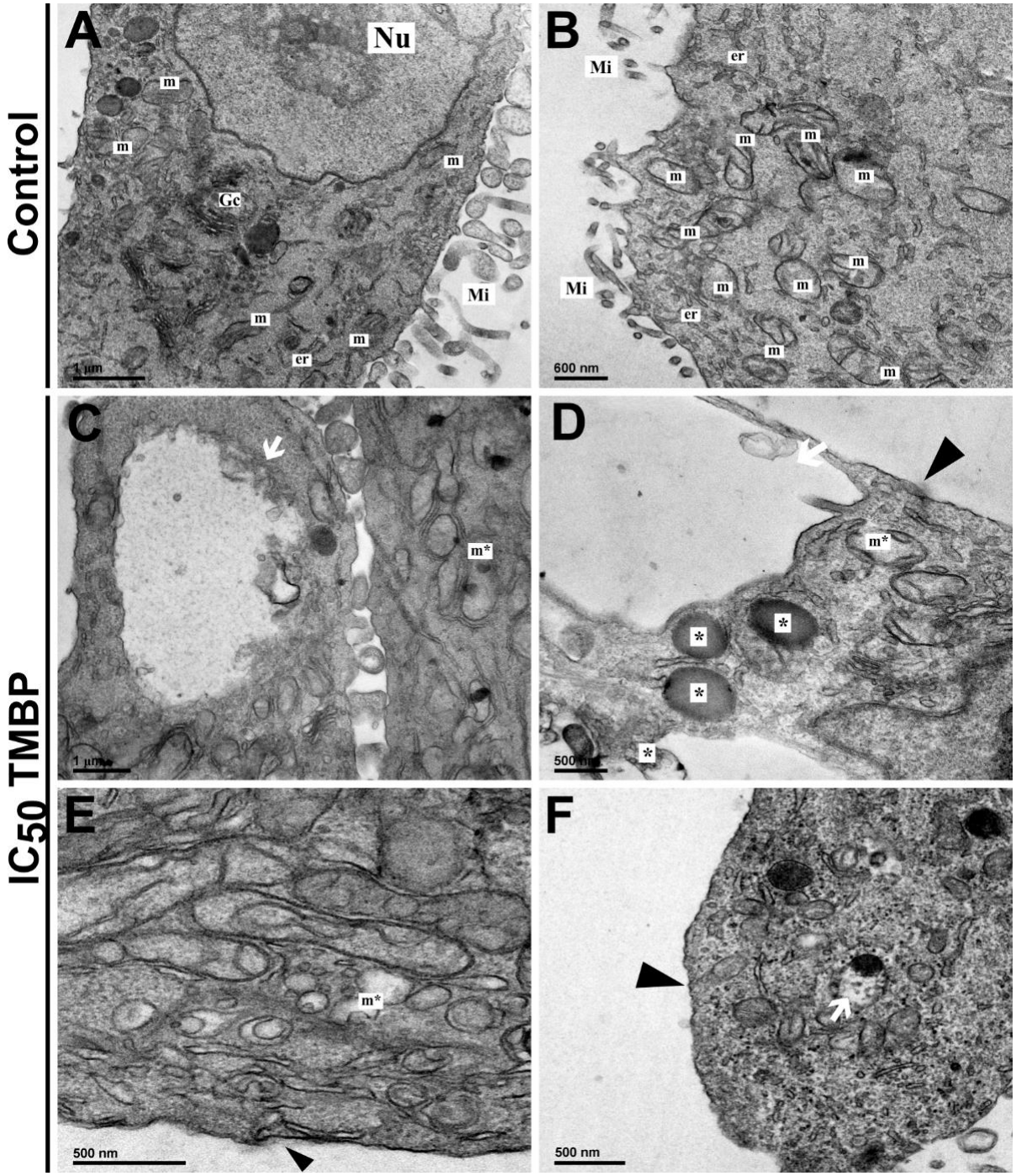

Figure 6: Ultrastructural changes in NCI-H460 cells treated with TMBP for 24 h and analyzed by transmission electron microscopy. (**A-B**) untreated cells; (**C-F**) cells treated with IC_{50} TMBP (152 µM); (m) mitochondria; (Gc) Golgi complex; (er) endoplasmic reticulum; (m*) mitochondrial swelling; (Nu) nucleus; (white arrow) cytoplasmic autophagic vacuole (black arrowhead) absence of microvilli; (*) lipid droplets storage areas. Scale bars = 1 µm (A, C), 600 nm (B) and 500 nm (D-F).

3.7 TMBP promotes cell cycle arrest in the G2/M phase and apoptosis via caspase-3/STAT-3

Analysis of cell cycle distribution also revealed a reduction in the G1 and S phases (51.1% ± 0.86 and 9.5% ± 1.40, respectively) and an accumulation of cells in the G2/M phase (52.7% ± 1.31) (**Fig. 7 A-B**). **Figure 7 C-D** shows that TMBP-treated cells promoted reduced cell viability by 49.75% (± 0.72), increased annexin (24.7% ± 0.85), and co-marking (annexin/PI) (25.15% ± 0.22) compared to the control, indicating cell death by an apoptosis-like process. This was confirmed by the increase in caspase-3/7 activity observed in these cells (**Fig. 7E**). Also, when evaluated by immunofluorescence the signal transducer and activator of transcription 3 (STAT-3), a reduction of this protein was observed in cells treated with TMBP ($p \leq 0.0001$) (**Fig. 7F-G**). In contrast, higher staining was observed in the untreated group. These data show that TMBP promoted metabolic damage that disrupted mitosis and progression leading to cell death.

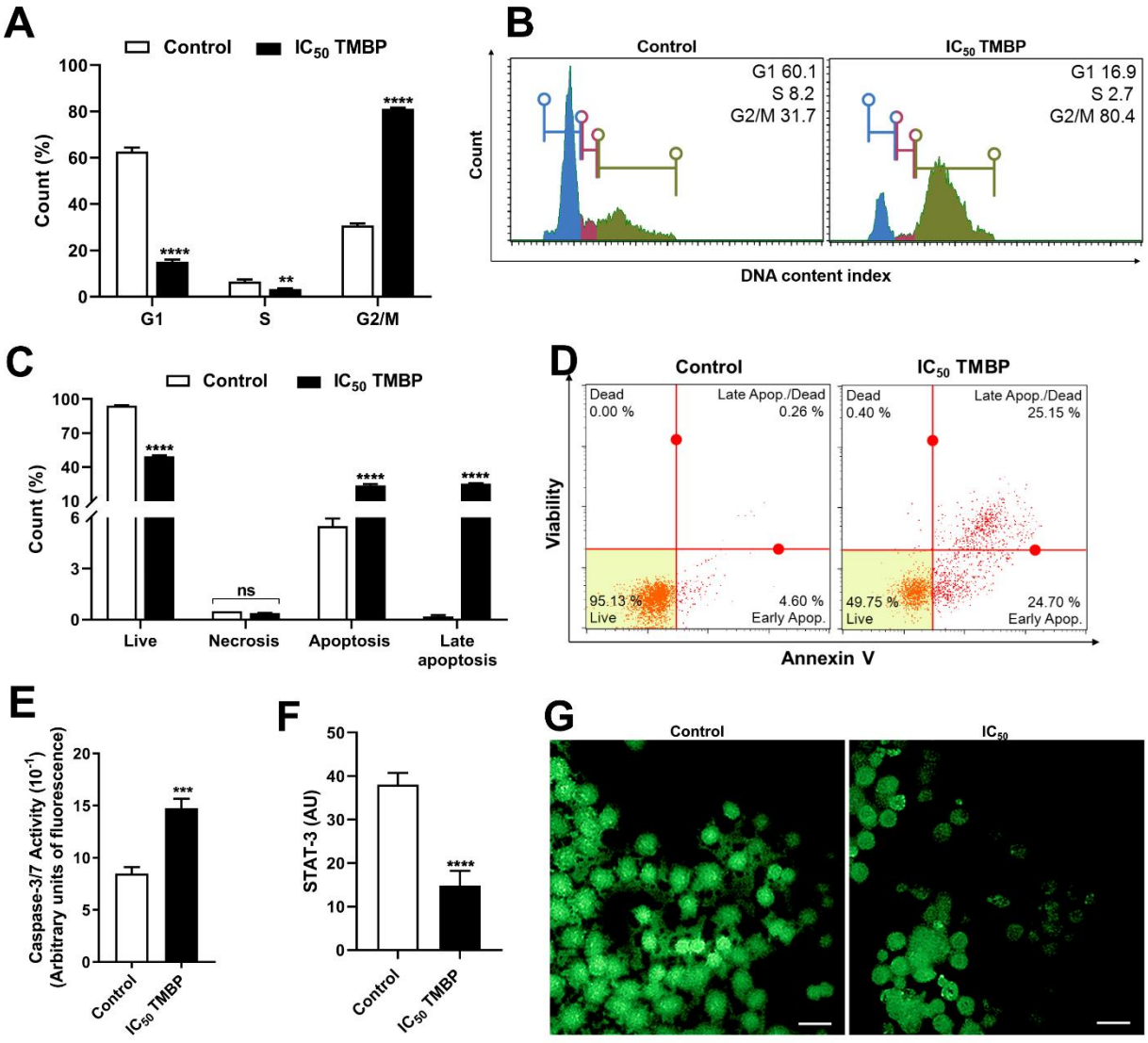

Figure 7: TMBP treatment induced cell cycle arrest in the G2/M phase, apoptosis, and reduced STAT-3 immunofluorescence staining in NCI-H460 cells. Cells were treated with IC_{50} of TMBP for 24 h and cell cycle distribution and histogram were quantified (**A**) and analyzed (**B**), respectively by flow cytometry. Quantitative analysis of viable, apoptotic, and necrotic NCI-H460 cells was evaluated in 24 h (**C**). For analysis in dot plots of cytometry, the induction of viable cells, apoptosis, and necrosis were evaluated for 24 h (**D**). Caspase 3/7 was quantified by fluorescence (**E**). Immunofluorescence staining of TMBP-treated and control cells to show reduced STAT-3 presence (green) after 24 h (**F-G**). Values are expressed as mean ± SEM. Cytometry data are expressed as percentage vs. control; and mean ± standard deviation. $p \leq 0.01$; ***p ≤ 0.001; ****$p \leq 0.0001$ vs. control. Scale bars = 20 μm (G).

3.8 TMBP acts on the PI3K/AKT/NF-κB pathway and activates iNOS mediated pro-oxidant profile in NCI-H460 tumor cell line

The PI3K/AKT signaling pathway is frequently activated in cancer as it is involved in the regulation of proliferation, survival, inhibition of apoptosis, and cell invasion [34]. These proteins were therefore evaluated by ELISA after treatment with TMBP (**Fig. 8**). A decrease in PI3K ($p \leq 0.01$) and an increase in total AKT ($p \leq 0.0001$) were observed. The pAKT ($p \leq 0.01$) phosphorylated activated form, however, decreased.

After treatment with TMBP, we observed reduced levels of arginase-1 (ARG-1) ($p < 0.05$) and increased levels of inducible nitric oxide synthase (iNOS) ($p \leq 0.01$). Next, nuclear factor *kappa* B (NF-κB) was evaluated after treatment with TMBP. We observed a decrease in total NF-κB protein levels ($p \leq 0.01$) and its activated phosphorylated form (pNF-κB) ($p \leq 0.04$). Furthermore, when the nuclear factor erythroid 2 related factor 2 (Nrf2) was analyzed, we found that its levels did not significantly differ from the control group ($p > 0.05$).

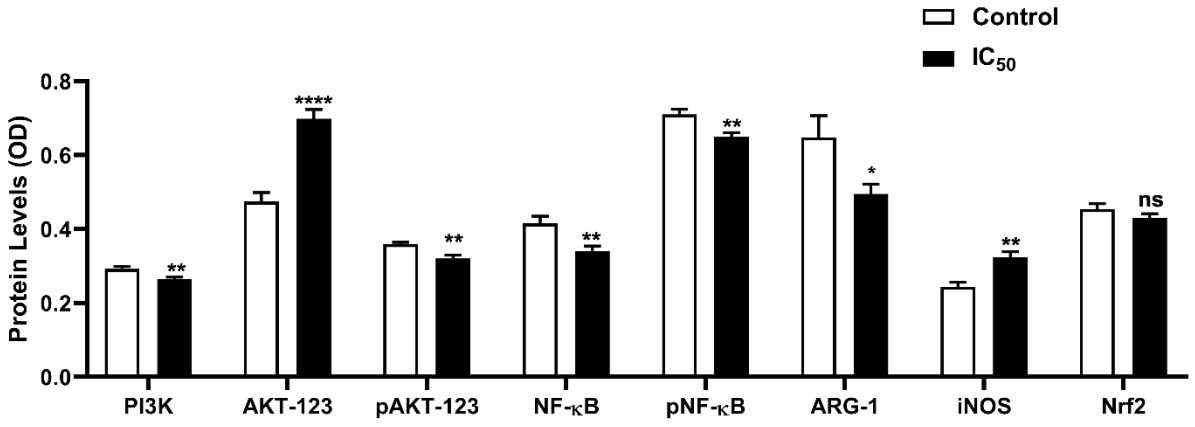

Figure 8: Evaluation of intracellular signaling mediators involved in the pathogenesis of lung cancer cells. ELISA measurement of PI3K, AKT, pAKT, ARG-1, iNOS, NF-κB, pNF-κB and Nrf2 levels, expressed as the natural logarithm of absorbance. White bars represent untreated NCI-H460 cells, while black bars represent 24-h TMBP-treated cells. Values represent the mean ± SEM. * ($p < 0.05$); ** ($p \leq 0.01$); **** ($p \leq 0.0001$); ns (not significant).

4. Discussion

Chemoresistance is a common feature and a major cause of treatment failure in NSCLC, leading to tumor recurrence and disease progression. This ability is associated with most available drugs, including cisplatin. The main factors associated with cisplatin resistance are reduced accumulation and inactivation of the drug by binding to various proteins, increased DNA repair, and alteration of various proteins signaling apoptosis [35–37]. In this context, there is a growing interest in microbial biotransformation of drugs and natural products with antitumor activity. This process allows the modification of the relevant chemical molecules, generating new compounds that may be more effective and less toxic. In addition, it is possible to take advantage of the mild conditions under which the reactions take place, with most transformations occurring at temperatures between 20°C and 40°C and with aqueous solvents. Although yields are sometimes limited, several options for biological reagents can be manipulated through mutants, aeration, temperature, and culture medium to improve these results [38, 39]. Thus, the development of therapeutic strategies that are effective in eliminating aberrant cells and preventing malignant growth is of great interest as it may can expand the possibilities of new approaches for therapeutic applications.

In a previous study, we demonstrated that TMBP exhibited direct cytotoxic effects on the A549 cell line. In addition, *in silico* predictions have shown promising drug-likeness potential for TMBP, indicating high oral bioavailability and intestinal absorption [19]. For the first time, the present study provides new insights into the type of cell death induced by TMBP against the NCI-H460 cell line, demonstrating anti-proliferative activity, metabolic and structural changes (reduced lamellipodia, filopodia, microvilli, and release of large oncosomes). A series of biochemical processes showed that TMBP acts by producing ROS and NO that potentially lead to cell death. Furthermore, TMBP treatment of the cell line reduced protein levels of PI3K/pAKT/ARG-1/pNF-κB and increased iNOS, which may favor increased oxidative stress and promote death in these tumor cells. The significance of our *in vitro* findings is reinforced by the fact that key components of the TMBP-mediated pathway described have

identified cellular self-destruction in lung cancer, and may lead to improved oncotherapy.

Cell proliferation and migration are considered an essential and regulated behavior in several normal physiological processes, such as morphogenesis, embryogenesis, immune cell responses, angiogenesis, tissue repair, cell differentiation, and tissue regeneration [40]. In cancer, cell migration, invasion, and adhesion are phenomena that determine cell plasticity and epithelial-mesenchymal transition (EMT). During the process of EMT, which involves the transformation of cancer cells from a non-motile epithelial phenotype to a migratory mesenchymal-like phenotype, several changes occur in the markers expression. Epithelial markers such as E-cadherin, α-catenin, and β-catenin are downregulated, while mesenchymal markers like N-cadherin and vimentin are upregulated. This transition closely correlates with increased cell migration and invasion, contributing to cancer progression [41–43].

It is worth noting that in the context of cancer, the stabilization of β-catenin and its subsequent translocation into the nucleus can promote cancer progression, cell proliferation, and metastasis [44–47]. By reducing β-catenin levels, the compound TMBP may actually inhibit the pro-metastatic effects associated with β-catenin. Similarly, the decrease in N-cadherin is in line with our hypothesis that TMBP counteracts the EMT process. N-cadherin is typically upregulated during EMT and contributes to cell migration and invasion [44,48–50]. Therefore, the reduction in N-cadherin levels supports the potential anti-metastatic activity of TMBP [51–53]. In addition to its effects on metastasis-related markers, our experimental data demonstrates that TMBP not only reduces cell proliferation but also diminishes the cells' migratory capacity. Moreover, we observed that TMBP decreases cell protrusion extensions, including lamellipodia and filopodia, as well as microvilli. These observations suggest that TMBP interferes with cell locomotion by altering their invasive morphology, leading to reduced actin filament content, which subsequently impacts their motility and cell-cell adhesion.

Oxidative stress is defined as an excess of oxidants over antioxidant activity and leads to many diseases. Understanding the role of oxidative stress in cancer pathophysiology is necessary since these biomolecules impact the whole organism. Regulation of the redox state in a normal environment is critical for cellular maintenance, including viability, proliferation, and metabolism. Cells generate ROS and reactive nitrogen species (RNS), as an unavoidable consequence of physiological processes and for intracellular signaling. The major components comprising ROS are superoxide radical anion ($O_2^{\bullet-}$), hydroxyl radical ($OH^{\bullet}$), and hydrogen peroxide (H_2O_2). The main site of $O_2^{\bullet-}$ production is the mitochondria, which are used for energy production and result from the process of OXPHOS. Superoxide anion radical can be dismutated spontaneously to H_2O_2 or by the action of SODs, mainly SOD2. H_2O_2 can be

653 catalytically converted to H_2O and O_2 by catalase, peroxiredoxins (PRDXs), and glutathione
654 peroxidases (GPXs). GPXs require glutathione (GSH); reducing the levels of H_2O_2. Superoxide
655 radical anion can also react with H_2O_2 to form OH•, a highly reactive radical that can damage
656 proteins, lipids, carbohydrates, and DNA [54–56]. It should also be noted that when SOD2
657 activity is increased, proliferating cells go into quiescence, *i.e*. they do not multiply, but remain
658 metabolically active, resulting in increased H_2O_2 activity [57].
659 Nitric oxide (NO) and peroxynitrite anion ($ONOO^-$) are the major RNS. GSH is highly
660 abundant in all cellular compartments and is the main soluble antioxidant and determinant of
661 oxidative stress. GSH also contributes to the scavenging of NO, the reduction of $ONOO^-$ and
662 the denitrosylation of proteins. Thus, $O_2•^-$ and $ONOO^-$ are highly reactive species that can
663 damage intracellular macromolecules, including polyunsaturated fatty acids and nucleic acids
664 [58, 59]. Therefore, in our study, TMBP was able to reduce cancer cell viability via a ROS- and
665 NO-dependent mechanism. Furthermore, TMBP treatment caused a reduction in $O_2•^-$ levels,
666 increased SOD2 activity, and decreased GSH, suggesting that the highly unstable superoxide
667 radical anions may be converted to peroxynitrite and/or hydroxyl radical.
668 Cancer cells exhibit aberrant metabolism, which is used to maintain their vital functions.
669 This leads to the activation of pro-tumorigenic signaling, increased cell proliferation, migration,
670 invasion, inhibition of apoptosis, therapeutic resistance, progression, and other aggressive
671 features. Therefore, when cancer cells are presented with a high demand for oxidative stress,
672 they initiate the process of adaptation in order to mitigate the damage and escape death [60, 61].
673 Another prominent feature is the Warburg effect, which refers to the metabolic shift in cancer
674 cells from OXPHOS to aerobic glycolysis. This glycolytic shift leads to a dramatic increase in
675 glucose uptake and consequent lactate production, which are essential in providing substrates
676 for cancer cells to sustain a high rate of proliferation [62–64]. Furthermore, glucose metabolism
677 is a hallmark of NSCLC [65, 66].
678 In addition to glycolysis, mitochondrial function, lipid biogenesis, and autophagy,
679 although essential in physiological processes, also play a critical role in cancer development by
680 providing cells with considerable flexibility, such as changes in utilization and energy supply,
681 and oxidative stress management. It has also been reported that when these processes become
682 irreparably damaged, the cell tends to undergo apoptosis [67–74]; [29–33]. In our study, we
683 observed that TMBP treatment of NCI-H460 cells was capable of reducing glucose and lactate
684 consumption, indicating that the cancer cells were under metabolic stress. We also found that
685 TMBP altered mitochondrial function, as demonstrated by [19], suggesting that the cells were
686 damaged, as confirmed by the intra- and extra-cellular LDH levels. Additionally, TMBP

687 treatment increased lipid droplets and autophagic vacuoles; indicative of a metabolic stress
688 profile, as confirmed by the TEM images. Taken together, these data suggest that TMBP-treated
689 NCI-H460 cells were damaged and initiated a process of metabolic stress in an attempt for the
690 cells to regain viability.

691 Controlling or terminating the uncontrolled growth of cancer cells using their own death
692 mechanism is a highly effective method of treating cancer. Apoptosis is an essential event in
693 the regulation of a wide range of physiological cellular processes. However, dysfunction of the
694 apoptotic machinery is implicated in many diseases, particularly cancer. Failure to activate the
695 apoptotic pathway can lead to chemotherapeutic resistance, tumor recurrence, and cell
696 migration [75, 76]. DNA damage, cellular and metabolic stress are known triggers of cell death
697 by apoptosis or senescence that can eliminate dysfunctional and dangerous conditions in cells.
698 According to our data, TMBP was able to induce cell cycle arrest, culminating in apoptosis
699 with activation of caspase-3 and -7. The functions of these proteases in apoptosis overlap,
700 although they have different functions [77], with caspase-3 controlling DNA fragmentation and
701 morphological changes, while caspase-7 is associated with loss of cell viability [78,79]. TMBP
702 treatment was also able to reduce STAT-3 protein immunolabeling, which favors reduced
703 migration, invasion, and metastasis.

704 Another important transcription factor involved with the evolution of neoplastic cells is
705 NF-κB, which manifests a response against invading pathogens, and also promotes a metabolic
706 switch to glycolysis and controls the tumor microenvironment in several types of cancer [80].
707 Furthermore, NF-κB communicates with PI3K/AKT signaling to promote the survival and
708 proliferation of lung cancer cells [81]. The PI3K/AKT/mTOR pathway represents an attractive
709 target for novel anticancer therapies in NSCLC, as it is also involved in the regulation of cell
710 growth, metabolism, and resistance to therapeutic agents [34]. Judging from our data, TMBP
711 was able to act on this pathway by reducing the levels of PI3K/AKT/NF-κB.

712 Another molecule of interest in cancer is the enzyme ARG-1, which has been implicated
713 in cancer progression through several signaling pathways. ARG-1, when positively regulated,
714 increases the levels of phosphorylated AKT and ERK, leading to cancer cell viability and
715 proliferation. In addition, phosphorylated STAT-3 binds directly to the promoter region of
716 ARG-1, promoting a more aggressive cancer condition. Moreover, there is evidence that
717 patients with NSCLC have high plasma levels of ARG-1, which may be a promising target for
718 clinical use. ARG-1 may also regulate cellular NO production by competing with iNOS for the
719 substrate L-arginine. When produced by M2-type macrophages, ARG-1 can modulate NO
720 production and promote tissue repair and remodeling, production of collagen and other

components of the extracellular matrix. However, when iNOS metabolizes arginine to L-citrulline and NO, the latter at high concentrations (μM range) induce cellular cytotoxicity, DNA damage, nitrosation/oxidative stress, and apoptosis [82]. Thus, TMBP treatment was able to decrease ARG-1 levels and increase iNOS in NCI-H460 cells.

The effective response of TMBP against the NCI-H460 tumor cell line was due to the reduction in cell proliferation, invasive and metastatic activity, and induced morphological and ultrastructural changes in the lung cancer cells by increasing toxic mediators as oxidative species and metabolic stress, leading to a resolution of the tumor environment.

5. Conclusion

The development of therapies is a recent research trend as these are capable of reducing side effects and can improve efficacy. The use of the biotransformed compound TMBP in lung cancer has not been reported, and our study is the first to evaluate the effect of TMBP treatment on the viability of lung cancer cells and its biological mechanism and focused on the development of cell growth and apoptosis. TMBP was capable of reducing proliferation, migration, and invasion, as well as morphological and ultrastructural changes in NCI-H460 cells. TMBP treatment increased oxidative stress parameters and induced metabolic changes culminating in apoptotic death. TMBP negatively regulated proliferation-related proteins such as PI3K/AKT/NF-κB/ARG-1 and positively regulated the pro-oxidant profile mediated by the iNOS pathway.

Considering that non-small cell lung cancer (NSCLC) encompasses diverse histological subtypes, including large cell carcinoma, squamous cell carcinoma, adenocarcinoma, and adenosquamous carcinoma, our study focuses primarily on the NCI-H460 large cell carcinoma cell line and the A549 adenocarcinoma cell line, as indicated by previous research (Concato et al., 2020). These results suggest the potential broad-spectrum efficacy of TMBP against various lung cancer cells. However, it is essential to emphasize that additional investigations in different NSCLC cell lines are imperative to confirm these findings.

In light of these promising outcomes, compounds with the ability to induce cancer cell death are potential candidates for oncotherapy. Future studies should deeper into exploring the potential tumor-suppressing effects of TMBP, thereby advancing our understanding and potentially contributing to the development of novel therapeutic approaches for lung cancer.

Acknowledgments

This work was supported by the Coordenação de Aperfeiçoamento de Pessoal de Nível Superior (CAPES, Brazil), Conselho Nacional de Pesquisa (CNPq, Brazil), Financiadora de Estudos e Projetos (FINEP) and Universidade Estadual de Londrina (UEL, Brazil).

Funding

Not applicable.

CReditT Contributions

Virginia Marcia Concato: Conceptualization; Data curation; Formal analysis; Investigation; Methodology; Roles/Writing - original draft. **Taylon Felipe Silva:** Conceptualization; Formal analysis; Investigation; Resources; Methodology; Roles/Writing - original draft. **Mariana Barbosa Detoni:** Conceptualization; Data curation; Formal analysis; Investigation; Methodology; Roles/Writing - original draft. **Ellen Mayara Souza Cruz:** Data curation; Formal analysis; Investigation; Methodology. **Manoela Daiele Gonçalves:** Data curation; Formal analysis; Investigation; Resources; Methodology. **Bruna Taciane da Silva Bortoleti:** Data curation; Formal analysis; Investigation; Resources; Methodology. **Fernanda Tomiotto-Pellissier:** Formal analysis; Investigation; Resources; Methodology. **Ana Carolina Jacob Rodrigues:** Formal analysis; Investigation; Resources; Methodology. **Amanda Cristina Carloto:** Formal analysis; Investigation; Resources; Methodology. **Maria Beatriz Madureira** Investigation; Methodology. **Jéseka Gabriela Schirmann:** Formal analysis; Investigation; Resources; Methodology. **Aneli M. Barbosa-Dekker**: Formal analysis; Investigation; Resources; Methodology. **Robert F. H. Dekker:** Data curation; Formal analysis; Investigation; Resources; Methodology; Roles/Writing - original draft. **Ivete Conchon-Costa:** Funding acquisition; Writing - review & editing; Resources. **Carolina Panis:** Methodology; Writing - review & editing. **Danielle Bidóia Lazarin:** Methodology; Writing - review & editing. **Milena Menegazzo Miranda-Sapla:** Writing - review & editing; Data curation; Formal analysis. **Mario Sergio Mantovani:** Data curation; Formal analysis; Investigation; Resources; Methodology; Roles/Writing - original draft. **Wander Rogério Pavanelli:** Funding acquisition; Project administration; Supervision; Validation; Writing - review & editing; Resources. All authors read and approved the final manuscript.

Competing interests

The authors declare that they have no competing interests.

References

[1]Bray F, Ferlay J, Soerjomataram I, Siegel RL, Torre LA, Jemal A. Global cancer statistics 2018: GLOBOCAN estimates of incidence and mortality worldwide for 36 cancers in 185 countries. CA Cancer J Clin 2018;68:394–424. https://doi.org/10.3322/caac.21492.

[2]Schabath MB, Cote ML. Cancer Progress and Priorities: Lung Cancer. Cancer Epidemiol Biomarkers Prev 2019;28:1563–79. https://doi.org/10.1158/1055-9965.EPI-19-0221.

[3]Iglesias VS, Giuranno L, Dubois LJ, Theys J, Vooijs M. Drug Resistance in Non-Small Cell Lung Cancer: A Potential for NOTCH Targeting? Front Oncol 2018;8:267. https://doi.org/10.3389/FONC.2018.00267.

[4]Dasari S, Bernard Tchounwou P. Cisplatin in cancer therapy: molecular mechanisms of action. Eur J Pharmacol 2014;740:364–78. https://doi.org/10.1016/J.EJPHAR.2014.07.025.

[5]Von Nussbaum F, Brands M, Hinzen B, Weigand S, Häbich D. Antibacterial natural products in medicinal chemistry--exodus or revival? Angew Chem Int Ed Engl 2006;45:5072–129. https://doi.org/10.1002/ANIE.200600350.

[6]Rasines-Perea Z, Jacquet R, Jourdes M, Quideau S, Teissedre PL. Ellagitannins and Flavano-Ellagitannins: Red Wines Tendency in Different Areas, Barrel Origin and Ageing Time in Barrel and Bottle. Biomolecules 2019;9. https://doi.org/10.3390/BIOM9080316.

[7]Schirmann JG, Dekker RFH, Borsato D, Barbosa-Dekker AM. Selective control for the laccase-catalyzed synthesis of dimers from 2,6-dimethoxyphenol: Optimization of 3,3',5,5'-tetramethoxy-biphenyl-4,4'-diol synthesis using factorial design, and evaluation of its antioxidant action in biodiesel. Appl Catal A Gen 2018;555:88–97. https://doi.org/10.1016/J.APCATA.2018.02.015.

[8]Schirmann JG, Angilelli KG, Dekker RFH, Borsato D, Barbosa-Dekker AM. 3,3″,5,5″-Tetramethoxybiphenyl-4,4″-diol: A new antioxidant enhancing oxidative stability of soybean biodiesel. Fuel 2019;237:593–6. https://doi.org/10.1016/J.FUEL.2018.10.044.

[9]Gonçalves MD, Tomiotto-Pellissier F, de Matos RLN, Assolini JP, da Silva Bortoleti BT, Concato VM, et al. Recent Advances in Biotransformation by Cunninghamella Species. Curr Drug Metab 2021;22:1035–64. https://doi.org/10.2174/1389200222666211126100023.

[10] Kobayashi A, Koguchi Y, Kanzaki H, Kajiyama I, Kawazu K. Production of a New Type of Bioactive Phenolic Compound. Biosci Biotechnol Biochem 1994;58:133–4. https://doi.org/10.1271/BBB.58.133.

[11] Bang KH, Kim YK, Min BS, Na MK, Rhee YH, Lee JP, et al. Antifungal Activity of Magnolol and Honokiol. Arch Pharm Res 2000;23:46–9. https://doi.org/10.1007/BF02976465/METRICS.

[12] Hawkshaw C, Kiamanesh O, Walton R. The Effects of the Antimicrobial Honokiol on the Intracellular pH of Bacillus subtilis WB746 and Escherichia coli B23. Journal of Experimental Microbiology and Immunology 2008;12:14–20.

[13] Kobayashi A, Koguchi Y, Kanzaki H, Kajiyama I, Kawazu K. Production of a New Type of Bioactive Phenolic Compound. Biosci Biotechnol Biochem 1994;58:133–4. https://doi.org/10.1271/BBB.58.133.

[14] Uta R, François C, Marvin H, Philipp A, Andrea PP, Henrik W, et al. Anti-inflammatory properties of Honokiol in activated primary microglia and astrocytes. J Neuroimmunol 2018;323:78–86. https://doi.org/10.1016/J.JNEUROIM.2018.07.013.

[15] MURAKAMI Y, ISHII H, HOSHINA S, TAKADA N, UEKI A, TANAKA S, et al. Antioxidant and Cyclooxygenase-2-inhibiting Activity of 4,4′-Biphenol, 2,2′-Biphenol and Phenol. Anticancer Res 2009;29.

[16] Ramachandran C, Wilk B, Melnick SJ, Eliaz I. Synergistic Antioxidant and Anti-Inflammatory Effects between Modified Citrus Pectin and Honokiol. Evid Based Complement Alternat Med 2017;2017. https://doi.org/10.1155/2017/8379843.

[17] Hsiao C-H, Yao C-J, Lai G-M, Lee L-M, Whang-Peng J, Shih P-H. Honokiol induces apoptotic cell death by oxidative burst and mitochondrial hyperpolarization of bladder cancer cells. Exp Ther Med 2019;17:4213. https://doi.org/10.3892/ETM.2019.7419.

[18] Huang K, Chen Y, Zhang R, Wu Y, Ma Y, Fang X, et al. Honokiol induces apoptosis and autophagy via the ROS/ERK1/2 signaling pathway in human osteosarcoma cells in vitro and in vivo. Cell Death & Disease 2018 9:2 2018;9:1–17. https://doi.org/10.1038/s41419-017-0166-5.

[19] Concato VM, Tomiotto-Pellissier F, Silva TF, Gonçalves MD, Bortoleti BT da S, Detoni MB, et al. 3,3',5,5'-tetramethoxybiphenyl-4,4'diol induces cell cycle arrest in G2/M phase and apoptosis in human non-small cell lung cancer A549 cells. Chem Biol Interact 2020;326. https://doi.org/10.1016/J.CBI.2020.109133.

[20] Schirmann JG, Dekker RFH, Borsato D, Barbosa-Dekker AM. Selective control for the laccase-catalyzed synthesis of dimers from 2,6-dimethoxyphenol: Optimization of 3,3',5,5'-tetramethoxy-biphenyl-4,4'-diol synthesis using factorial design, and evaluation of its antioxidant action in biodiesel. Appl Catal A Gen 2018;555:88–97. https://doi.org/10.1016/J.APCATA.2018.02.015.

[21] Tomiotto-Pellissier F, Alves DR, Miranda-Sapla MM, de Morais SM, Assolini JP, da Silva Bortoleti BT, et al. Caryocar coriaceum extracts exert leishmanicidal effect acting in promastigote forms by apoptosis-like mechanism and intracellular amastigotes by Nrf2/HO-1/ferritin dependent response and iron depletion: Leishmanicidal effect of Caryocar coriaceum leaf exracts. Biomedicine & Pharmacotherapy 2018;98:662–72. https://doi.org/10.1016/J.BIOPHA.2017.12.083.

[22] Duplancic R, Kero D. Novel approach for quantification of multiple immunofluorescent signals using histograms and 2D plot profiling of whole-section panoramic images. Scientific Reports 2021 11:1 2021;11:1–17. https://doi.org/10.1038/s41598-021-88101-1.

[23] Cataneo AHD, Tomiotto-Pellissier F, Miranda-Sapla MM, Assolini JP, Panis C, Kian D, et al. Quercetin promotes antipromastigote effect by increasing the ROS production and anti-amastigote by upregulating Nrf2/HO-1 expression, affecting iron availability. Biomed Pharmacother 2019;113:108745–108745. https://doi.org/10.1016/J.BIOPHA.2019.108745.

[24] MARKLUND S, MARKLUND G. Involvement of the superoxide anion radical in the autoxidation of pyrogallol and a convenient assay for superoxide dismutase. Eur J Biochem 1974;47:469–74. https://doi.org/10.1111/J.1432-1033.1974.TB03714.X.

[25] LOWRY OH, ROSEBROUGH NJ, FARR AL, RANDALL RJ. PROTEIN MEASUREMENT WITH THE FOLIN PHENOL REAGENT. Journal of Biological Chemistry 1951;193:265–75. https://doi.org/10.1016/S0021-9258(19)52451-6.

[26] Rahman I, Kode A, Biswas SK. Assay for quantitative determination of glutathione and glutathione disulfide levels using enzymatic recycling method. Nature Protocols 2007 1:6 2007;1:3159–65. https://doi.org/10.1038/nprot.2006.378.

878 [27] Khan FH, Dervan E, Bhattacharyya DD, McAuliffe JD, Miranda KM, Glynn SA. The
879 Role of Nitric Oxide in Cancer: Master Regulator or NOt? Int J Mol Sci 2020;21:1–30.
880 https://doi.org/10.3390/IJMS21249393.
881 [28] Griess B, Tom E, Domann F, Teoh-Fitzgerald M. Extracellular Superoxide Dismutase
882 and its Role in Cancer. Free Radic Biol Med 2017;112:464.
883 https://doi.org/10.1016/J.FREERADBIOMED.2017.08.013.
884 [29] Yun CW, Lee SH. The Roles of Autophagy in Cancer. Int J Mol Sci 2018;19.
885 https://doi.org/10.3390/IJMS19113466.
886 [30] Grasso D, Zampieri LX, Capelôa T, Van De Velde JA, Sonveaux P. Mitochondria in
887 cancer. Cell Stress 2020;4:114. https://doi.org/10.15698/CST2020.06.221.
888 [31] Cruz ALS, Barreto E de A, Fazolini NPB, Viola JPB, Bozza PT. Lipid droplets:
889 platforms with multiple functions in cancer hallmarks. Cell Death & Disease 2020 11:2
890 2020;11:1–16. https://doi.org/10.1038/s41419-020-2297-3.
891 [32] Wang C, Youle RJ. The Role of Mitochondria in Apoptosis. Annu Rev Genet
892 2009;43:95. https://doi.org/10.1146/ANNUREV-GENET-102108-134850.
893 [33] Boren J, Brindle KM. Apoptosis-induced mitochondrial dysfunction causes
894 cytoplasmic lipid droplet formation. Cell Death Differ 2012;19:1561.
895 https://doi.org/10.1038/CDD.2012.34.
896 [34] Tan AC. Targeting the PI3K/Akt/mTOR pathway in non-small cell lung cancer
897 (NSCLC). Thorac Cancer 2020;11:511. https://doi.org/10.1111/1759-7714.13328.
898 [35] Iglesias VS, Giuranno L, Dubois LJ, Theys J, Vooijs M. Drug Resistance in Non-
899 Small Cell Lung Cancer: A Potential for NOTCH Targeting? Front Oncol 2018;8:267.
900 https://doi.org/10.3389/FONC.2018.00267.
901 [36] Ashrafizadeh M, Zarrabi A, Hushmandi K, Hashemi F, Moghadam ER, Owrang M, et
902 al. Lung cancer cells and their sensitivity/resistance to cisplatin chemotherapy: Role of
903 microRNAs and upstream mediators. Cell Signal 2021;78:109871.
904 https://doi.org/10.1016/J.CELLSIG.2020.109871.
905 [37] Ghosh S. Cisplatin: The first metal based anticancer drug. Bioorg Chem
906 2019;88:102925. https://doi.org/10.1016/J.BIOORG.2019.102925.
907 [38] Gao F, Zhang JM, Wang ZG, Peng W, Hu HL, Fu CM. Biotransformation, a
908 promising technology for anti-cancer drug development. Asian Pac J Cancer Prev
909 2013;14:5599–608. https://doi.org/10.7314/APJCP.2013.14.10.5599.
910 [39] Gonçalves MD, Tomiotto-Pellissier F, de Matos RLN, Assolini JP, da Silva Bortoleti
911 BT, Concato VM, et al. Recent Advances in Biotransformation by Cunninghamella
912 Species. Curr Drug Metab 2021;22:1035–64.
913 https://doi.org/10.2174/1389200222666211126100023.
914 [40] Lauffenburger DA, Horwitz AF. Cell Migration: A Physically Integrated Molecular
915 Process. Cell 1996;84:359–69. https://doi.org/10.1016/S0092-8674(00)81280-5.
916 [41] Janiszewska M, Primi MC, Izard T. Cell adhesion in cancer: Beyond the migration of
917 single cells. J Biol Chem 2020;295:2495–505.
918 https://doi.org/10.1074/JBC.REV119.007759.
919 [42] Bush M, Alhanshali BM, Qian S, Stanley CB, Heller WT, Matsui T, et al. An
920 ensemble of flexible conformations underlies mechanotransduction by the cadherin–
921 catenin adhesion complex. Proc Natl Acad Sci U S A 2019;116:21545–55.
922 https://doi.org/10.1073/PNAS.1911489116/SUPPL_FILE/PNAS.1911489116.SAPP.PDF.
923 [43] Péglion F, Etienne-Manneville S. N-cadherin expression level as a critical indicator of
924 invasion in non-epithelial tumors. Cell Adh Migr 2012;6:327.
925 https://doi.org/10.4161/CAM.20855.
926 [44] Loh CY, Chai JY, Tang TF, Wong WF, Sethi G, Shanmugam MK, et al. The E-
927 Cadherin and N-Cadherin Switch in Epithelial-to-Mesenchymal Transition: Signaling,

928 Therapeutic Implications, and Challenges. Cells 2019;8.
929 https://doi.org/10.3390/CELLS8101118.
930 [45] Valenta T, Hausmann G, Basler K. The many faces and functions of β-catenin. EMBO
931 J 2012;31:2714–36. https://doi.org/10.1038/EMBOJ.2012.150.
932 [46] Jin J, Zhan P, Katoh M, Kobayashi SS, Phan K, Qian H, et al. Prognostic significance
933 of β-catenin expression in patients with non-small cell lung cancer: a meta-analysis. Transl
934 Lung Cancer Res 2017;6:97–108. https://doi.org/10.21037/TLCR.2017.02.07.
935 [47] Zhu W, Wang H, Zhu D. Wnt/β-catenin signaling pathway in lung cancer. Med Drug
936 Discov 2022;13:100113. https://doi.org/10.1016/J.MEDIDD.2021.100113.
937 [48] Kang Y, Massagué J. Epithelial-mesenchymal transitions: Twist in development and
938 metastasis. Cell 2004;118:277–9. https://doi.org/10.1016/j.cell.2004.07.011.
939 [49] Angadi P V., Patil P V., Angadi V, Mane D, Shekar S, Hallikerimath S, et al.
940 Immunoexpression of Epithelial Mesenchymal Transition Proteins E-Cadherin, β-Catenin,
941 and N-Cadherin in Oral Squamous Cell Carcinoma. Int J Surg Pathol 2016;24:696–703.
942 https://doi.org/10.1177/1066896916654763.
943 [50] Miao Y, Li AL, Wang L, Fan CF, Zhang XP, Xu HT, et al. Overexpression of NEDD9
944 is associated with altered expression of E-Cadherin, β-Catenin and N-Cadherin and
945 predictive of poor prognosis in non-small cell lung cancer. Pathol Oncol Res 2013;19:281–
946 6. https://doi.org/10.1007/S12253-012-9580-2.
947 [51] Sun H, Liu M, Wu X, Yang C, Zhang Y, Xu Z, et al. Overexpression of N-cadherin
948 and β-catenin correlates with poor prognosis in patients with nasopharyngeal carcinoma.
949 Oncol Lett 2017;13:1725. https://doi.org/10.3892/OL.2017.5645.
950 [52] Wu J shun, Jiang J, Chen B jun, Wang K, Tang Y ling, Liang X hua. Plasticity of
951 cancer cell invasion: Patterns and mechanisms. Transl Oncol 2021;14:100899.
952 https://doi.org/10.1016/J.TRANON.2020.100899.
953 [53] Mrozik KM, Blaschuk OW, Cheong CM, Zannettino ACW, Vandyke K. N-cadherin
954 in cancer metastasis, its emerging role in haematological malignancies and potential as a
955 therapeutic target in cancer. BMC Cancer 2018 18:1 2018;18:1–16.
956 https://doi.org/10.1186/S12885-018-4845-0.
957 [54] Birben E, Sahiner UM, Sackesen C, Erzurum S, Kalayci O. Oxidative Stress and
958 Antioxidant Defense. World Allergy Organ J 2012;5:9.
959 https://doi.org/10.1097/WOX.0B013E3182439613.
960 [55] Hayes JD, Dinkova-Kostova AT, Tew KD. Oxidative Stress in Cancer. Cancer Cell
961 2020;38:167. https://doi.org/10.1016/J.CCELL.2020.06.001.
962 [56] Azmanova M, Pitto-Barry A. Oxidative Stress in Cancer Therapy: Friend or Enemy?
963 ChemBioChem 2022;23:e202100641. https://doi.org/10.1002/CBIC.202100641.
964 [57] Wang M, Kirk JS, Venkataraman S, Domann FE, Zhang HJ, Schafer FQ, et al.
965 Manganese superoxide dismutase suppresses hypoxic induction of hypoxia-inducible
966 factor-1alpha and vascular endothelial growth factor. Oncogene 2005;24:8154–66.
967 https://doi.org/10.1038/SJ.ONC.1208986.
968 [58] Beligni MV, Lamattina L. Is nitric oxide toxic or protective? Trends Plant Sci
969 1999;4:299–300. https://doi.org/10.1016/s1360-1385(99)01451-x.
970 [59] Radi R. Oxygen radicals, nitric oxide, and peroxynitrite: Redox pathways in molecular
971 medicine. Proc Natl Acad Sci U S A 2018;115:5839–48.
972 https://doi.org/10.1073/PNAS.1804932115/ASSET/52782DFA-96E3-4150-AB66-
973 C339B5F09458/ASSETS/GRAPHIC/PNAS.1804932115FIG03.JPEG.
974 [60] Arfin S, Jha NK, Jha SK, Kesari KK, Ruokolainen J, Roychoudhury S, et al.
975 Oxidative Stress in Cancer Cell Metabolism. Antioxidants 2021, Vol 10, Page 642
976 2021;10:642. https://doi.org/10.3390/ANTIOX10050642.

[61] Xing F, Hu Q, Qin Y, Xu J, Zhang B, Yu X, et al. The Relationship of Redox With Hallmarks of Cancer: The Importance of Homeostasis and Context. Front Oncol 2022;12:1437. https://doi.org/10.3389/FONC.2022.862743/BIBTEX.
[62] Yap KM, Sekar M, Wu YS, Gan SH, Rani NNIM, Seow LJ, et al. Hesperidin and its aglycone hesperetin in breast cancer therapy: A review of recent developments and future prospects. Saudi J Biol Sci 2021;28:6730–47. https://doi.org/10.1016/J.SJBS.2021.07.046.
[63] Wee P, Wang Z. Epidermal Growth Factor Receptor Cell Proliferation Signaling Pathways. Cancers (Basel) 2017;9. https://doi.org/10.3390/CANCERS9050052.
[64] Cassim S, Vučetić M, Ždralević M, Pouyssegur J. Warburg and Beyond: The Power of Mitochondrial Metabolism to Collaborate or Replace Fermentative Glycolysis in Cancer. Cancers (Basel) 2020;12. https://doi.org/10.3390/CANCERS12051119.
[65] Boren J, Brindle KM. Apoptosis-induced mitochondrial dysfunction causes cytoplasmic lipid droplet formation. Cell Death Differ 2012;19:1561. https://doi.org/10.1038/CDD.2012.34.
[66] Xu JQ, Fu YL, Zhang J, Zhang KY, Ma J, Tang JY, et al. Targeting glycolysis in non-small cell lung cancer: Promises and challenges. Front Pharmacol 2022;13. https://doi.org/10.3389/FPHAR.2022.1037341.
[67] Cassim S, Vučetić M, Ždralević M, Pouyssegur J. Warburg and Beyond: The Power of Mitochondrial Metabolism to Collaborate or Replace Fermentative Glycolysis in Cancer. Cancers (Basel) 2020;12. https://doi.org/10.3390/CANCERS12051119.
[68] White E. Role of Metabolic Stress Responses of Apoptosis and Autophagy in Tumor Suppression. Ernst Schering Found Symp Proc 2007:23. https://doi.org/10.1007/2789_2008_087.
[69] Guo W, Du K, Luo S, Hu D. Recent Advances of Autophagy in Non-Small Cell Lung Cancer: From Basic Mechanisms to Clinical Application. Front Oncol 2022;12. https://doi.org/10.3389/FONC.2022.861959.
[70] Chuang CH, Dorsch M, Dujardin P, Silas S, Ueffing K, Holken JM, et al. Altered mitochondria functionality defines a metastatic cell state in lung cancer and creates an exploitable vulnerability. Cancer Res 2021;81:567. https://doi.org/10.1158/0008-5472.CAN-20-1865.
[71] Luo W, Wang H, Ren L, Lu Z, Zheng Q, Ding L, et al. Adding fuel to the fire: The lipid droplet and its associated proteins in cancer progression. Int J Biol Sci 2022;18:6020–34. https://doi.org/10.7150/IJBS.74902.
[72] Grasso D, Zampieri LX, Capelôa T, Van De Velde JA, Sonveaux P. Mitochondria in cancer. Cell Stress 2020;4:114. https://doi.org/10.15698/CST2020.06.221.
[73] Petan T, Jarc E, Jusović M. Lipid Droplets in Cancer: Guardians of Fat in a Stressful World. Molecules 2018, Vol 23, Page 1941 2018;23:1941. https://doi.org/10.3390/MOLECULES23081941.
[74] Yun CW, Lee SH. The Roles of Autophagy in Cancer. Int J Mol Sci 2018;19. https://doi.org/10.3390/IJMS19113466.
[75] Mehdizadeh K, Ataei F, Hosseinkhani S. Treating MCF7 breast cancer cell with proteasome inhibitor Bortezomib restores apoptotic factors and sensitizes cell to Docetaxel. Medical Oncology 2021;38:1–8. https://doi.org/10.1007/S12032-021-01509-7/FIGURES/4.
[76] Pfeffer CM, Singh ATK. Apoptosis: A Target for Anticancer Therapy. Int J Mol Sci 2018;19. https://doi.org/10.3390/IJMS19020448.
[77] Walsh JG, Cullen SP, Sheridan C, Lüthi AU, Gerner C, Martin SJ. Executioner caspase-3 and caspase-7 are functionally distinct proteases. Proc Natl Acad Sci U S A 2008;105:12815–9. https://doi.org/10.1073/PNAS.0707715105/SUPPL_FILE/0707715105SI.PDF.

[78] Brentnall M, Rodriguez-Menocal L, De Guevara RL, Cepero E, Boise LH. Caspase-9, caspase-3 and caspase-7 have distinct roles during intrinsic apoptosis. BMC Cell Biol 2013;14:1–9. https://doi.org/10.1186/1471-2121-14-32/FIGURES/5.

[79] Lakhani SA, Masud A, Kuida K, Porter GA, Booth CJ, Mehal WZ, et al. Caspases 3 and 7: Key Mediators of Mitochondrial Events of Apoptosis. Science 2006;311:847. https://doi.org/10.1126/SCIENCE.1115035.

[80] Taniguchi K, Karin M. NF-κB, inflammation, immunity and cancer: coming of age. Nat Rev Immunol 2018;18:309–24. https://doi.org/10.1038/NRI.2017.142.

[81] Chen W, Li Z, Bai L, Lin Y. NF-kappaB, a mediator for lung carcinogenesis and a target for lung cancer prevention and therapy. Front Biosci 2011;16:1172. https://doi.org/10.2741/3782.

[82] Niu F, Yu Y, Li Z, Ren Y, Li Z, Ye Q, et al. Arginase: An emerging and promising therapeutic target for cancer treatment. Biomedicine & Pharmacotherapy 2022;149:112840. https://doi.org/10.1016/J.BIOPHA.2022.112840.

Trilobolide-6-*O*-isobutyrate from *Sphagneticola trilobata* acts by inducing oxidative stress, metabolic changes and apoptosis-like processes by caspase 3/7 activation of human lung cancer cell lines

Virginia Marcia Concato-Lopes[a,*], Manoela Daiele Gonçalves-Lens[b], Fernanda Tomiotto-Pellissier[a,c,d], Mariana Barbosa Detoni[a], Ellen Mayara Souza Cruz[a], Bruna Taciane da Silva Bortoleti[a,c], Amanda Cristina Machado Carloto[a], Ana Carolina Jacob Rodrigues[a,c], Taylon Felipe Silva[a], Elaine da Silva Siqueira[a], Ricardo Luís Nascimento de Matos[b], Ian Lucas Alves Cardoso[b] Ivete Conchon-Costa[a], Danielle Lazarin-Bidoia[a], Nilton Syogo Arakawa[b], Robert F. H. Dekker[e], Mário Sérgio Mantovani[f], Wander Rogério Pavanelli[a]

Author information:

[a] Laboratory of Immunoparasitology of Neglected Diseases and Cancer, Department of Immunology, Parasitology and General Pathology, State University of Londrina, PR, Brazil.

[b] Laboratory of Biotransformation and Phytochemical, Department of Chemistry, State University of Londrina, PR, Brazil.

[c] Graduate Program in Biosciences and Biotechnology, Carlos Chagas Institute (ICC), Fiocruz, Curitiba, PR, Brazil.

[d] Department of Medical Pathology, Federal University of Paraná, Curitiba, PR, Brazil.

[e] Beta-Glucan Produtos Farmoquímicos-EIRELI, Lote 24[A] - Bloco Zirconia, Universidade Tecnológica Federal do Paraná, Avenida João Miguel Caram 731, CEP: 86036-700, Londrina, Paraná, Brazil.

[f] Laboratory of Toxicological Genetics, Department of Biology, State University of Londrina, PR, Brazil.

[*] **Corresponding author:** Virginia Marcia Concato-Lopes, Department of Immunology, Parasitology and General Pathology, Laboratory of Immunopathology of Neglected Diseases and Cancer, State University of Londrina – UEL. Rodovia Celso Garcia Cid Campus, CEP: 86057-970, Post Box 10.011. Londrina, PR.

Tel: +055 4333714539. *E*-mail: vir_93_@hotmail.com

Highlights

- TBB exhibits drug-likeness parameters and pharmacological characteristics.
- TBB treatment reduces cell viability and alters morphology in A549 and NCI-H460.
- The treatment reduces migratory capacity in tumor cell lines.
- TBB treatment promotes oxidative and metabolic stress in A549 and NCI-H460.
- TBB induces cell death through caspase activation in A549 and NCI-H460.

Abstract

Background: Lung cancer, a chronic and heterogeneous disease, is the leading cause of cancer-related death on a global scale. Presently, despite a variety of available treatments, their effectiveness is limited, often resulting in considerable toxicity and adverse effects. Additionally, the development of chemoresistance in cancer cells poses a challenge. Trilobolide-6-*O*-isobutyrate (TBB), a natural sesquiterpene lactone extracted from *Sphagneticola trilobata*, has exhibited antitumor effects. Its pharmacological properties in NSCLC lung cancer, however, have not been explored.

Purpose: This study evaluated the impact of TBB on the A549 and NCI-H460 tumor cell lines in vitro, examining its antiproliferative properties and initial mechanisms of cell death.

Methods: TBB, obtained at 98% purity from S. trilobata leaves, was characterized using chromatographic techniques. Subsequently, its impact on inhibiting tumor cell proliferation in vitro, TBB-induced cytotoxicity in LLC-MK2, THP-1, AMJ2-C11 cells, as well as its effects on sheep erythrocytes, and the underlying mechanisms of cell death, were assessed.

Results: In silico predictions have shown promising *drug-likeness* potential for TBB, indicating high oral bioavailability and intestinal absorption. Treatment of A549 and NCI-H460 human tumor cells with TBB demonstrated a direct impact, inducing significant morphological and structural alterations. TBB also reduced migratory capacity without causing toxicity at lower concentrations to LLC-MK2, THP-1 and AMJ2-C11 cell lines. This antiproliferative effect correlated with elevated oxidative stress, characterized by increased levels of ROS, superoxide anion radicals and NO, accompanied by a decrease in antioxidant markers: SOD and GSH. TBB-stress-induced led to changes in cell metabolism, fostering the accumulation of lipid droplets and autophagic vacuoles. Stress also resulted in compromised mitochondrial integrity, a crucial aspect of cellular function. Additionally, TBB prompted apoptosis-like cell death through activation of caspase 3/7 stressors.

Conclusion: These findings underscore the potential of TBB as a promising candidate for future studies and suggest its viability as an additional component in the development of novel anticancer drugs prototypes.

Key words: NSCLC - A549, NCI-H460 cell lines; Natural Product; Oral bioavailability; Cytotoxicity; Cell Death.

Graphical abstract

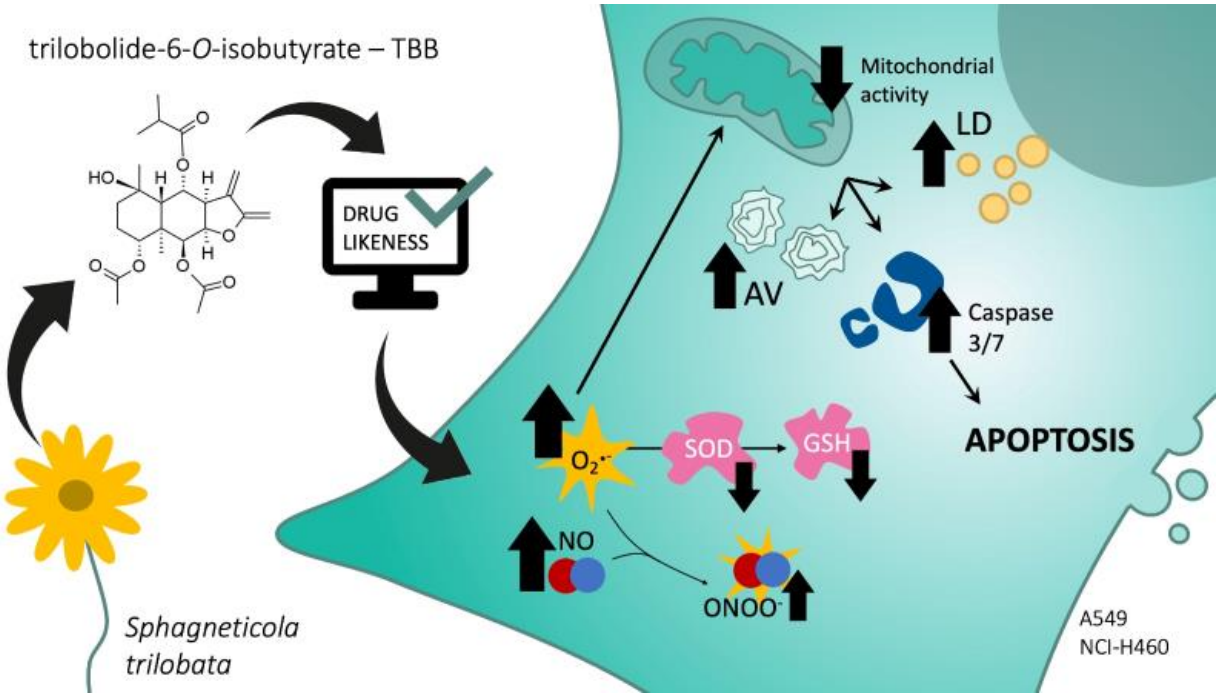

Abbreviations: ADMET, Absorption, distribution, metabolism, excretion and toxicity; CCCP, Carbonyl cyanide *m*-chlorophenylhydrazone; DMEM, Dulbecco's Modified Eagle Medium; DMSO, Dimethyl sulfoxide; DNA, Deoxyribonucleic acid; FBS, Fetal bovine serum; FDA, Food and Drug Administration; GSH, Reduced L-glutathione; H_2DCFDA, 2',7'-dichlorofluorescein diacetate; H_2O_2, Hydrogen peroxide; H-Acc, Number of Hydrogen bond acceptor; H-Don, Number of Hydrogen bond donor; $IC_{50,}$ Inhibitory concentration at 50%; IL-6, Interleucin-6; LD, lipid droplets; MDC, Monodansylcadaverine; miLog P, Log of partition-coefficient; m.p, Melting point; MTT, 3-(4,5-dimethylthiazol-2-yl)-2,5-diphenyltetrazolium bromide; MW, Molecular weight; NBT, Nitro blue tetrazolium; NH, Non-hemolytic; NMR, Nuclear magnetic resonance; NO, Nitric oxide; NR, Nile red; NSCLC, Non-small cell lung cancer; $O_2^{\bullet -}$, Superoxide anion radical; PBS, Phosphate-buffered saline; NMR, Magnetic resonance; PCNA, Proliferating cell nuclear antigen; P-gp, Permeability glycoprotein; PI, Propidium iodide; PMA,

Phorbol myristate acetate; RB, Number of rotatable bonds; ROS, Reactive Oxygen Species; SCLC, Small cell lung cancer; SEM, Scanning electron microscopy; SL, Sesquiterpene lactone; SOD, Superoxide dismutase; TBB, Trilobolide-6-*O*-isobutyrate; TEM, Transmission electron microscopy; TMRE, Tetramethyl rhodamine-ethyl-ester; TPSA, Molecular Polar Surface Area; TSI, Tumor selectivity index; VLC, Vacuum liquid chromatography; CIS, cisplatin.

1. Background

Lung-related cancers have presented more than 2.2 million novel cases worldwide, and in 2020 resulted in an estimated 1.8 million deaths (Sung et al., 2021, ranking this as the primary cause of cancer-related mortality globally. Lung cancer is a heterogeneous disease that encompasses various biologically distinct tumors. Broadly categorized into non-small cell lung cancer (NSCLC, 85% of total diagnoses) and small cell lung cancer (SCLC, 15% of total diagnoses). NSCLC is further segregated into adenocarcinoma - the prevailing subtype and is succeeded by squamous-cell carcinoma and large-cell carcinoma (Thai et al., 2021; Travis et al., 2015).

Although there is a plethora of therapeutic options (chemotherapy, target therapy and immunotherapy) for systemic treatment, chemotherapy remains a critical component of lung cancer treatment, especially for patients with advanced stages of the disease, pre-existing autoimmune disease, and toxicity associated with combination immunotherapy. Consequently, platinum-based duplex regimens (e.g., cisplatin in combination with carboplatin or paclitaxel, or another cytotoxic drug) are commonly employed in this setting. The combination of cisplatin is a preferred treatment regimen, especially in combination with new-generation drugs, but it still results in adverse side-effects for patients, such as gastrointestinal toxicity, nephrotoxicity, neurotoxicity, ototoxicity, hypersensitivity, and myelosuppression. In addition, patients continue to experience disease recurrence and drug resistance during platinum-based therapy, which reduces the efficacy of NSCLC treatment (Guo et al., 2022; Lee, 2019; Mithoowani and Febbraro, 2022; Ryan et al., 2021).

Plant-derived compounds possess a broad spectrum of biomedical applications, primarily attributed to their diminished adverse effects, cost-effectiveness relative to pharmaceuticals, and their endorsement by the Food and Drug Administration (FDA) (Atanasov et al., 2021; Dutta et al., 2019). *Sphagneticola trilobata* (L.) J.F. Pruski, also popularly known as "*margaridão"* and "*Wedelia*", belongs to the *Asteraceae* plant family and has been a traditional medicinal resource in India, China, the Caribbean, and Central and South America (Mardina et al., 2020) . Despite

its classification as an invasive weed, this medicinal plant is noted for its high molecular diversity and its diverse biological activity that encompasses antibacterial, antidiabetic, hepatoprotective, antipyretic-analgesic, and anticancer activities (Shankar and Thomas, 2014; Mardina et al., 2020; Mardina et al., 2021; Zhang et al., 2021).

The principal chemical constituents from *S. trilobata* are the ent-kaurane diterpenes, eudesmane sesquiterpene lactones, and triterpenes (Hui et al., 2019) . Recent investigations have demonstrated the therapeutic potential of sesquiterpene lactones (SLs), especially within the domain of cancer research (Dhyani et al., 2022; Dong et al., 2022; Shoaib et al., 2017) . Among these is trilobolide-6-*O*-isobutyrate (TBB), molecular formula $C_{23}H_{32}O_9$, a notable natural sesquiterpene lactone extracted from *S. trilobata* (Bohlmann et al., 1981).

In a recent *in vitro* investigation utilizing TBB against the human hepatocellular carcinoma cell lines: HuH7, HepG2, SK-Hep1 and Bel7402, TBB from *S. trilobata* was found to inhibit growth and colony formation in a time- and concentration- dependent manner. TBB treatment exhibited inhibitory effects on migration, invasion, and glycolysis, ultimately culminating in cell cycle arrest within the G2/M phase, mitochondrial dysfunction, and apoptosis-driven cell death. TBB was furthermore, also able to regulate the expression of pivotal genes associated with proliferation, migration, and metastasis as PCNA (proliferating cell nuclear antigen), Ki67, Cyclin B1, Cyclin E, Bax, Bcl2, MMP2/9 (metalloproteinase 2/9) and PGK1 (phosphoglycerate kinase 1), primarily via the inhibition of the interleukin-6/signal transducers and activators of the transcription-3 (IL-6/STAT3) signaling pathway. The *in vivo* efficacy of TBB's anticancer attributes was validated through experimentation with a xenograft tumor model in male BALB/c nude mice, where TBB was effective in eliminating tumor growth (weight and volume) without causing toxicity to the experimental animals (Zhou et al., 2021).

Here, we report for the first time, the biological activity of TBB isolated from *S. trilobata* in NSCLC cell lines, A549 (lung adenocarcinoma) and NCI-H460 (large cell carcinoma), employing diverse experimental methodologies. This study encompasses an evaluation of TBB's theoretical drug-likeness predictions and an investigation into its *in vitro* antiproliferative effects on NSCLC cell lines. Furthermore, we explore the potential mechanistic actions of TBB in inducing cell death and assess its cytotoxicity across a spectrum of cell types, including epithelial cells, monocytes, and erythrocytes.

2. Material and Methods

2.1 Animals and ethics committee

This study was approved by the Animal Ethics Committee of the State University of Londrina (approval Nº 8286.2016.60 on 1/6/2016) and all methods performed were conducted following the Arouca Guideline and all ethical international regulations.

2.1.1 Hemolytic Assay

Sheep red blood cells were used to evaluate direct membrane toxicity through the hemolytic assay. In this assay, erythrocytes were treated with TBB (3, 6, 12, 25, 50, 100, 200 μM) or cisplatin (CIS) (12, 25, 50, 100, 200 μM) following the protocol established by Concato et al., 2020).

2.2 Cell lines and reagents

We conducted a comprehensive characterization of a panel of cell lines, including Rhesus monkey renal epithelial cells (LLC-MK2), human leukemia monocytic cells (THP-1), murine alveolar macrophages (AMJ2-C11), and the established NSCLC lines, A549 and NCI-H460, sourced from the ATCC. All cells were cultured in Roswell Park Memorial Institute (RPMI) 1640 medium (Life Technologies, CA, USA) supplemented with 10% fetal bovine serum (FBS) (GIBCO, Invitrogen, New York, USA), 100 U/mL Penicillin and 100 μg/mL Streptomycin (Santa Cruz Biotechnologies, Dallas, TX, USA) and maintained at 37 °C in 5% CO_2.

2.3 Plant material and isolation of trilobolide-6-*O*-isobutyrate (TBB)

The leaves of *S. trilobata* were collected in February 2013 at Horto de Plantas Medicinais do Centro de Ciências Agrárias da Universidade Estadual de Londrina (23˚32' 64" N, 51˚20' 63" W). A voucher specimen (Nº. 49306, collected by one of the authors N.S.A.) was deposited at the Herbarium of the State University of Londrina, Brazil.

After drying the leaves of *S. trilobata* to a constant mass, a crude extract was obtained through maceration with dichloromethane until the total exhaustion of the plant material. Subsequently, the extract was dried under reduced pressure using a rotary evaporator. The resulting crude extract was re-dissolved in a solvent mixture of 10% (v/v) methanol (MeOH) in water and subjected to sequential partitioning with hexane (hex) and dichloromethane. The solvent fractions were subsequently dried under reduced pressure. The dichloromethane fraction was further subjected to vacuum liquid chromatography (VLC) using an increasing polarity gradient (Hex: ethyl acetate (EtOAc): MeOH) and monitored by Comparative Thin Layer Chromatography (TLC). The fraction obtained with a ratio of 7:3 (EtOAc: Hex) was subjected

to a subsequent round of VLC. Fraction F54, obtained during this process, yielded crystals (495 mg) which were subjected to a low temperature acetone wash.

The isolated compound (75 mg, 97% purity) (**Fig. 1**) by Ian Lucas Alves Cardoso was identified through ^{1}H and ^{13}C nuclear magnetic resonance (NMR) spectroscopy (Bruker Avance Model III, 400 MHz for ^{1}H and 100 MHz for ^{13}C), in $CDCl_3$. The compound's identity was confirmed by comparison with spectral data obtained through literature values (Ferreira et al., 1994). The melting point (m.p) was determined using a hotplate device (Microquímica MQAPF 302, Campinas, SP, Brazil). A stock solution of TBB was prepared in 1% dimethyl sulfoxide (DMSO) (GIBCO). The concentration of DMSO in the experiments never exceeded 0.06%.

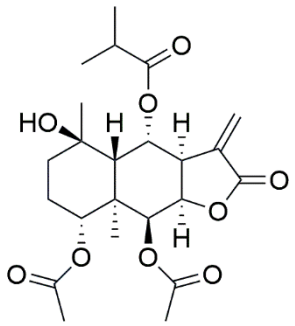

Figure 1: Chemical structure of trilobolide-6-*O*-isobutyrate (TBB).

2.4 *In silico* studies for *drug-likeness* analysis

An in-silico study was conducted to analyze the structure of TBB and assess various theoretical parameters. Initially, the Molinspiration Property Calculator program (accessible at: www.molinspiration.com) was used to determine parameters associated with oral bioavailability, in alignment with Lipinski's Rule of Five (Ro5) (Lipinski, 2004). Subsequently, Veber's rule (Veber et al., 2002) employed for further analysis. Following this, pharmacokinetic predictions were made regarding the similarity of drugs in terms of oral bioavailability, absorption, distribution, metabolism, excretion, and toxicity properties. These predictions were obtained from the SwissADME online database (http://www.swissadme.ch/index.php). The properties assessed included blood-brain barrier penetration, human intestinal absorption, analysis of the five most critical cytochrome P450 isoforms, AMES toxicity, carcinogens and carcinogenicity, and the human ether-à-go-go related gene (hERG)—a potassium channel crucial for cardiac repolarization. Additionally, an evaluation was conducted to determine whether TBB acts as a substrate for permeability glycoprotein (P-gp), which is responsible for assessing active efflux across biological membranes (Cheng et al., 2012; Yang et al., 2019).

2.5 Viability assay

To assess the impact of TBB on the viability of LLC-MK2, THP-1 and AMJ2-C11 cell lines, we employed the MTT assay, following the protocol outlined by Mosmann (1983). Specifically, cells were seeded (1×10^4 cells/well) in 96-well plates and exposed to varying concentrations of TBB (12.5, 25, 50, 100, 200, and 400 μM) for a duration of 24 h at 37 °C in a 5% CO_2 atmosphere. For A549 and NCI-H460 cells (1×10^4 cells/well), TBB was administered at concentrations of 3, 6, 12, 25, 50, and 100 μM, and cytotoxicity was evaluated at 24, 48, and 72 h. The MTT assay was performed at the end of each respective incubation period, wherein cells were washed and MTT solution (0.05 mg/ml) was added, followed by a 3-h incubation. Formazan crystals formed were then diluted with 100 μL of DMSO and their optical density (OD) was measured at 540 nm using a spectrophotometer (Thermo Scientific, Multiskan GO). Experimental groups in this study were categorized as follows: a control group, a vehicle group (0.06% DMSO, representing the highest vehicle concentration used in treated groups), groups exposed to the specified TBB concentrations, and a CIS group (50 μM) serving as a positive control. The results were expressed as percentage of viability compared to the control group calculated with the following formula: % (viable cells) = (OD of TBB-treated samples/OD control-sample) × 100.

2.6.1 Half-maximal concentration (IC_{50}) calculation and tumor selectivity index (TSI)

The IC_{50} curves for all cell lines were calculated using logarithmic regression. The values obtained for A549 and NCI-H460 were utilized to conduct further experiments. The TSI was determined through the following calculation: IC_{50} cell lines / IC_{50} of tumor cells at 24 h.

2.6.2 Morphological and ultrastructural analysis of lung cancer cell lines

Scanning electron microscopy (SEM) was performed on A549 and NCI-H460 cells to analyze morphology cell surface following the procedure outlined by Tomiotto-Pellissier et al., (2018). Briefly, cells (1×106 cells/well) were exposed to IC_{50}-TBB [A549 (73 μM ± 0.03); NCI-H460 (54 μM ± 0.06)] for 24 h at 37 °C. Subsequently, the cells were fixed with 2.5% glutaraldehyde in 0.1 M sodium cacodylate buffer (pH 7.4) and gradually dehydrated using increasing concentrations of ethanol (30-100%). Following dehydration, the samples underwent critical point drying (Baltec SCD-030, Balzer's, Liechtenstein), were gold-coated, and visualized using a high-resolution FEI SCIOS double-beam electron microscope (Thermo Fisher Scientific, Massachusetts, USA) for imaging purposes.

To assess ultrastructure in the TBB-treated cells by transmission electron microscopy (TEM) (JEOL USA JEM 1400, Tokyo, Japan), cells were treated and fixed similarly as described above. The samples were then post-fixed with 1% OsO_4, 0.8% potassium ferrocyanide and 10.0 mM $CaCl_2$ in 0.1 M sodium cacodylate buffer (pH 7.4) for 1 h at room temperature and protected from light. The samples were subsequently rinsed in 0.1 M sodium cacodylate buffer and dehydrated using increasing concentrations of acetone (30-100%). The acetone was gradually substituted with EPON™ epoxy resin (Electron Microscopy Sciences, Hatfield, United States) through cell diffusion, followed by allowing polymerization at 60 °C for 72 h. Subsequently, the resin-embedded cells were sliced (nanoscale sections, 60-70 nm) using an ultramicrotome (Power Tomer BMC - Germany), and then the sectioned slices were contrasted using 5% uranyl acetate and 2% lead citrate. In addition, the samples were subjected to analysis using TEM. The A549 and NCI-H460 cell lines, maintained in RPMI culture medium without TBB treatment, served as the negative control.

2.6.3 Wound healing assay

A549 and NCI-H460 cells (1×10^6 cells/well) were plated in 6-well plates and incubated at 37 °C with 5% CO_2 to confluence. The cell monolayer was then gently "scratched" with a 200 µL pipette tip, creating a gap in the monolayer where cells at the edges began migrating into the open space. Cells were then treated with IC_{50}-TBB [A549 (73 µM ± 0.03); NCI-H460 (54 µM ± 0.06)] and photomicrographs (40× objective) were taken at different time points (0, 12 and 24 h) using an EVOS FL Auto2 microscope (Thermo Scientific). The extent of cell migration was evaluated by measuring the free area (the area without cells) using Image-Pro Plus software (ImageJ). The percentage decrease in area was quantified as the cell migration index. All assays were performed in triplicate for each tested group.

2.6.4 Production of Reactive Oxygen Species (ROS)

ROS generation was assessed by the conversion of non-fluorescent 2',7'-dichlorofluorescein diacetate (H_2DCFDA) to highly fluorescent 2',7'-dichlorofluorescein (DCF) by intracellular free radicals. A549 and NCI-H460 cells (1×10^4 cells/well) were treated with IC_{50}-TBB [A549 (73 µM ± 0.03); NCI-H460 (54 µM ± 0.06)] for 24 h, and the assay performed according to Concato et al., (2020). Untreated cells were used as a negative control, and H_2O_2 (0.04%) was used as a positive control. Data were normalized and expressed in arbitrary units.

2.6.5 Determination of nitrite, an estimate of nitric oxide (NO) levels

NO levels were determined based upon the Griess method. A549 and NCI-H460 cells (1×10^5 cells/well) were treated with IC_{50}-TBB [A549 (73 μM ± 0.03); NCI-H460 (54 μM ± 0.06)] and incubated for 24 h. The supernatant of the samples was collected and analyzed according to Cataneo et al., (2019).

2.6.6 Superoxide anion radical production

The generation of O2•- was determined through the reduction of the redox dye nitro blue tetrazolium (1 mg/mL; NBT, Sigma-Aldrich). A549 and NCI-H460 cell lines (1×10^4 cells/well) were exposed to IC_{50}-TBB [A549 (73 μM ± 0.03); NCI-H460 (54 μM ± 0.06)] and incubated for 24 h. Subsequently, the cells were washed with PBS, and 100 μL of NBT solution was added and incubated at 37 °C for 1 h. After centrifugation, the supernatant was discarded, and the formazan precipitate was dissolved by adding 60 μL of 2.0 M KOH and 60 μL of DMSO. The optical density was measured at 600 nm using a microplate reader (Multiskan GO Microplate Spectrophotometer, Thermo Scientific). Untreated cells served as the negative control, while treatment with phorbol myristate acetate (PMA) served as the positive control.

2.6.7 Superoxide Dismutase (SOD)

For the determination of SOD activity, A549 and NCI-H460 cell lines (1×10^5 cells/well) were seeded in 6-wells plate, treated with the IC_{50}-TBB [A549 (73 μM ± 0.03); NCI-H460 (54 μM ± 0.06)], and incubated for 24 h at 37 °C. Thereafter, the cells were lysed according to Concato-Lopes et al., (2023). The method used for assaying SOD activity was as described by Marklund and Marklund (1974), based on the enzyme's ability to inhibit auto-oxidation of pyrogallol. Total protein was determined on the cell lysate by the Lowry method (Lowry et al., 1951). The data were normalized as mg protein/mL. Untreated cells were used as negative control.

2.6.8 Reduced glutathione (GSH)

To assess the degree of oxidative stress, the levels of reduced L-glutathione (GSH) were measured. Cells were seeded in 6-well plates at a density of 1×10^5 cells per well and treated with IC_{50}-TBB concentrations [A549 (73 μM ± 0.03); NCI-H460 (54 μM ± 0.06)]. Following a 24-h incubation period, GSH quantification was carried out following the methodology outlined by Rahman et al., (2006). Concentrations were determined by reference to a standard curve generated using serial dilutions of GSH. Untreated cells served as the negative control.

2.6.9 Determination of Mitochondrial Membrane Potential (ΔΨm)

The evaluation of ΔΨm was conducted through cell labeling with tetramethyl rhodamine-ethyl ester (TMRE) (Sigma-Aldrich, St. Louis, MO, USA). A549 and NCI-H460 cell lines (1×10^4 cells/well) were exposed to IC_{50}-TBB concentrations [A549 (73 μM ± 0.03); NCI-H460 (54 μM ± 0.06)] for 24 h, and the procedure followed the methodology outlined by Concato et al., (2020). Untreated cells served as the negative control, while carbonyl cyanide m-chlorophenylhydrazone (CCCP) (100 μM) was employed as the positive control. Data were expressed in arbitrary units.

2.6.10 Detection of lipid droplets (LD)

A549 and NCI-H460 cells (1×10^4 cells/well) were treated with IC_{50}-TBB [A549 (73 μM ± 0.03); NCI-H460 (54 μM ± 0.06)] for 24 h and analyzes performed by staining with Nile Red (NR) (Sigma-Aldrich) as described by Concato et al., (2020). Untreated cells were used as a negative control, and PBS treatment was used as a positive control. Data were normalized and expressed in arbitrary units.

2.6.11 Determination of the formation of autophagic vacuoles

For the assessment of the formation of autophagic vacuoles, cells were labeled using monodansylcadaverine (MDC, Sigma-Aldrich). A549 and NCI-H460 cells (1×10^4 cells/well) were exposed to IC_{50}-TBB [A549 (73 μM ± 0.03); NCI-H460 (54 μM ± 0.06)] for 24 h. The assay procedure closely followed the methodology outlined by Concato et al., (2020). Untreated cells were used as a negative control, and PBS treatment was used as a positive control. Data were normalized and expressed in arbitrary units.

2.6.12 Cell apoptosis assay

A549 and NCI-H460 cells (1×10^6 cells/well) were treated with IC_{50}-TBB [A549 (73 μM ± 0.03); NCI-H460 (54 μM ± 0.06)] for 24 h and the analysis was performed using Annexin V and iodete propidium (PI) (Millipore, Billerica, MA, USA) labeling**.** The assay was achieved as described by Concato et al., (2020).

2.6.13 Caspase-3/7 Assay

A549 and NCI-H460 cells (1×10^6 cells/well) were treated with IC_{50}-TBB [A549 (73 μM ± 0.03); NCI-H460 (54 μM ± 0.06)] for 24 h and caspase-3/7 protease activity was measured using the EnzChek Caspase-3/7 Assay Kit (Invitrogen). The assay was achieved as described by Concato-Lopes et al., (2023). Data were normalized and expressed in arbitrary units.

2.7 Statistical analysis

The data are presented as the mean ± standard error of the mean (SEM). Three independent experiments were conducted, each with duplicate datasets, and subjected to analysis using GraphPad Prism 8 statistical software (GraphPad Software, Inc., USA, 500.288). Significant distinctions between groups were determined through t-tests or one-way ANOVA, followed by Tukey's test for multiple comparisons. A result was regarded statistically significant if the $p < 0.05$.

3 RESULTS

3.6 Chemical and drug-likeness properties of TBB

To validate the identification of the isolated compound (TBB; 495 mg), a thorough analysis was conducted using ^{1}H and ^{13}C NMR spectroscopy (**Supp. Tables 1-2**), which closely matched the values reported by (Ferreira et al., 1994). The m.p. of TBB was 218.52 °C For predicting the potential suitability of the molecule as an oral medication, Lipinski's (Ro5) and Veber rules were employed as reliable parameters. The results of the *in-silico* analysis of the TBB molecule indicated full compliance with the established rules, with no violation (**Table 1**). Theoretical predictions evaluated by the ADMET program revealed specific characteristics of TBB based on its chemical structure. Notably, the compound demonstrated a propensity for mitochondrial accumulation, high absorption in the human intestine, and was identified as a substrate and inhibitor of permeability glycoprotein. Importantly, TBB does not inhibit the human ether-a-go-go related gene (hERG), lacks carcinogenic components in its structure, does not induce toxicity according to the Ames test, and is non-carcinogenic. Furthermore, in accordance with theoretical predictions, TBB exhibited the potential to penetrate the blood-brain barrier and displayed interactions with several cytochrome P450 (CYP) isoforms, specifically CYP1A2, CYP2C9, CYP2D6, and CYP2C19. Also presented low CYP inhibitory promiscuity, *i.e.*, it does not alter the general functionality of CYP450 (**Table 2**) (Cheng et al., 2012; Yang et al., 2019).

Supp. Table 1: ^{1}H NMR data (400 MHz, $CDCl_3$, *J* in Hz, ™ in ppm)

Position	Ferreira et al. (1994) ™$_H$ (ppm)	This work TBB ™$_H$ (ppm), *m*, *J* (Hz)
1	4.59 (*dd*, 10.5, 4.2)	4.59 (*dd*, 10.6, 4.2)

2	1.7 - 1.5	1.8 - 1.5
3	1.7 - 1.6	1.7 - 1.6
5	1.88 (*d,* 3.0)	1.88 (*d*, 2.9)
6	5.98 (*dl*, 3.0)	5.95 (*d*l, 3.0)
7	3.30 (*m*)	3.16 (*m*)
8	4.91 (*dd*, 8.1; 4.5)	4.88 (*dd*, 8.0, 4.5)
9	5.24 (*d*, 4.5)	5.21 (*d*, 4.5)
13α	6.26 (*d*, 3.8)	6.23 (*d*, 3.8)
13β	5.65 (*d*, 3.5)	5.66 (*d*, 3.5)
14	1.38 (s)	1.36 (*s*)
15	1.37 (s)	1.34 (*s*)
2’	2.6 (*spt*, 7.0)	2.58 (*spt*)
3’	1.23 (*d*, 7.0)	1.22 (*d*, 7.0)
4’	1.22 (*d*, 7.0)	1.20 (*d*, 7.0)
2’’	1.99 (s)	2.02 (*s*)
2’’’	1.96 (s)	1.93 (*s*)

(dd) double doublet, (d) doublet, (dl) doublet large, (m) multiplets, (s) singlet, (spt) septet.

Supp. Table 2: ^{13}C NMR data (100 MHz, $CDCl_3$, ™ in ppm)

Position	Ferreira et al. (1994) ™$_C$ (ppm)	This work TBB ™$_C$ (ppm)
1	72.9	73.0
2	23.7	24.0
3	41.3	41.6
4	70.6	70.6
5	43.1	43.4
6	67.9	68.0
7	44.5	44.9
8	71.9	72.1
9	70.4	71.0

10	41.3	41.3
11	133.9	134.1
12	168.9	169.2
13	118.9	119.2
14	14.0	14.3
15	26.1	26.4
1’	175.9	176.2
2’	34.1	34.4
3’	18.2	18.4
4’	18.7	19.0
1’’	170.3	170.6
2’’	20.0	20.2
1’’’	169.3	169.4
2’’’	20.8	21.0

Table 1: Molecular properties of trilobolide-6-*O*-isobutyrate (TBB) based on Lipinski and Veber’s criteria.

		Limits	**TBB**
Lipinski’s rules	**MW**	≤500	452.50
	miLog P	≤5	1.72
	H-Acc	≤10	9
	H-Don	≤5	1
Veber’s rules	**RB**	≤10	7
	tPSA	≤140°Å²	125.45
	H-Acc + H-Don	≤12	10
N°. of Violations			None

MW: molecular weight; **miLog P**: Log of partition-coefficient; **H-Acc**: number of Hydrogen bond acceptor; **H-Don**: number of Hydrogen bond donor; **RB**: number of rotatable bonds; **tPSA**: molecular polar surface area.

Table 2: Prediction of pharmacological parameters evaluating TBB using ADMETSar toolbox.

ADMET Properties	**TBB***

Subcellular localization	Mitochondria
Blood-Brain Barrier permeant	High
Human Intestinal Absorption	High
Caco-2 Permeability	Non
P-glycoprotein Substrate	Yes
P-glycoprotein Inhibitor	Yes
CYP450 2C9 Substrate	Non
CYP450 2D6 Substrate	Non
CYP450 3A4 Substrate	Yes
CYP450 1A2 Inhibitor	Non
CYP450 2C9 Inhibitor	Non
CYP450 2D6 Inhibitor	Non
CYP450 2C19 Inhibitor	Non
CYP450 3A4 Inhibitor	Yes
CYP Inhibitory Promiscuity	Low
hERG	Non
AMES Toxicity	Non
Carcinogens	Non
Carcinogenicity	Non
Predicted aqueous solubility	Soluble

hERG, human Ether-a-go-go-Related Gene Inhibition. * (Cheng et al., 2012; Yang et al., 2019).

3.7 TBB exhibits antiproliferative activity in A549 and NCI-H460 tumor cells and low toxicity in epithelial, alveolar macrophage, monocytic and blood red cells.

The potential cytotoxicity of TBB was evaluated in epithelial, alveolar macrophage, monocytic, blood red cells and lung tumoral cell lines. Initially, we investigated whether treatment with TBB altered the viability of renal epithelial cells (LLC-MK2 from monkey), mouse alveolar macrophage (AMJ2-C11), human-derived leukemia monocytes (THP-1), and sheep erythrocytes employing the MTT and hemolytic assays. AMJ2-C11 cell line showed toxicity above 100 μM TBB ($p < 0.0001$), while LLC-MK2 and THP-1 showed toxicity above 200 μM TBB (both $p < 0.0001$), when compared to control (**Fig. 2A**). Data from the hemolytic assay demonstrated that TBB did not cause hemolysis of sheep erythrocytes at any of the concentrations tested (3-200 μM), while CIS (12-200 μM) caused hemolysis at 50, 100 and 200

μM ($p < 0.001$, $p < 0.01$, $p < 0.0001$, respectively) (data not shown), confirming the low toxicity of TBB for these red blood cells.

The effect of TBB on the lung cancer cell lines A549 and NCI-H460 was investigated for 24, 48 and 72 h (**Fig. 2B-C**). Treatment of A549 cells with TBB for 24 h at a concentration of 100 μM was able to reduce the viability of the cells by 61% ($p < 0.0001$). Treatment with TBB at concentrations of 50 μM and 100 μM for 48 h reduced cell viability by more than 50% ($p < 0.0001$), while at 72 h, we observed that concentrations of 25, 50, and 100 μM reduced cell viability by 51.35%, 78.85%, and 98.30%, respectively ($p < 0.0001$) (**Fig. 2B**). Further, in the NCI-H460 cells treated with TBB at concentrations of 50 and 100 μM for 24 h, cell viability was reduced by 53.44% and 83.38%, respectively ($p < 0.0001$). At 48 h, concentrations of TBB of 25, 50 and 100 μM caused reduced cell viabilities of 46.01%, 72.48%, and 91.34%, respectively ($p < 0.0001$), while at 72 h, we observed that treatment with 25, 50, and 100 μM TBB caused reductions of 70.73%, 84.82%, and 96.64%, respectively ($p < 0.0001$) (**Fig. 2C**). The vehicle (DMSO 0.06%) exhibited no toxic effect at any of the time-points tested, and CIS (50 μM) as a positive control, inhibited cell viability in both lung cancer lines.

The IC_{50} values of TBB were determined for LLC-MK2, THP-1, and AMJ2-C11 cells following a 24-h treatment period (**Table 3**). In the case of the tumor cells, A549 and NCI-H460, IC_{50} values were calculated at 24, 48, and 72 h (**Table 3 and Suppl. Table 3**). The TSI was also calculated, where a favorable TSI > 1.0 indicates a drug with efficacy against tumor cells greater than toxicity to normal cells. Our data showed TSI values >1 for both tumor cells relative to epithelial, monocytic and alveolar macrophage cells (**Table 3**).

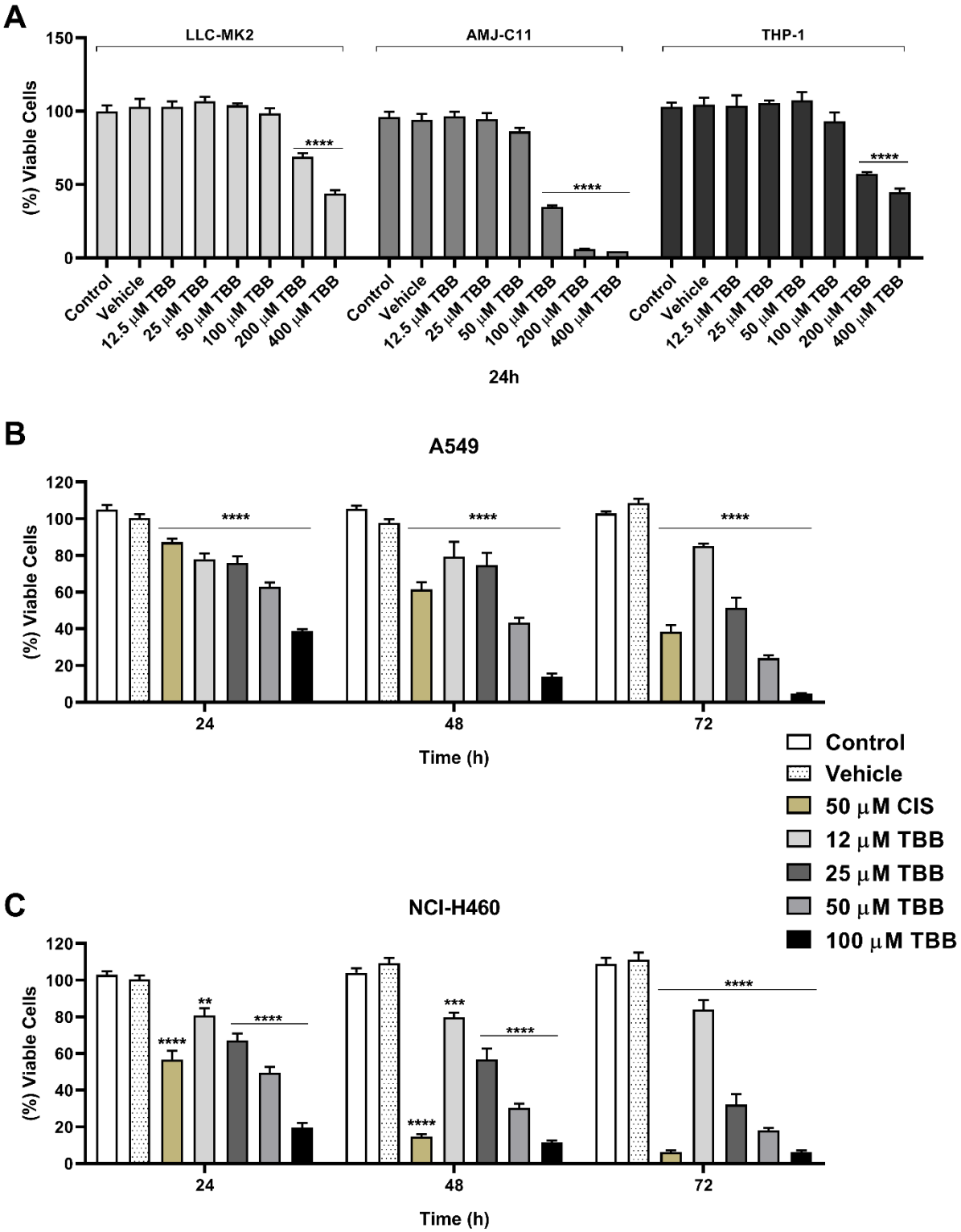

Figure 2: TBB exhibited superior efficacy against tumor cells and low toxicity to epithelial, monocytic, and alveolar macrophage. Cell lines LLC-MK2, THP-1, and AMJ2-C11 (**A**) treated with TBB at different concentrations (12.5-400 μM) for 24 h and analyzed by the MTT assay. Lung cancer cell lines A549 (**B**) and NCI-H460 (**C**) treated with TBB (12 - 100 μM) for 24 h, were also evaluated by MTT. Values are expressed as mean ± SEM. Significant difference

with $^{**}p \leq 0.01$, $^{***}p \leq 0.001$, and $^{****}p \leq 0.0001$ vs. control (untreated cells); vehicle (DMSO 0.06%); CIS (cisplatin, 50 µM).

Table 3

IC_{50} of cell lines: LLC-MK2, THP-1 and AMJ2-C11, and TSI of lung cancer cells A549 and NCI-H460 following treatment with trilobolide-6-*O*-isobutyrate (TBB).

Compound		LLC-MK2 IC_{50} µM (±SEM)	THP-1 IC_{50} µM (±SEM)	AMJ-C11 IC_{50} µM (±SEM)	A549 IC_{50} µM (±SEM)	NCI-H460 IC_{50} µM (±SEM)
TBB		335 µM (±0.01)	305 µM (±0.04)	81 µM (±0.03)	73 µM (±0.06)	54 µM (±0.03)
	TSI A549	5	4	1	-	-
	TSI NCI-H460	6.2	6	1.5	-	-

Rhesus monkey kidney epithelial cells (LLC-MK2), human leukemia monocytic cell line (THP-1), alveolar macrophage murine (AMJ2-C11), lung adenocarcinoma (A549) and large cell lung cancer (NCI-H460). SEM – standard error of the mean.

Supp. Table 3: Half-maximal inhibitory concentration (IC_{50}) in lung cancer cells at 24-72 h after treatment with TBB.

Cell line	**IC_{50}** (µM ± SEM) **Time of treatment** (h)		
	24	**48**	**72**
A549	73 (± 0.06)	47 (± 0.03)	27 (± 0.02)
NCI-H460	54 (± 0.03)	30 (± 0.03)	21 (± 0.02)

SEM – standard error of the mean.

3.8 TBB induces morphological and ultrastructural changes in lung cancer cell lines treated with TBB

Having observed the inhibitory effect of TBB on the proliferation of the lung cancer cells, a comprehensive investigation was conducted to assess its impact on the morphological and ultrastructural aspects of A549 and NCI-H460 cells using SEM and TEM. SEM analysis revealed distinct morphological changes: untreated A549 cells (**Fig. 3A, C**) exhibited typical characteristics, such as strong adhesion to the glass coverslips, presence of an intact cell membrane, the presence of lamellipodia (L), filopodia (F) and microvilli (Mi) across the cell

surface, and well-preserved cellular structures. Following treatment with IC_{50}-TBB, these cells displayed altered morphologies, characterized by a transition to rounded shapes, reduced lamellipodia, irregularities on the cell surface (arrowhead), diminished or absent microvilli (Mi*), and evidence of nuclear and cytoplasmic disruptions (arrow) (**Fig. 3B, D**). Similarly, untreated NCI-H460 cells showed a normal appearance consistent with the features (**Fig. 3E, G**). Upon treatment with TBB, NCI-H460 cells also showed reduced or absent microvilli (Mi*), irregularities on the cell surface (arrowhead), and along with nuclear and cytoplasmic disruptions (arrow) (**Fig. 3F, H**).

Ultrastructural evaluation by TEM showed that the control groups of A549 and NCI-H460 cells presented a homogeneous cytoplasm with regular organelles (mitochondria and endoplasmic reticulum) and without the presence of vacuole-like structures, indicating whole cell integrity (**Fig. 4A, C and E, G**). After treatment with TBB, A549 showed the absence of microvilli (arrowhead), changes in mitochondrial structures such as swelling and enlargement of these organelles (m*). Accumulation of lipid storage droplets (*) and autophagic vacuoles (arrow) were also observed. In NCI-H460 cells, we observed reduced microvilli (Mi*), accumulation of lipid storage droplets (*) and autophagic vacuoles (arrow) following treatment with TBB. Furthermore, the presence of substances inside the vacuoles can be observed (**Fig. 4B, D and F, H**).

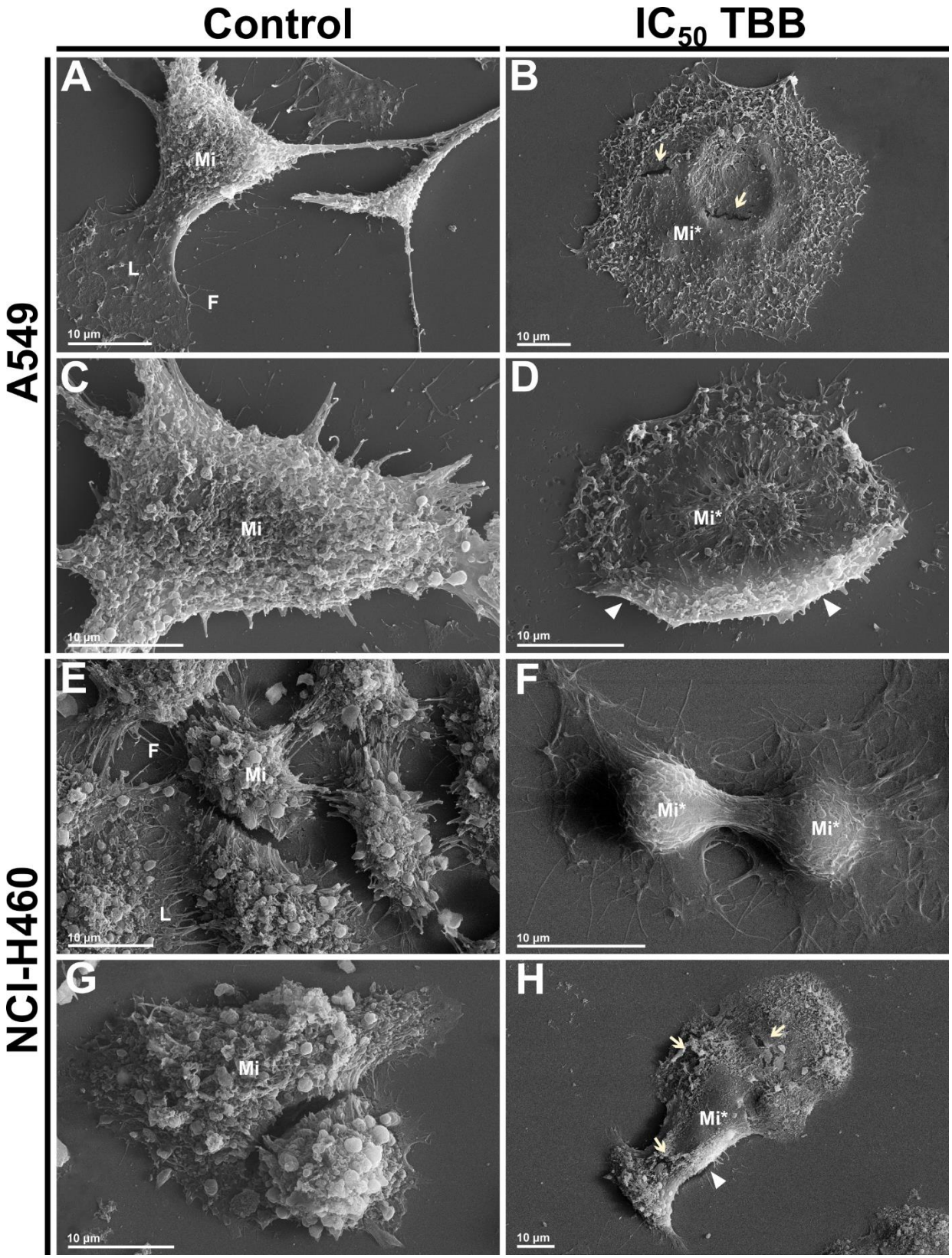

Figure 3: Effect of TBB treatment on the morphology of lung cancer cell lines. Morphological changes observed by scanning electron microscopy after treatment with TBB for 24 h. (**A and C**) Control A549 cell line, untreated cells; (**B and D**) A549 cells treated with IC_{50} of TBB (73 µM). (**E and G**) Control NCI-H460 cell line, untreated cells; (**F and H**) NCI-H460

cells treated with IC_{50} of TBB. (54 µM). (Mi) microvilli, (L) lamellipodia and (F) filopodia, altered microvilli (Mi*), (arrowhead) lamellipodia and filopodia alterations, (arrow) cell disruption. Scale bars = 10 µm (A-I).

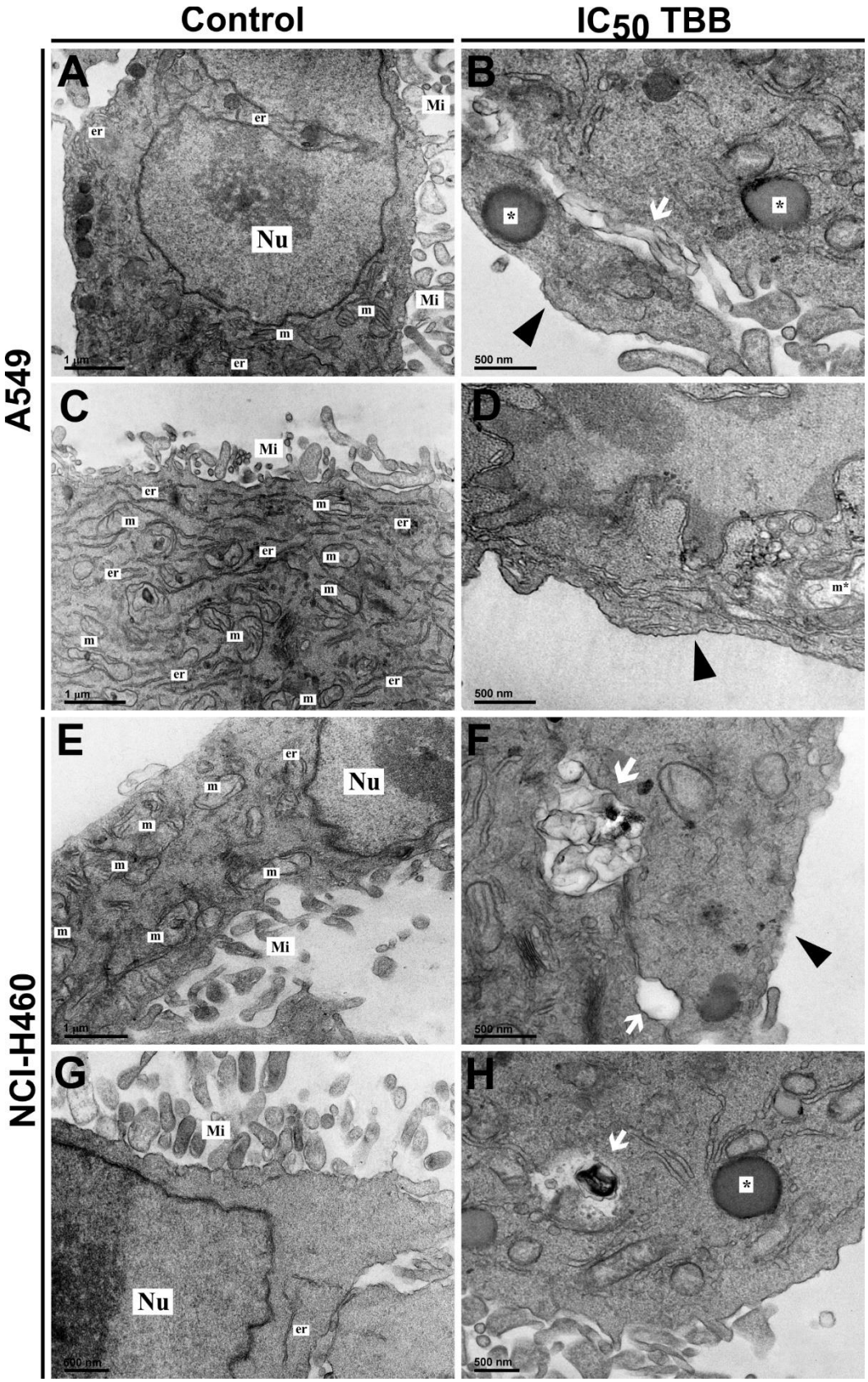

Figure 4: Ultrastructural changes in lung cancer cell lines treated with TBB for 24 h and analyzed by transmission electron microscopy. (**A and C**, A549; **E and G**, NCI-H460) untreated cells; (**B and D**, A549; **F and H**, NCI-H460) cells treated with IC_{50} TBB (73 and 54 µM, respectively); (m) mitochondria; (Gc) Golgi complex; (er) endoplasmic reticulum; (m*) mitochondrial swelling; (Nu) nucleus; (arrow) cytoplasmic autophagic vacuole; (arrowhead) absence of microvilli; (*) lipid droplets storage areas. Scale bars = 1 µm (A, C), 600 nm (B) and 500 nm (D-F).

3.9 TBB reduces migratory capacity in A549 and NCI-H460 cell lines.

A wound healing assay was performed to evaluate migration of lung cancer cells after treatment with TBB (**Fig. 5**). Cell movements at the wound margins were photographed immediately at the start of scratching and at regular time intervals (0, 12, and 24 h) (**Fig. 5A**). Thereafter quantification, the control group of A549 cells showed an increase in migration in relation to the elapsed time, while the TBB-treated group showed a reduction in migration time at 24 h ($p \leq 0.001$) compared to the untreated group (**Fig. 5B**). A549 cells also showed a significant difference between the time points analyzed, with an increase in migration at 12 and 24 h ($p \leq 0.0001$) compared to 0 h. For NCI-H460 cells, the migration effect was even more pronounced. The untreated group also showed an increase in migratory capacity, but the treated group showed a discrepant reduction at 12 h ($p \leq 0.01$) and 24 h ($p \leq 0.001$) (**Fig. 5B**). It is noteworthy that there were no discernible variations in the temporal outcomes among the TBB-treated group for this cell line, elucidating the compound's impact during the initial phases of treatment.

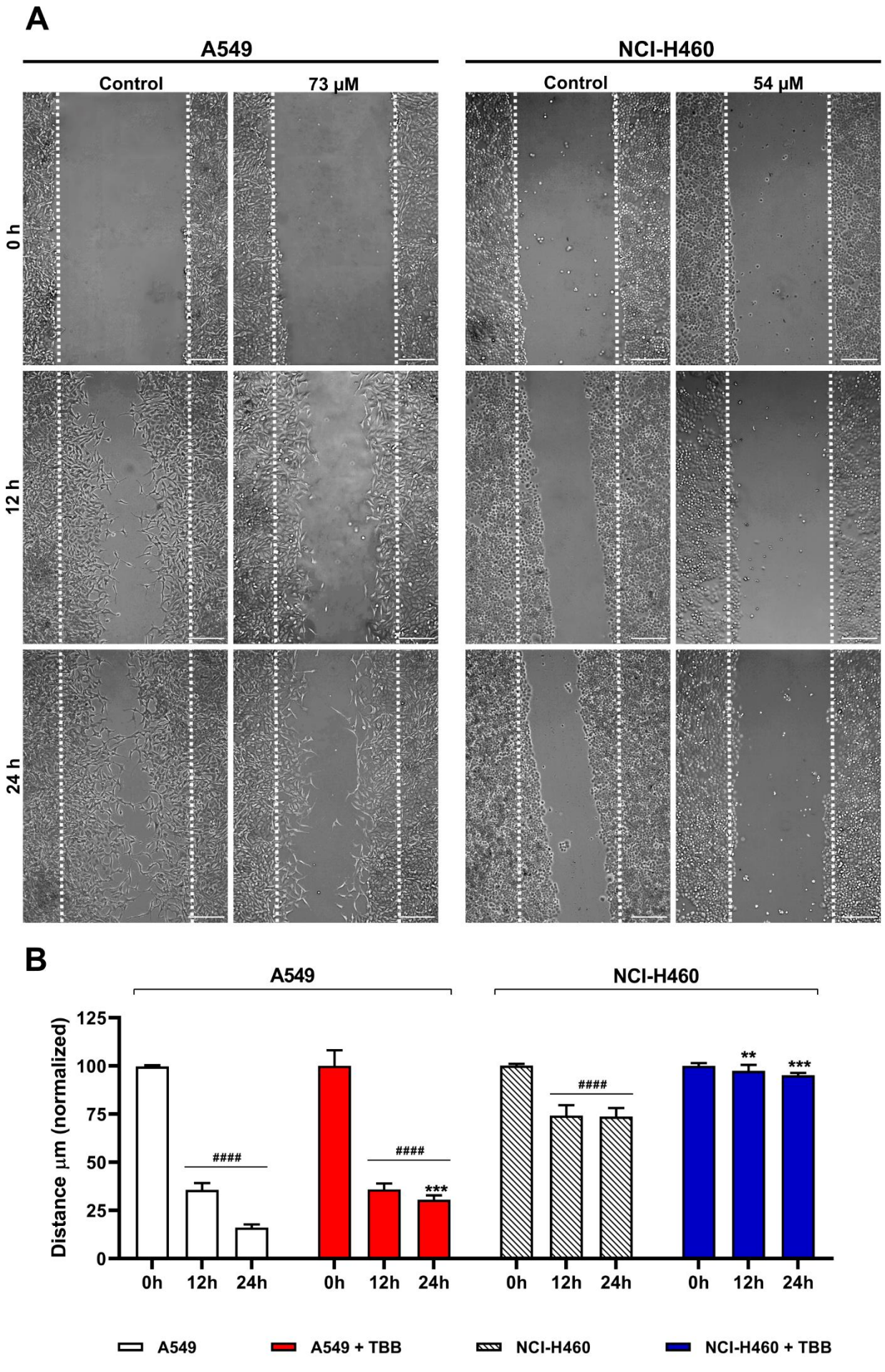
A
A549
NCI-H460
Control
73 μM
Control
54 μM
0 h
12 h
24 h
B
A549
NCI-H460
Distance μm (normalized)
125
100
75
50
25
0
####
####
***
####
**
***
0h
12h
24h
0h
12h
24h
0h
12h
24h
0h
12h
24h
A549
A549 + TBB
NCI-H460
NCI-H460 + TBB

Figure 5: TBB treatment inhibited lung cancer cell line's migration. The scratch assay procedure was performed to observe the effect of TBB treatment on cell migration over time (0, 12 and 24 h) (**A**). The distance of the free surface of these treated cells (**B**) was quantified. Values represent the mean ± SEM of three different experiments performed in triplicate. Significant difference versus control ** ($p \leq 0.01$); *** ($p \leq 0.001$). Significant difference inters groups #### ($p < 0.0001$). Scale bar = 200 µm.

3.10 TBB promotes oxidative stress in lung cancer cells by increasing free radicals and reducing the activity of *in-situ* antioxidant enzymes.

As treatment of lung cancer cells with TBB demonstrated antiproliferative activity and halted cell migration, we investigated whether TBB would act as a pro- or antioxidant in these cells. Therefore, in evaluating total ROS production after 24 h, treatment with TBB showed high levels of these reactive species in the A549 (22.23 AU ± 4.15) and NCI-H460 (62.61 AU ± 9.52) (**Fig. 6A**) cell lines. One of the reactive oxygen species produced intracellularly mainly by mitochondria is $O_2^{\bullet-}$. When evaluating whether TBB would alter the production of these radicals, we found that the treatment promoted a significant increase in both A549 ($p = 0.0075$) and NCI-H460 ($p < 0.0001$) (**Fig. 6C**) cell lines. Reactive nitrogen species also have a highly potent pro-oxidant capacity. When evaluating the levels of NO after treatment with TBB, both A549 and NCI-H460 showed an increase of levels ($p \leq 0.0001$) compared to the control groups (**Fig. 6B**).

Parameters related to the antioxidant profile were also altered by TBB-treatment of the cells. The data showed a decrease in SOD activity and level of GSH for the A549 ($p = 0.0086$, $p = 0.0009$, respectively) and NCI-H460 ($p = 0.0445$, $p = 0.0002$, respectively) cell lines (**Fig. 6D-E**). Overall, these data suggest that TBB acts by increasing oxidative stress in these cancer cells.

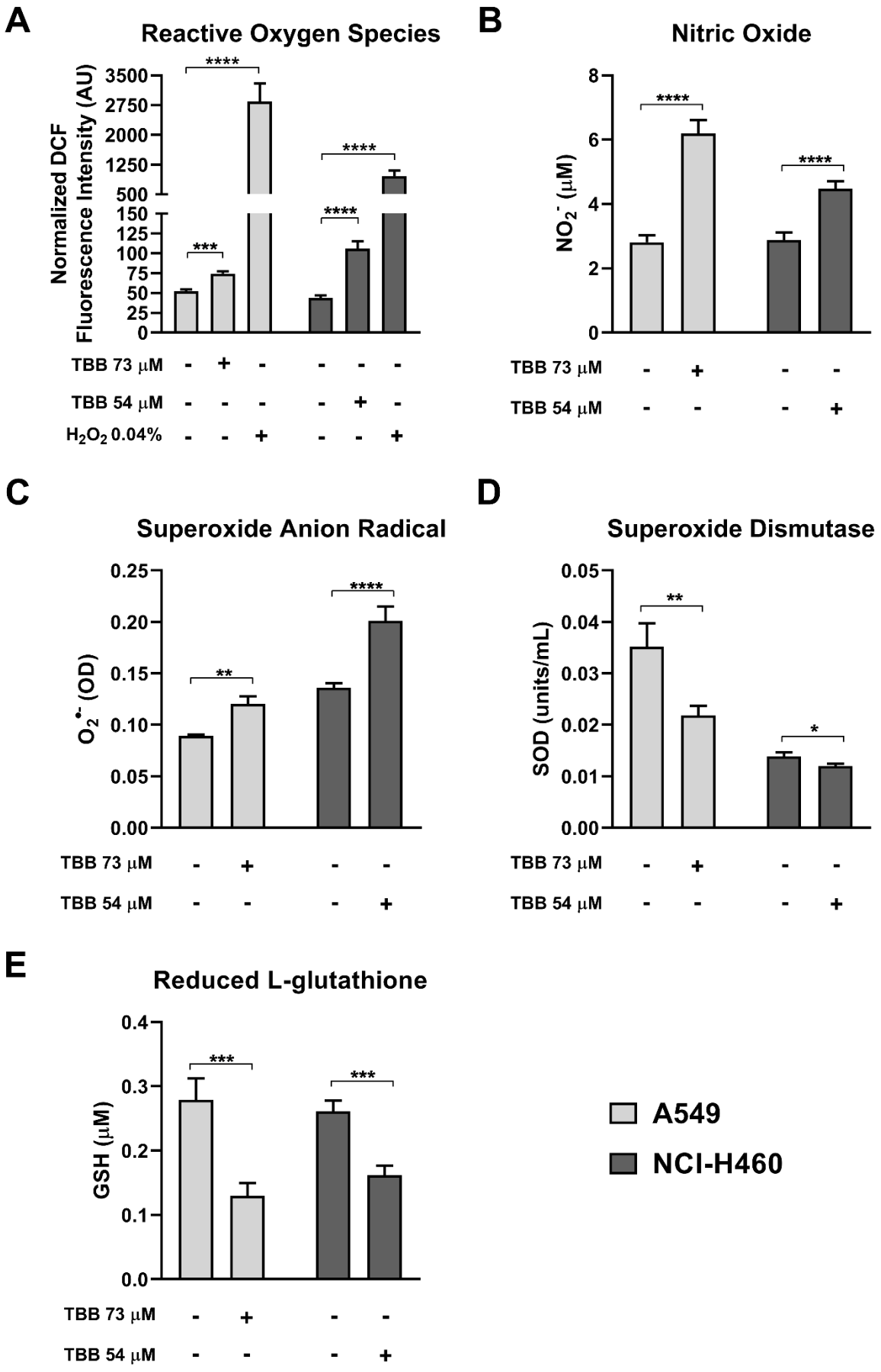
A
Reactive Oxygen Species
Normalized DCF Fluorescence Intensity (AU)
3500
2750
2000
1250
500
150
125
100
75
50
25
0
****
***
****
****
TBB 73 μM - + - - - -
TBB 54 μM - - - - + -
H2O2 0.04% - - + - - +
B
Nitric Oxide
NO2- (μM)
8
6
4
2
0
****
****
TBB 73 μM - + - -
TBB 54 μM - - - +
C
Superoxide Anion Radical
O2•- (OD)
0.25
0.20
0.15
0.10
0.05
0.00
**
****
TBB 73 μM - + - -
TBB 54 μM - - - +
D
Superoxide Dismutase
SOD (units/mL)
0.05
0.04
0.03
0.02
0.01
0.00
**
*
TBB 73 μM - + - -
TBB 54 μM - - - +
E
Reduced L-glutathione
GSH (μM)
0.4
0.3
0.2
0.1
0.0
***
***
TBB 73 μM - + - -
TBB 54 μM - - - +
A549
NCI-H460

Figure 6: The TBB treatment of lung cancer cells trigger oxidative stress, while decreasing levels of antioxidant molecules. Both A549 and NCI-H460 cells were exposed to TBB at IC_{50} concentrations (73 μM for A549, and 54 μM for NCI-H460) for a duration of 24 h. To measure the extent of oxidative stress, ROS levels were assessed using the H_2DCFDA probe (**A**). Nitric oxide (NO) levels were quantified using the Griess method (**B**). Additionally, superoxide radical anion ($O_2^{\bullet-}$) levels were determined through the NBT assay (**C**). The activity of superoxide dismutase (SOD) (**D**), and the reduced levels of glutathione (GSH) (**E**) were evaluated in these lung cancer cell lines. Data are expressed as mean ± SEM of three independent experiments performed in triplicate. * ($p < 0.05$); ** ($p \leq 0.01$); *** ($p \leq 0.001$); **** ($p \leq 0.0001$) vs. control.

3.11 TBB causes metabolic stress in A549 and NCI-H460 cancer cells

Cellular metabolism is essential for the maintenance and acquisition of energy. We evaluated the ΔΨm using the TMRE assay and found that treatment with TBB in A549 cells caused depolarization of ΔΨm, with a decrease in the total fluorescence intensity of TMRE compared to the control ($p < 0.0001$) (**Fig. 7A**), indicating a loss of organelle integrity. In NCI-H460 cells, however, the opposite effect was obtained, i.e., treatment with TBB caused hyperpolarization of ΔΨm, and induced an increase in TMRE-mitochondria complexation ($p < 0.0001$) (**Fig. 7A**), indicating an increase in function and damage in this organelle.

Considering the observed mitochondrial alterations, our investigation then assessed the formation of lipid droplets (LDs) and autophagic vacuoles in the TBB-exposed cells, with the objective to substantiate the presence of metabolic and/or energy imbalances induced by TBB treatment of the lung cancer cells. Nile Red (NR) fluorescence was utilized since it serves as a reliable indicator of LDs. The results clearly demonstrated a substantial increase in LD formation in both A549 ($p < 0.0001$) and NCI-H460 ($p < 0.0001$) cells following treatment with TBB, as compared to the control group (**Fig. 7B**). This observation supports the premise of altered cellular metabolism and energy dynamics induced by treatment with TBB.

The presence of autophagic vacuoles was identified using monodansylcadaverine (MDC) fluorescence. Notably, we observed a significant elevation in fluorescence intensity in A549 (58.68 AU ± 4.12) and NCI-H460 (82.29 AU ± 2.06) cells post-TBB treatment (**Fig. 7C**). These findings align with the results presented in **figure 4**, where TBB induced marked changes in the cellular environment, indicative of an adaptive process aimed at maintaining cell viability.

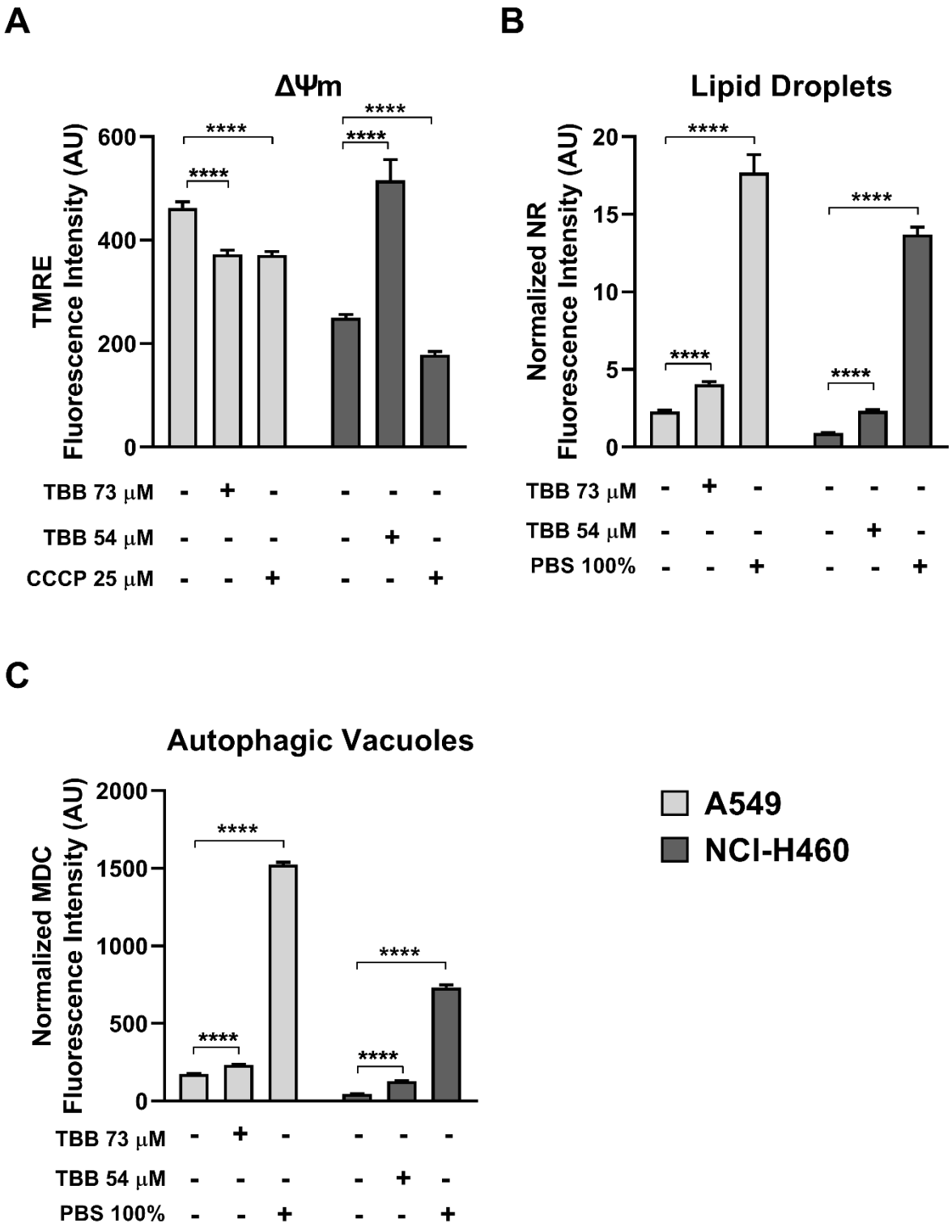

Figure 7: TBB treatment alters metabolism in lung cancer cells. A549 and NCI-H460 cells were treated with IC_{50}-TBB (73 and 54 μM, respectively) for 24 h. (**A**) ΔΨm, (**B**), lipid droplets and (**C**) autophagic vacuoles were quantified by fluorescence. Data are expressed as mean ± SEM of three independent experiments, each performed in triplicate. **** ($p < 0.0001$) vs. control.

3.12 TBB induces apoptosis-like cell death and caspase-3 activation

Cell staining with Annexin V, which binds to phosphatidylserine when externalized, and PI, which diffuses through permeable membranes and binds DNA. This labeling technique allows us to identify the mechanism of cell death induced by IC_{50}-TBB treatment in the lung cancer cells. We differentiated the cell death mechanism into necrotic (PI+), apoptotic (Annexin V+) or late apoptotic (co-staining V+/PI+) processes. Our data revealed that A549 cells treated with TBB increased V+ labeling (31.55% ± 0.93) compared to the control group, while PI or co-staining labeling were not different from the control (**Fig. 8A, B**). In NCI-H460 cells, treatment with TBB was able to increase the percentage of annexin V+ cells (22.30 ± 1.17) and Annexin V+/PI+ double positive cells (11.85% ± 0.40), and PI-stained cells did not differ from the control group (**Fig. 8D, E**).

In support of these data, we found that IC_{50}-TBB treatment also induced an increase in caspase 3/7 activity in both cancer cell lines (**Fig. 8C, F**). A549 and NCI-H460 cells showed an increase in fluorescence intensity of 64.37% (± 1.30) (**Fig. 8C**) and 50% (± 0.70) (**Fig. 8F**), respectively, compared to the control. These data indicate a predominance of apoptotic-type cell death processes resulting from TBB treatment.

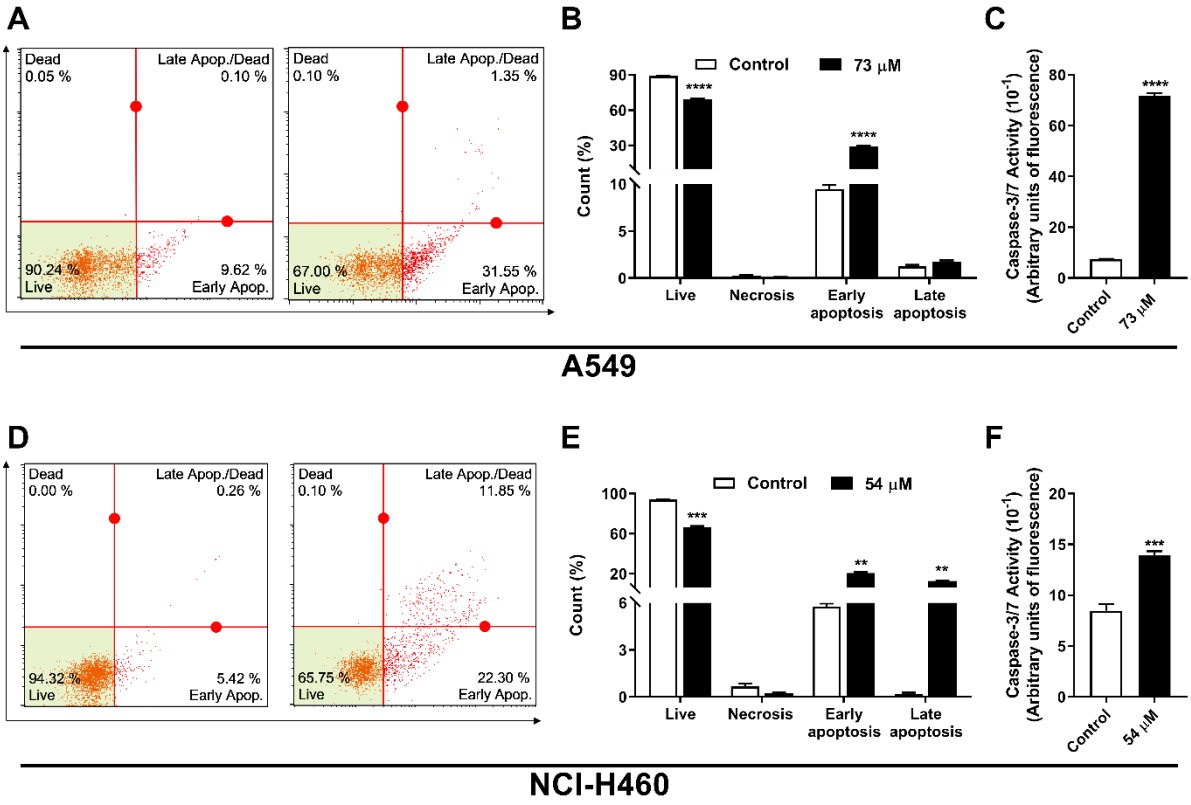

Figure 8: TBB treatment induces apoptosis via increased caspase 3/7 activity in lung cancer cells. A549 and NCI-H460 cell lines treated with IC_{50} of TBB for 24 h and evaluated in dot plots

of cytometry, the induction of viable cells, apoptosis, and necrosis (**A, D**). Quantitative analysis of the dot plots of both cell lines (**B, E**). Caspase 3/7 was quantified by fluorescence for A549 (**C**) and NCI-H460 (**F**) cells. Values are expressed as mean ± standard deviation. Cytometry data are expressed as % vs. control; and mean ± standard deviation. $^{**}p \leq 0.01$; $^{***}p \leq 0.001$; $^{****}p < 0.0001$ vs. control.

4 DISCUSSION

Chemotherapy consists of a group of drugs, either alone or in combination, which represents a therapeutic strategy aimed at inhibiting cell growth as the standard treatment for non-small cell lung cancer. The FDA has compiled a list of approved drugs for combating NSCLC, but both the treatments and the disease itself can lead to several adverse effects. These side effects can vary significantly among patients, even when they are administered the same drug. This variability primarily arises from the substantial heterogeneity observed in NSCLC patients (Majeed et al., 2021; Araghi et al., 2023). Consequently, there remains an ongoing imperative for the development of novel, or newer, therapies to address and mitigate this complex condition (Zappa and Mousa, 2016).

Within this framework, we perform preliminaries study and offers novel insights into the mechanism underlying the *in vitro* action of trilobolide-6-*O*-isobutyrate (TBB) on NSCLC cells, particularly the A549 and NCI-H460 cell lines. Initially, we presented the characterization and obtention of the compound, in addition, revealed that TBB meets the critical criteria for drug-likeness *in silico*. Our findings revealed that TBB reduced cell viability in the A549 and NCI-H460 cell lines while exhibiting low toxicity in epithelial cells, alveolar macrophages, and blood cells. Treatment with TBB reduced migration ability and induced morphological and ultrastructural changes. These observed outcomes were accompanied by an increase in oxidative stress, leading to an adaptive response aimed at mitigating damage and evading cell death. However, TBB ultimately induced cell death through apoptosis-like processes in both cell lines, activating caspase 3/7.

Sesquiterpene lactones (SLs) are naturally occurring products found in *Asteraceae* plants. They hold significant promise for advancing human health due to history of traditional medicine use, and the biomolecular diversity for drug discovery (Chadwick et al., 2013). They can serve as valuable pharmaceutical agents with promising applications in oncotherapy due to their anticancer properties (Liang et al., 2008; Chan et al., 2016; Wang et al., 2017). One noteworthy compound is TBB, classified as a SL, which boasts advantageous pharmacological attributes. *In silico* studies have consistently demonstrated its adherence to Lipinski and Veber's rules,

exhibiting excellent parameters of drug-likeness predictions, such as bioavailability, metabolic stability, and intestinal absorption without any violations (Lipinski, 2004; Veber et al., 2002). Moreover, the structural characteristics of TBB demonstrated favorable calculation of ADMET (Absorption, Distribution, Metabolism, Excretion, and Toxicity) properties, including a high potential for oral bioavailability (Cheng et al., 2012). It's important to note that unfavorable or poor ADMET properties often represent a significant challenge for drug candidates during clinical trials (van de Waterbeemd and Gifford, 2003).

The primary objective of chemotherapy is to achieve a high degree of selective cytotoxicity against cancer cells while minimizing harm to healthy cells. Following the administration of chemotherapy drugs, such as docetaxel, cisplatin, and fluorouracil, several issues arise. These include immunosuppression, leading to conditions like monocytopenia, which involves a reduction in the number of monocytes in peripheral blood. Additionally, renal toxicity becomes evident, as the kidney is susceptible to damage from drugs due to its vital role in the elimination of ingested, injected, or administered chemicals, toxic metabolites, and medications (Poprac et al., 2017; Griffin et al., 2019; Patysheva et al., 2022).

Furthermore, during-chemotherapy, hematological toxicity is a significant concern. This complication is a leading cause of treatment discontinuation, primarily due to its adverse effects on red blood cells, causing anemia, white blood cells, leading to neutropenia or granulocytopenia, and platelets, resulting in thrombocytopenia. These conditions can pose a significant risk to the patient's well-being (Ouyang et al., 2013). Therefore, it is crucial to note that treatment with TBB showed low toxicity towards renal epithelial cells, monocytic cells, and red blood cells. This suggests a promising potential for reduced side effects and a more favorable outcome for patients undergoing this treatment.

The TSI evaluates the cytotoxicity of a compound with respect to tumor and normal cells. A high value (>1) indicates greater selectivity for tumor cells (Badisa et al., 2009; Lica et al., 2021). The present study demonstrated for the first time the anticancer activity of TBB against A549 and NCI-H460 cell lines. Our results revealed that TBB inhibited proliferation of the lung tumor cells with low toxicity to epithelial cells, monocytic and alveolar macrophage, with TSI values >1. Furthermore, we observed a decrease in cell migration, a crucial factor in metastasis (Stuelten et al., 2018), along with significant morphological and ultrastructural alterations indicating the hallmarks of apoptosis-induced cell death and loss of mobility in both A549 and NCI-H460 cancer cells.

In the study conducted by Zhou et al. (2021), they demonstrated the effectiveness of TBB, isolated from *S. trilobata,* against various cell lines of hepatocellular carcinoma (HCC), including

Huh7, SK-Hep-1, HepG2, and Bel7402. Their study assessed multiple time points and revealed that TBB treatment significantly inhibited tumorigenesis. Building upon the findings regarding TBB's action on HCC cells, the primary focus of our investigation was to explore the mechanistic aspects of cell death induced by TBB in NSCLC cells.

Generally, cancer cells have elevated levels of ROS compared to normal cells. The presence of small amounts of ROS in cells promotes cancer development. However, when ROS production exceeds the toxic threshold, this can be associated with mitochondrial dysfunction and can trigger apoptosis in cancer cells. Therefore, a highly effective approach used by cytotoxic agents to induce cell death, is to generate oxygen-containing species. Our results demonstrated that TBB was effective in increasing total ROS and superoxide anion radical production beyond the threshold in both lung cancer cells. In addition, these results were accompanied by increased NO levels, while decreased levels of SOD and GSH in both A549 and NCI-H460 cell lines after treatment with TBB.The literature database has highlighted the dual activities exhibited by NO, which are contingent upon cellular response, redox status, and concentration of NO (Kolb, 2000). Physiologically (nM range) relevant levels of NO have been observed to inhibit apoptosis in diverse cell types, including lung cancer cells. However, at higher concentrations (μM range), NO is known to induce apoptosis through mechanisms involving oxidative stress and time-dependent activation of caspases 1, 3 and 6 (Mintz et al., 2021; Umansky et al., 2000).

The cellular defense against oxidative stress is a fundamental aspect of maintaining cellular homeostasis and preventing cellular death. The enzymes SOD and GSH play pivotal roles in orchestrating the antioxidant response within cells. SOD catalyzes $O_2^{\bullet-}$ into less harmful species like hydrogen peroxide (H_2O_2), thereby mitigating the initial burst of oxidative damage. Subsequently, GSH participates in detoxifying H_2O_2 through the action of glutathione peroxidases, preventing the formation of highly reactive hydroxyl radicals ($^{\bullet}OH$). Together, SOD and GSH act synergistically, forming an essential frontline defense mechanism against oxidative stress, and their proper regulation and activity are crucial for maintaining cellular viability (Poprac et al., 2017). Consequently, our findings indicate that TBB employs a strategy of promoting oxidative stress in tumor cells in two ways: (1) increasing the production of reactive oxygen and nitrogen species and (2) reducing the levels of antioxidant enzymes. This reinforces its potential to combat the proliferation of lung cancer cells.

Cellular responses to stress can trigger either the activation of cell death pathways, or an adaptive response that ensures cell survival. The adaptive response empowers cells to better withstand stress-induced damage. Throughout the adaptive process, cells undergo significant metabolic and physiological adjustments to safeguard against damage and maintain internal

balance (homeostasis). One of the primary mechanisms through which cells promote survival is by removing damaged organelles and recycling nutrients via the autophagic process (Chern and Tai, 2020; Labrie et al., 2022). However, when subjected to TBB treatment, A549 and NCI-H460 cells exhibited an increase of lipid droplets and autophagic vacuoles. Despite this, the treatment resulted in mitochondrial depolarization (MDP) and hyperpolarization (MHP) in the respective cancer cell lines, indicating functional loss and organelle damage that culminates in the loss of the electron transport chain and energy synthesis.

Maintaining the integrity of mitochondria is of paramount importance for efficient energy production and overall cellular survival, especially when exposed to environmental stressors such as nutrient scarcity or genotoxic agents. Disruptions in mitochondrial membrane potential, as indicated by MDP and MHP, are critical events associated with cell death. These mitochondrial dysfunctions represent a crucial "point of no return" in cascade signaling leading to the loss of efficiency in the electron transport chain and reduction in energy synthesis. These events culminate in cell death, and the release of factors such as cytochrome c, into the cytosol (Ganta et al., 2017; Kroemer and Reed, 2000; Susin et al., 1997). Among the various mechanisms of cell death explored, two prominent pathways stand out: apoptosis, a programmed process, and necrosis, which can act as a precursor to several chronic illnesses, including cancer, due to initiation of an inflammatory cascade. Therefore, there is a distinct preference for therapeutic agents that can selectively induce apoptosis in cancer cells (Pfeffer and Singh, 2018).

Apoptosis can be initiated by the intrinsic (mitochondrial) and extrinsic (death receptor) pathways, leading to the activation of effector caspases (caspase 3, -6, and -7) that trigger apoptotic death. DNA damage, oxidative and nitrosative stress, and cytotoxic agents, ultimately lead to permeabilization of the mitochondrial outer membrane and subsequently release cytochrome c, typically initiating the intrinsic pathway. The released cytochrome c leads to the formation of the apoptosome complex, which in turn activates effector caspases. Notable features of apoptotic cell death include some hallmarks such as chromatin condensation, nuclear fragmentation, mitotic cell rounding, reduced cell volume (pyknosis), membrane blebbing formation, ultrastructural modification of cytoplasmic organelles, loss of membrane integrity, and withdrawal of pseudopodia (Chaudhry et al., 2022; Gottlieb et al., 2003; Wong, 2011). In our study, we identified several features associated with apoptosis and, in support of these data, we also observed cell death such as apoptosis with 3/7 caspase activation. However, further experiments are required to substantiate this hypothesis.

Thus, our data showed that cells treated with TBB exhibited morphological and ultrastructural changes indicative of cell damage and death. These changes indicated a profile

favorable to oxidative stress, evidenced by increased levels of ROS and NO, potentially leading to the production of highly reactive radicals, such as peroxynitrite and hydroxyls. Furthermore, tumor cell lines exhibited adaptations that culminated in cell death through processes similar to apoptosis and caspase 3/7 activation (**Fig. 9**).

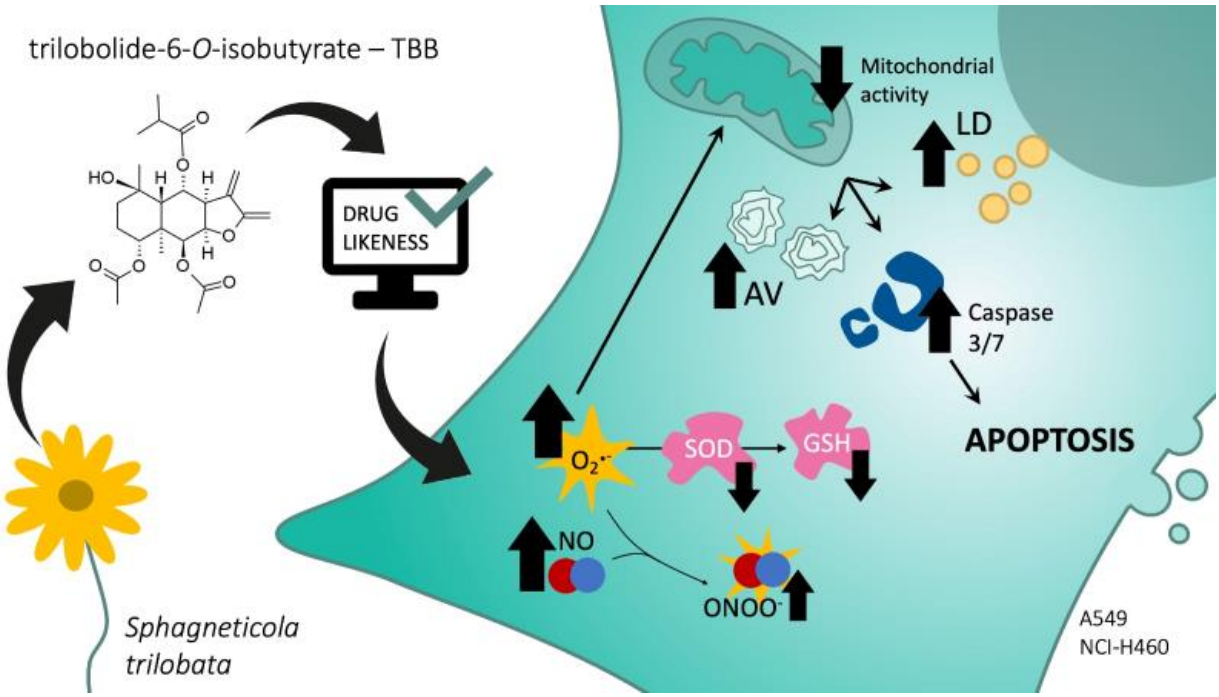

Figure 9: Representative scheme of the antiproliferative action of TBB on human lung tumor cell lines, A549 and NCI-H460. Captions: LD, lipid droplets; NO, Nitric oxide; $O_2^{\bullet -}$, Superoxide anion radical; SOD, Superoxide dismutase; GSH, Reduced L-glutathione; AV, Autophagic vacuoles; $ONOO^-$, Peroxynitrite.

CONCLUSION

This research provided for the first-time new insights into the *in vitro* activity of trilobolide-6-*O*-isobutyrate in lung cancer cell lines, as well as its characterization and predictions based on the *in-silico* study. This research has provided novel insights into the *in vitro* activity of trilobolide-6-*O*-isobutyrate in lung cancer cell lines. TBB exerts a direct inhibitory effect, leading to a reduction in cell proliferation and migration, accompanied by notable morphological, ultrastructural, and biochemical alterations. Additionally, TBB induced elevated levels of oxidative and metabolic stress, culminating in a process resembling apoptosis, as evidenced by the activation of effector caspases. These findings, coupled with theoretical assessments of drug-likeness analysis, position TBB as a promising candidate for further exploration in cancer studies. Furthermore, this study represents a pioneering effort in unraveling

the mechanisms underlying the *in vitro* treatment of lung cancer cells with TBB, and more studies need to be explored to develop as a potential lead in drug development in cancer treatment.

Credit author statement

All persons who meet authorship criteria are listed as authors, and all authors certify that they have participated sufficiently in the work to take public responsibility for the content, including participation in the concept, design, analysis, writing, or revision of the manuscript. Furthermore, each author certifies that this material or similar material has not been and will not be submitted to or published in any other publication before its appearance in *Phytomedicine*.

Author's contribution

V.M.C.L. Conceptualization; Formal analysis; Investigation; Resources; Methodology; Roles/Writing - original draft. **M.D.G. and F.T.P.:** Formal analysis; Investigation; Methodology; Roles/Writing - original draft. **M.B.D., E.M.S.C and B.T.S.B:** Investigation; Methodology; Roles/Writing - original draft. **AC.M.C.:** Formal analysis; Investigation; Methodology; Roles/Writing - original draft. **A.C.J.R.:** Formal analysis; Methodology. **T.F.S.:** Formal analysis; Methodology; Roles/Writing - original draft. **E.S.S.:** Investigation; Methodology. **R.L.N.M.:** Formal analysis; Investigation; Roles/Writing - original draft. **I.L.A.C.:** Investigation; Methodology. **I.C.C.:** Writing - review & editing. **D.B.L.:** Methodology and writing - review & editing. **N.S.A.:** Data curation; Formal analysis; Investigation; Resources; Methodology and revised the manuscript. **R.F.H.D.:** Data curation, formal analysis, and revised the manuscript. **M.S.M.:** supervised the study and revised the manuscript. **W.R.P.:** supervised the study and revised the manuscript. All authors read and approved the final manuscript. All data were generated in-house, and no paper mill was used. All authors agree to be accountable for all aspects of work ensuring integrity and accuracy.

Acknowledgments

This research was conducted with the generous funding and support provided by the Coordenação de Aperfeiçoamento de Pessoal de Nível Superior (CAPES, Brazil), the Conselho Nacional de Desenvolvimento Científico e Tecnológico (CNPq, Brazil), Financiadora de Estudos e Projetos (FINEP) and the Universidade Estadual de Londrina (UEL, Brazil).

Funding

Not applicable.

Ethics approval

This study was approved by the ethics committee (8286.2016.60 and approved in 1/6/2016) of the State University of Londrina.

Competing interests

The authors declare that they have no competing interests.

REFERENCES

Araghi, M., Mannani, R., Heidarnejad Maleki, A., Hamidi, A., Rostami, S., Safa, S. H., Faramarzi, F., Khorasani, S., Alimohammadi, M., Tahmasebi, S., & Akhavan-Sigari, R. (2023). Recent advances in non-small cell lung cancer targeted therapy; an update review. Cancer cell international, 23(1), 162. https://doi.org/10.1186/s12935-023-02990-y

Atanasov AG, Zotchev SB, Dirsch VM, Orhan IE, Banach M, Rollinger JM, et al. Natural products in drug discovery: advances and opportunities. Nat Rev Drug Discov 2021; 20:200–16. https://doi.org/10.1038/S41573-020-00114-Z.

Badisa RB, Darling-Reed SF, Joseph P, Cooperwood JS, Latinwo LM, Goodman CB. Selective Cytotoxic Activities of Two Novel Synthetic Drugs on Human Breast Carcinoma MCF-7 Cells. Anticancer Res 2009; 29:2993.

Bohlmann F, Ziesche J, King RM, Robinson H. Eudesmanolides and diterpenes from Wedelia trilobata and an ent-kaurenic acid derivative from *Aspilia parvifolia*. Phytochemistry 1981; 20:751–6. https://doi.org/10.1016/0031-9422(81)85167-9.

Carrascosa C, Raheem D, Ramos F, Saraiva A, Raposo A. Microbial Biofilms in the Food Industry—A Comprehensive Review. Int J Environ Res Public Health 2021; 18:1–31. https://doi.org/10.3390/IJERPH18042014.

Cataneo AHD, Tomiotto-Pellissier F, Miranda-Sapla MM, Assolini JP, Panis C, Kian D, et al. Quercetin promotes antipromastigote effect by increasing the ROS production and anti-amastigote by upregulating Nrf2/HO-1 expression, affecting iron availability. Biomed Pharmacother 2019; 113:108745–108745. https://doi.org/10.1016/J.BIOPHA.2019.108745.

Chadwick M, Trewin H, Gawthrop F, Wagstaff C. Sesquiterpenoids Lactones: Benefits to Plants and People. Int J Mol Sci 2013; 14:12780. https://doi.org/10.3390/IJMS140612780.

Chan CK, Chan G, Awang K, Kadir HA. Deoxyelephantopin from *Elephantopus scaber* Inhibits HCT116 Human Colorectal Carcinoma Cell Growth through Apoptosis and Cell Cycle Arrest. Molecules 2016;21. https://doi.org/10.3390/MOLECULES21030385.

Chaudhry GES, Md Akim A, Sung YY, Sifzizul TMT. Cancer and apoptosis: The apoptotic activity of plant and marine natural products and their potential as targeted cancer

therapeutics. Front Pharmacol 2022; 13:842376. https://doi.org/10.3389/FPHAR.2022.842376/BIBTEX.

Cheng F, Li W, Zhou Y, Shen J, Wu Z, Liu G, et al. admetSAR: a comprehensive source and free tool for assessment of chemical ADMET properties. J Chem Inf Model 2012; 52:3099–105. https://doi.org/10.1021/CI300367A.

Chern YJ, Tai IT. Adaptive response of resistant cancer cells to chemotherapy. Cancer Biol Med 2020; 17:842. https://doi.org/10.20892/J.ISSN.2095-3941.2020.0005.

Concato VM, Tomiotto-Pellissier F, Silva TF, Gonçalves MD, Bortoleti BTDS, Detoni MB, Siqueira EDS, Rodrigues ACJ, Schirmann JG, Barbosa-Dekker AM, Costa IN, Conchon-Costa I, Miranda-Sapla MM, Mantovani MS, Pavanelli WR. 3,3',5,5'-tetramethoxybiphenyl-4,4'diol induces cell cycle arrest in G2/M phase and apoptosis in human non-small cell lung cancer A549 cells. Chem Biol Interact. 2020 Aug 1;326:109133. https://doi.org/10.1016/j.cbi.2020.109133

Concato-Lopes VM, Silva TF, Detoni MB, Cruz EMS, Gonçalves MD, da Silva Bortoleti BT, Tomiotto-Pellissier F, Carloto ACM, Madureira MB, Rodrigues ACJ, Schirmann JG, Barbosa-Dekker AM, Dekker RFH, Conchon-Costa I, Panis C, Lazarin-Bidóia D, Miranda-Sapla MM, Mantovani MS, Pavanelli WR. 3,3',5,5'-Tetramethoxybiphenyl-4,4'diol triggers oxidative stress, metabolic changes, and apoptosis-like process by reducing the PI3K/AKT/NF-κB pathway in the NCI-H460 lung cancer cell line. Biomed Pharmacother. 2023 Dec 6;170:115979. https://doi.org/10.1016/j.biopha.2023.115979

Dhyani P, Sati P, Sharma E, Attri DC, Bahukhandi A, Tynybekov B, et al. Sesquiterpenoid lactones as potential anti-cancer agents: an update on molecular mechanisms and recent studies. Cancer Cell International 2022 22:1 2022; 22:1–18. https://doi.org/10.1186/S12935-022-02721-9.

Dong Y, Qian X, Li J. Sesquiterpene Lactones and Cancer: New Insight into Antitumor and Anti-inflammatory Effects of Parthenolide-Derived Dimethylaminomicheliolide and Micheliolide. Comput Math Methods Med 2022. https://doi.org/10.1155/2022/3744837.

Dutta S, Mahalanobish S, Saha S, Ghosh S, Sil PC. Natural products: An upcoming therapeutic approach to cancer. Food and Chemical Toxicology 2019; 128:240–55. https://doi.org/10.1016/J.FCT.2019.04.012.

Ferreira D, LevoRato A, Faria T De, De Carvalho M, Braz-Filho R. Eudesmanolide Lactones From *Wedelia paludosa*. Nat Prod Lett 1994; 4:1–7. https://doi.org/10.1080/10575639408043884.

Ganta KK, Mandal A, Chaubey B. Depolarization of mitochondrial membrane potential is the initial event in non-nucleoside reverse transcriptase inhibitor efavirenz induced cytotoxicity. Cell Biol Toxicol 2017; 33:69–82. https://doi.org/10.1007/S10565-016-9362-9.

1889 Gottlieb E, Armour SM, Harris MH, Thompson CB. Mitochondrial membrane potential regulates
1890 matrix configuration and cytochrome c release during apoptosis. Cell Death & Differentiation
1891 2003; 10:709–17. https://doi.org/10.1038/sj.cdd.4401231.

1892 Griffin, B.R., Faubel, S., Edelstein, C.L. Biomarkers of Drug-Induced Kidney Toxicity. Ther.
1893 Drug Monit. 2019; 41, 213–226. https://doi.org/10.1097/FTD.0000000000000589

1894 Guo Q, Liu L, Chen Z, Fan Y, Zhou Y, Yuan Z, et al. Current treatments for non-small cell lung
1895 cancer. Front Oncol 2022; 12:945102. https://doi.org/10.3389/FONC.2022.945102/BIBTEX.

1896 Hui Y, Zhou XQ, Chen GY, Han CR, Song XP, Dai CY, et al. Chemical Constituents of the
1897 Flowers of Wedelia trilobata. Chem Nat Compd 2019; 55:160–3.
1898 https://doi.org/10.1007/s10600-019-02643-5.

1899 Kolb JP. Mechanisms involved in the pro- and anti-apoptotic role of NO in human leukemia.
1900 Leukemia 2000; 14:1685–94. https://doi.org/10.1038/SJ.LEU.2401896.

1901 Kroemer G, Reed JC. Mitochondrial control of cell death. Nature Medicine 2000; 6:513–9.
1902 https://doi.org/10.1038/74994.

1903 Labrie M, Brugge JS, Mills GB, Zervantonakis IK. Therapy resistance: opportunities created by
1904 adaptive responses to targeted therapies in cancer. Nat Rev Cancer 2022; 22:323–39.
1905 https://doi.org/10.1038/S41568-022-00454-5.

1906 Lee SH. Chemotherapy for Lung Cancer in the Era of Personalized Medicine. Tuberc Respir Dis
1907 (Seoul) 2019; 82:179–89. https://doi.org/10.4046/TRD.2018.0068.

1908 Liang QL, Min Z Da, Tang YP. A new elemanolide sesquiterpene lactone from *Elephantopus*
1909 *scaber*. J Asian Nat Prod Res 2008; 10:403–7. https://doi.org/10.1080/10286020801966526.

1910 Lica JJ, Wieczór M, Grabe GJ, Heldt M, Jancz M, Misiak M, et al. Effective Drug Concentration
1911 and Selectivity Depends on Fraction of Primitive Cells. Int J Mol Sci 2021; 22.
1912 https://doi.org/10.3390/IJMS22094931.

1913 Lipinski CA. Lead- and drug-like compounds: the rule-of-five revolution. Drug Discov Today
1914 Technol 2004; 1:337–41. https://doi.org/10.1016/J.DDTEC.2004.11.007.

1915 Lowry, O.H., Rosebrough, N.J., Farr, A.L., Randall, R.J. protein measurement with the folin
1916 phenol reagent. J. Biol. Chem. 1951; 193, 265–275.

1917 Majeed, U., Manochakian, R., Zhao, Y., & Lou, Y. (2021). Targeted therapy in advanced non-
1918 small cell lung cancer: current advances and future trends. Journal of hematology &
1919 oncology, 14(1), 108. https://doi.org/10.1186/s13045-021-01121-2

1920 Mardina V, Ilyas S, Halimatussakdiah H, Harmawan T, Tanjung M, Yusof F. Anticancer,
1921 Antioxidant, and Antibacterial Activities of the Methanolic Extract from Sphagneticola
1922 trilobata (L.) J. F Pruski Leaves. J Adv Pharm Technol Res. 2021 Jul-Sep;12(3):222-226.
1923 https://doi.org/10.4103/japtr.JAPTR_131_21

Mardina V, Ilyas S, Harmawan T, Halimatussakdiah H, Tanjung M. Antioxidant and cytotoxic activities of the ethyl acetate extract of *Sphagneticola trilobata* (L.) J.F. Pruski on MCF-7 breast cancer cell. J Adv Pharm Technol Res 2020; 11:123. https://doi.org/10.4103/japtr.JAPTR_31_20

Marklund, S., Marklund, G. Involvement of the superoxide anion radical in the autoxidation of pyrogallol and a convenient assay for superoxide dismutase. Eur. J. Biochem. 1974; 47, 469–474.

Mintz, J., Vedenko, A., Rosete, O., Shah, K., Goldstein, G., Hare, J. M., Ramasamy, R., & Arora, H. (2021). Current Advances of Nitric Oxide in Cancer and Anticancer Therapeutics. Vaccines, 9(2), 94. https://doi.org/10.3390/vaccines9020094

Mithoowani H, Febbraro M. Non-Small-Cell Lung Cancer in 2022: A Review for General Practitioners in Oncology. Curr Oncol 2022; 29:1828–39. https://doi.org/10.3390/CURRONCOL29030150.

Mosmann, T. Rapid colorimetric assay for cellular growth and survival: application to proliferation and cytotoxicity assays. J. Immunol. Methods 1983; 65, 55–63.

Ouyang, Z., Peng, D., & Dhakal, D. P. (2013). Risk factors for hematological toxicity of chemotherapy for bone and soft tissue sarcoma. Oncology letters, 5(5), 1736–1740. https://doi.org/10.3892/ol.2013.1234

Patysheva, M., Frolova, A., Larionova, I., Afanas'ev, S., Tarasova, A., Cherdyntseva, N., Kzhyshkowska, J. Monocyte programming by cancer therapy. Front. Immunol. 2022; 13. https://doi.org/10.3389/FIMMU.2022.994319

Poprac, P., Jomova, K., Simunkova, M., Kollar, V., Rhodes, C.J., Valko, M. Targeting Free Radicals in Oxidative Stress-Related Human Diseases. Trends Pharmacol. Sci. 2017; 38, 592–607. https://doi.org/10.1016/j.tips.2017.04.005

Pfeffer CM, Singh ATK. Apoptosis: A Target for Anticancer Therapy. Int J Mol Sci 2018;19. https://doi.org/10.3390/IJMS19020448.

Rahman, I., Kode, A. & Biswas, S. Assay for quantitative determination of glutathione and glutathione disulfide levels using enzymatic recycling method. Nat Protoc 1, 3159–3165 (2006). https://doi.org/10.1038/nprot.2006.378

Ryan SL, Dave KA, Beard S, Gyimesi M, McTaggart M, Sahin KB, et al. Identification of Proteins Deregulated by Platinum-Based Chemotherapy as Novel Biomarkers and Therapeutic Targets in Non-Small Cell Lung Cancer. Front Oncol 2021; 11:615967. https://doi.org/10.3389/FONC.2021.615967/BIBTEX.

Shankar R, Thomas T. Antibacterial activity of flower heads of *Wedelia trilobata* (L.) A. S. HITCHC. Journal of Biological & Scientific Opinion 2014; 2:409–12. https://doi.org/10.7897/2321-6328.02692.

Shoaib M, Shah I, Ali N, Adhikari A, Tahir MN, Shah SWA, et al. Sesquiterpene lactone! a promising antioxidant, anticancer and moderate antinociceptive agent from *Artemisia macrocephala jacquem*. BMC Complement Altern Med 2017; 17:1–11. https://doi.org/10.1186/S12906-016-1517-Y/TABLES/6.

Sung, H., Ferlay, J., Siegel, R.L., Laversanne, M., Soerjomataram, I., Jemal, A., Bray, F., 2021. Global Cancer Statistics 2020: GLOBOCAN Estimates of Incidence and Mortality Worldwide for 36 Cancers in 185 Countries. CA Cancer J Clin 71. https://doi.org/10.3322/caac.21660

Susin SA, Zamzami N, Castedo M, Daugas E, Wang HG, Geley S, et al. The Central Executioner of Apoptosis: Multiple Connections between Protease Activation and Mitochondria in Fas/APO-1/CD95- and Ceramide-induced Apoptosis. J Exp Med 1997; 186:25. https://doi.org/10.1084/JEM.186.1.25.

Stuelten, C.H., Parent, C.A., Montell, D.J. Cell motility in cancer invasion and metastasis: insights from simple model organisms. Nat. Rev. Cancer 2018; 18, 296–312. https://doi.org/10.1038/NRC.2018.15

Thai AA, Solomon BJ, Sequist L V., Gainor JF, Heist RS. Lung cancer. Lancet 2021; 398:535–54. https://doi.org/10.1016/S0140-6736(21)00312-3.

Tomiotto-Pellissier F, Alves DR, Miranda-Sapla MM, de Morais SM, Assolini JP, da Silva Bortoleti BT, et al. *Caryocar coriaceum* extracts exert leishmanicidal effect acting in promastigote forms by apoptosis-like mechanism and intracellular amastigotes by Nrf2/HO-1/ferritin dependent response and iron depletion: Leishmanicidal effect of *Caryocar coriaceum* leaf exracts. Biomed Pharmacother 2018; 98:662–72. https://doi.org/10.1016/J.BIOPHA.2017.12.083.

Travis WD, Brambilla E, Nicholson AG, Yatabe Y, Austin JHM, Beasley MB, et al. The 2015 World Health Organization Classification of Lung Tumors: Impact of Genetic, Clinical and Radiologic Advances Since the 2004 Classification. J Thorac Oncol 2015; 10:1243–60. https://doi.org/10.1097/JTO.0000000000000630.

Umansky V, Ushmorov A, Ratter F, Chlichlia K, Bucur M, Lichtenauer A, et al. Nitric oxide-mediated apoptosis in human breast cancer cells requires changes in mitochondrial functions and is independent of CD95 (APO-1/Fas). Int J Oncol 2000; 16:109–17. https://doi.org/10.3892/IJO.16.1.109.

Veber DF, Johnson SR, Cheng HY, Smith BR, Ward KW, Kopple KD. Molecular properties that influence the oral bioavailability of drug candidates. J Med Chem 2002; 45:2615–23. https://doi.org/10.1021/JM020017N/SUPPL_FILE/JM020017N_S.PDF.

Wang Y, Zhang J, Huang ZH, Huang XH, Zheng W Bin, Yin XF, et al. Isodeoxyelephantopin induces protective autophagy in lung cancer cells via Nrf2-p62-keap1 feedback loop. Cell Death & Disease 2017 8:6: e2876–e2876. https://doi.org/10.1038/cddis.2017.265.

van de Waterbeemd H, Gifford E. ADMET in silico modelling: towards prediction paradise? Nat Rev Drug Discov 2003; 2:192–204. https://doi.org/10.1038/NRD1032.

Wong RSY. Apoptosis in cancer: from pathogenesis to treatment. J Exp Clin Cancer Res 2011; 30:87. https://doi.org/10.1186/1756-9966-30-87.

Yang H, Lou C, Sun L, Li J, Cai Y, Wang Z, et al. admetSAR 2.0: web-service for prediction and optimization of chemical ADMET properties. Bioinformatics 2019; 35:1067–9. https://doi.org/10.1093/BIOINFORMATICS/BTY707.

Zappa, C., Mousa, S.A. Non-small cell lung cancer: current treatment and future advances. Transl. Lung Cancer Res. 2016; 5, 288–300. https://doi.org/10.21037/tlcr.2016.06.07

Zhang B, Wang L, Wang L, Wang Y, Xu J, He X. Anti-proliferative and anti-inflammatory eudesmanolides from the flowers of Sphagneticola trilobata (L.) Pruski. Phytochemistry. 2023 Jun;210:113666. doi: 10.1016/j.phytochem.2023.113666. Epub 2023 Mar 31. PMID: 37003362.

Zhou XQ, Mao XM, Fan R, Li SY, Shang J, Zhang T, et al. Trilobolide-6-*O*-isobutyrate suppresses hepatocellular carcinoma tumorigenesis through inhibition of IL-6/STAT3 signaling pathway. Phytotherapy Research 2021; 35:5741–53. https://doi.org/10.1002/PTR.7233.